UNIVERSITY OF OKLAHOMA

GRADUATE COLLEGE

TOWARD ENHANCED WIRELESS COEXISTENCE IN THE 2.4GHZ ISM BAND VIA TEMPORAL CHARACTERIZATION AND EMPIRICAL MODELING OF 802.11B/G/N NETWORKS

A DISSERTATION

SUBMITTED TO THE GRADUATE FACULTY

in partial fulfillment of the requirements for the

Degree of

DOCTOR OF PHILOSOPHY

By

SAMER RAJAB
Norman, Oklahoma
2016

TOWARD ENHANCED WIRELESS COEXISTENCE IN THE 2.4GHZ ISM BAND VIA TEMPORAL CHARACTERIZATION AND EMPIRICAL MODELING OF 802.11B/G/N NETWORKS

A DISSERTATION APPROVED FOR THE
SCHOOL OF ELECTRICAL AND COMPUTER ENGINEERING

BY

_____
Dr. Hazem H. Refai, Chair

_____
Dr. Curt Adams

_____
Dr. John Dyer

_____
Dr. Ali Imran

_____
Dr. Thordur Runolfsson

To the soul of my Father, my beloved mother, siblings and wife, and my little yet to be born bliss

Acknowledgements

The work in this dissertation wouldn't have been possible without the continuous support of individuals whom I'd like to take this opportunity to acknowledge.

My guiding beacon and first idol, Dr. Adel Rajab may your soul rest in peace.

Love and appreciation goes to my mother Amal, Khaled, Reem, Majd, my wife Mayssaa and all of my family for their unconditional love and support.

Special thanks go to my advisor Dr. Hazem Refai for his invaluable guidance, and support. His help and directions have been the major reason for this dissertation success.

My PhD committee; Dr. John Dyer, Dr. Thordur Runolfsson, Dr. Ali Imran and Dr. Curt Adams are highly appreciated for their valuable support.

Acknowledgment goes to my friends whose help and support was a major motive for me to succeed.

Michelle Farabough is acknowledged for her instrumental help in editing this dissertation.

The University of Oklahoma is very well appreciated and acknowledged for support and embracement

Table of Contents

List of Tables

List of Figures

Abstract

This dissertation presents an extensive experimental characterization and empirical modelling of 802.11 temporal behavior. A detailed characterization of 802.11b/g/n homogeneous and heterogeneous network traffic patterns is featured, including idle time distribution and channel utilization.

Duty cycle serves as a measure for spectrum busyness. Higher duty cycle levels directly impact transceivers using the spectrum, which either refrain from transmission or suffer from increased errors. Duty cycle results are provided for 802.11b, g and n Wi-Fi technologies at various throughput levels. Lower values are observed for 802.11b and g networks. Spectrum occupancy measurements are essential for wireless networks planning and deployment.

Detailed characterization of 802.11g/n homogeneous and heterogeneous network traffic patterns, including activity and idle time distribution are presented. Distributions were obtained from time domain measurements and represent time fragment distributions for active and inactive periods during a specific test. This information can assist other wireless technologies in using the crowded ISM band more efficiently and achieve enhanced wireless coexistence.

Empirical models of 802.11 networks in the 2.4 GHz Industrial, Scientific, and Medical (ISM) band are also presented. This information can assist other wireless technologies aiming to utilize the crowded ISM band more efficiently and achieve enhanced wireless coexistence. In this work models are derived for both homogeneous and heterogeneous 802.11 network idle time distribution.

Additionally, two applications of 802.11 networks temporal characterization are presented. The first application investigates a novel method for identifying wireless technologies through the use of simple energy detection techniques to measure the channel temporal characteristics including activity and idle time probability distributions. In this work, a wireless technology identification algorithm was assessed experimentally. Temporal traffic pattern for 802.11b/g/n homogeneous and heterogeneous networks were measured and used as algorithm input. Identification accuracies of up to 96.83% and 85.9% are achieved for homogeneous and heterogeneous networks, respectively. The second application provides a case study using 802.15.4 ZigBee transmitter packet size on-line adjustments is also presented. Packet size is adaptively modified based on channel idle time distribution obtained using simple channel power measurements. Results demonstrate improved ZigBee performance and significant enhancement in throughput as a result of using adaptive packet size transmissions.

Chapter 1: Introduction

With estimated annual Wi-Fi devices transactions reaching nearly $315 million dollars in 2014, it is clear that Wi-Fi has become a major contributor to today's global communications economy [1]. Demand for wireless data transfer has increased significantly in recent years, rendering wireless spectrum an expensive and scarce resource. The ability to operate in the free, unlicensed ISM (Industrial Scientific and Medical) band has prompted cost effective Wi-Fi chip production. Hence, a large number of modern day gadgets, such as laptops, smartphones, printers, cameras and wearable devices, are now equipped with Wi-Fi wireless communications technologies, making Wi-Fi one of today's prevailing wireless communications technologies. New bandwidth-hungry and distributed applications like HD video transfer, social media, Internet of Things, and cloud computing have exacerbated the problem. Recent telecommunication research has focused on developing more efficient means for exploiting available, yet limited, frequency spectrum.

Various wireless technologies are uniquely characterized according to time, frequency, and power domains. Wireless technology characterization and identification provides a wireless device attempting to access the medium with valuable information, including anticipated transmission periodicity, frequency bandwidth, and transmit power, among other parameters. Awareness about these characteristics is useful, especially in heterogeneous frequency bands like the ISM band.

Spectrum scarcity has risen significantly in the past few years, triggering intensified research in multiple areas, such as spectrum occupancy measurements and cognitive radio.

An ever-increasing reliance on wireless communications makes frequency spectrum an expensive resource. Although a number of spectrum occupancy measurement campaigns have been presented in literature, as discussed in following sections, most target to study underutilized spectrum and multiple bands scanning. Limited work has investigated 2.4GHz ISM band spectrum occupancy.

Spectrum scarcity makes heterogeneous spectrum access a necessity in current wireless networks primarily because the scarcity forces wireless technologies to share the same frequency band [2]. As a consequence, wireless coexistence among various wireless technologies sharing the same medium is gaining increased attention as an integral feature for reliable operation. Coexistence is defined as "the ability of one system to perform a task in a given shared environment where other systems have an ability to perform their tasks and may or may not be using the same set of rules" [3]. Knowledge of both anticipated and current spectrum occupancy levels enables efficient planning and parameter adaption for coexisting wireless technologies, thus enhancing transmission efficiency.

The ISM band is unlicensed, making it an attractive solution for wireless device manufacturers. Several protocols (e.g., Wi-Fi, Bluetooth, Bluetooth Low Energy (BLE), and ZigBee) have been developed to operate in the ISM band. Wireless chips for these protocols are now manufactured in large scale, further reducing their prices. Consequently, the ISM band is widely recognized as one of the most crowded frequency bands and serves as a timely example of issues related to heterogeneous spectrum access. Spectrum occupancy measurement serves as a tool to assist wireless device manufacturers to make cognizant decisions when choosing transmission parameters, including transmission

power, frequency, and frame size, among others. This is performed using algorithms to intelligently characterize the spectrum occupancy and identify wireless technologies utilizing the spectrum at a particular time.

Wi-Fi is a primary causes of interference in the ISM band due to the technology's high power and data rate when compared with other technologies sharing the 2.4 GHz ISM band. Hence, characterizing spectrum occupancy behavior of Wi-Fi is vital for both frequency channel planning and wireless device development in the 2.4 GHz ISM band. A means to analyze spectrum occupancy for Wi-Fi is measuring channel duty cycle (DC), modelling idle time distributions and using this information to identify wireless technologies sharing the medium. Notably, DC is defined as the fraction of time at which the received signal strength is above a certain threshold [4].

Wi-Fi networks operating in the ISM band are typically heterogeneous, as they include 802.11b/g/n Wi-Fi standards, which have significant differences in both PHY and MAC layers, as will be discussed in greater detail in chapters that follow. Networks supporting any of these standards could exist within close proximity of one another. Thus, understanding spectrum occupancy for heterogeneous Wi-Fi networks can aid in improving coexisting network performance. Measuring frequency channel DC is one method for assessing spectrum occupancy.

This work in part investigates time distributions modelling of 802.11 heterogeneous networks in the 2.4GHz ISM band, including a detailed characterization of 802.11b/g/n homogeneous and heterogeneous network traffic patterns. This type of study will facilitate better understanding of 802.11 temporal behavior, thus enabling improved design for coexisting wireless technologies. Time distribution modelling focuses on 802.11

networks, in particular, primarily due to their high power levels and extensive use. This makes 802.11 networks the foremost interferer in the exceedingly crowded 2.4GHz ISM band. This band is of special interest to wireless coexistence for two chief reasons:

1) The relatively limited 80MHz spectrum, and

2) The large number of wireless technologies that share the ISM band.

These aspects cause wireless coexistence difficulties for technologies sharing the ISM band with 802.11 networks. Consequently, interference between 802.11 and other technologies (e.g., Bluetooth, ZigBee, and BLE, among others) could have adverse effects depending on the application of devices sharing the same 802.11 frequency band [5][6][7].

A critical example of the effect of 802.11 interference with other coexisting technologies can be found in the medical device industry. Many medical device manufacturers implement wireless technologies in their devices for a number of practical reasons, including patient convenience. Medical device applications for wireless connectivity range from transmitting regular telemetry data to patient life-critical applications. Medical devices must utilize low-power consumption technologies to minimize service interruption. Several manufacturers employ ISM band wireless technologies as often as possible, primarily due to global availability and reduced costs due to standardization and large scale manufacturing. ZigBee, Bluetooth, and BLE are examples of popular wireless communication technologies currently implemented in medical devices. Devices using these technologies could suffer severe interference among ISM transmitters caused by 802.11 traffic [8][9], which can jeopardize medical device functionality and impose a risk to patient safety depending on the specific application of the medical device. Diligent wireless coexistence risk assessment of wireless medical systems must be performed

based on data-rate and delay requirements, as well as anticipated spectrum occupancy. Consequently, the United States Food and Drug Administration (FDA) has recommended that radiated coexistence testing should be performed during the wireless medical device certification process [10]. The experimental wireless technology identification techniques assessment presented in this work is directly related to the wireless medical devices example as measurements were performed in the 2.4 GHz ISM band. Note that from hereafter, wireless technologies sharing frequency bands with 802.11 will be referred to as coexisting technologies (CT); the 2.4 GHz ISM band is referred to as the ISM band.

Channel awareness in terms of temporal characteristics (e.g., DC, activity distribution, and idle time distribution) aids CTs' intelligent transmission decision-making. Frame size, channel access frequency, and time (and/or transmission frequency channel) can be modified for improved performance based on channel temporal traffic patterns.

Various wireless applications operating in different frequency bands will benefit from wireless technology characterization and identification techniques. For example, cognitive radio requires spectrum usage awareness for cognitive nodes to operate properly. Cognitive radio network requires spectrum usability assessment, particularly in licensed bands, before a cognitive node can access the medium. Threats to wireless coexistence increase with cognitive radio use regardless of advanced spectrum sensing. Hence, identification of wireless technologies operating in a specific spectrum band provides a cognitive node with an estimate of potential interference. A cognitive node can use gathered information to aid in decision-making about using an intended frequency band.

This dissertation presents a detailed temporal characterization of 802.11 homogeneous and heterogeneous wireless channels in the ISM band based on an energy detection technique. The contributions of this work include the following:

1. Provide a methodology for wireless channel temporal characterization using an energy detection technique.

2. Offer an extensive experimental study of traffic patterns and DC for homogeneous and heterogeneous 802.11 networks and a detailed scheme for DC measurements for Wi-Fi 802.11b/g/n. The presented study links measured DC to data throughput level and the number of coexisting networks. Also, a comparison between obtained results using two developed measurement tools for time domain (TD) and frequency domain (FD) is presented. DC measurement data is analyzed via conventional inferential statistical methods (i.e., null-hypothesis tests, linear regression, and others) to validate DC obtained in TD with DC measured in FD.

3. Provide detailed empirical modelling of 802.11 homogeneous and heterogeneous networks in the ISM band, including evaluation of idle time devised models compared with corresponding measured distributions for 802.11b/g/n single and multi-pair transmissions obtained via energy detection method.

4. Report findings for a study investigating wireless technology identification using energy detection and machine learning techniques. Wireless technology identification is possible through received signal demodulation. However, this method could prove impractical, primarily because a wireless terminal with such functionality must support many different demodulation schemes. A novel alternative method for wireless technology identification through the use of simple

energy detection techniques is presented. A developed algorithm a) constructs temporal activity and idle time distributions from measured received signal strength (RSS), b) extracts distinguishing features from distribution, and c) provides technology identification decision using machine-learning classifiers. Experimental assessment of a developed algorithm has been performed, yielding high identification accuracy: 96.83% for homogeneous Wi-Fi networks and 85.9% for heterogeneous Wi-Fi networks.

5. Deliver results from a case study investigating CT (ZigBee) performance improvement when coexisting with an 802.11g network through temporal characterization. A ZigBee simulation was implemented wherein ZigBee packet size was changed adaptively according to channel idle time distribution to improve ZigBee performance under interference. ZigBee throughput and packet error rate (PER) for both fixed packet sizes and variable packet sizes were tracked and reported.

This dissertation is organized as follows. Chapter 2 lists related work and provides an overview of the ISM band technologies investigated in this work. Chapter 3 details methodology and the experimental setup. Chapters 4 and 5 present 802.11 networks temporal characterization including; spectrum occupancy analysis and time distributions of 802.11 networks, respectively. 802.11 idle time distributions empirical modeling work is presented in Chapter 6. Chapter 7 offers two applications of 802.11 networks temporal characterization. The first reports adaptive ZigBee frame size based on 802.11g network for improving performance; the second identifies wireless technology using energy

detection and machine learning techniques for devices sharing the medium. Finally, a conclusion is provided in Chapter 8.

Chapter 2: Literature Review

This chapter provides an overview of earlier work related to spectrum occupancy monitoring. Studies researching energy detection spectrum sensing, spectrum temporal patterns modelling, throughput-sensing problem, frame aggregation techniques, and wireless technologies identification are examined in the following subsections. An overview of wireless technologies investigated in this work is provided, as well.

Energy detection spectrum sensing

Energy detection, also known as transmitter detection or radiometry, is a simple and widely recognized spectrum sensing technique—one that has been adopted in many applications, including cognitive radio [11]. Unlike other spectrum sensing techniques, those employing an energy detection algorithm do not need prior information about the channel or received signal. The energy detecting algorithm has three stages. In the first stage, received signal energy is measured within a frequency span (or bandwidth). In the second stage, the measured signal is compared with a predefined threshold to separate the desired signal from background noise. In the third stage, a decision is made as to whether or not there is an active signal (i.e., if the measured energy value is above or equal to the threshold). This energy detection technique is characterized by low computational cost and minimal implementation complexity. However, its performance degrades with a low signal-to-noise ratio (SNR) [12]. The lower the SNR, the higher the probability of false detection. This drawback can be overcome by introducing improved energy detection algorithms, which enhances the performance of the conventional energy detection method [13][14][15].

Presented work in this dissertation details an energy detection method to scan the wireless spectrum in the ISM band. A variety of tests with varying throughput and number of transmitters were performed. Idle time and activity distributions were extracted, and empirical models were devised for a number of 802.11 combinations at varying throughput. The purpose of these tests is three fold:

1. Describe idle time distribution mathematically with acceptable accuracy to facilitate a better understanding of 802.11 heterogeneous networks.
2. Characterize temporal spectrum utilization by 802.11 networks to provide channel occupancy awareness for wireless technologies coexisting with 802.11 networks. Occupancy awareness results in intelligent and more efficient design.
3. Utilize the activity and idle time distributions obtained via energy detection method to provide examples of using this approach to enhance the performance of coexisting technologies.

Spectrum temporal patterns modelling

Following is a summary of related work on spectrum measurement and temporal patterns modeling.

Earlier work investigating spectrum occupancy measurements in the ISM band is of particular interest, as it falls within the scope of work presented herein. Limited work has been found in literature for ISM band spectrum occupancy measurement. In [16], spectrum occupancy measurements using distributed directional antennas are presented. This work provides information on spatial dimension influence over duty cycle (DC). ISM band measurements were conducted in an office environment, and DC for uncontrolled

environment was reported. The work adopted conventional energy detection with fixed threshold for calculating DC. The work was extended in [17], wherein measurements acquired from two devices with multiple directional antennas were conjoined using different combining rules. DC average measurement for one day in an office area was presented.

In [18], a measurement approach in the ISM band using energy detection was proposed. Measurements were undertaken using frequency domain (FD) sweeping, wherein each measurement was performed for 30 minutes. DC was presented as a function of frequency. Notably, the paper focused on measurement tool parameters development. Although other studies investigated ISM band activity to model idle time distributions, DC results were not provided [19] [20].

Aforementioned studies focused on spectrum sensing and DC reporting of uncontrolled transmissions on the spectrum. Work presented in herein is unique in that it investigates 802.11 temporal patterns in a controlled environment for single and multiple homogeneous and heterogeneous 802.11 transmitters with varying throughput levels. The study also models 802.11 network idle time distributions, thus capturing temporal behavior of the main interference sources might exist in the band.

Examples of previous research investigating temporal behavior in a licensed, non-ISM band can be found in [21] [22]. Work presented in [21] models long term DC and activity/idle time distributions for measurements obtained from several bands. The paper provides an accurate model for DC for cellular bands GSM and DCS. Though measurements were taken for the ISM band, they were not presented nor discussed. The presented model for idle time distribution is provided for large scale (in order of seconds),

whereas presented distributions in this dissertation are for small scale distributions (i.e., micro seconds).

Modelling of wireless activity temporal patterns using Continuous-Time semi-Markov Chain CTMC was presented in [22]. Two measurement devices that provided high and low time resolution were employed. The longest time resolution achieved and reported was 128 μs, which is inadequate to accurately capture WLAN activity patterns. The work applied different distributions to various bands. Although the authors in [22] mentioned ISM measurement of ISM band spectrum utilization, results were not presented.

Throughput-sensing problem

In the ISM band, 802.11, and other Coexisting Technologies (CTs) have equal privilege to use the unlicensed band. Notably, the high power and data rate of 802.11 have made this technology the dominant transmitter. The 802.11 interference effect on CT far exceeds CT interference effect on 802.11. Hence, other CTs must optimize wireless coexistence with 802.11 to improve their performance. This phenomenon is analogous to cognitive radio networks where a secondary user (SU) must manage spectrum access to minimize interference with primary user (PU).

In a cognitive radio (CR) network, the SU frame transmission time is divided into sensing time and transmission time. The latter is one of the most important parameters effecting SU throughput [23]. Frame time must be optimized by minimizing sensing time and maximizing transmission time. Effects of PU traffic on SU throughput has been investigated in earlier literature [24][25][26][27][28].

Researchers in [24] were the first to examine the effect of PU altering transmission state during SU transmission on CR performance (i.e., throughput). Previous studies considered a channel to be either busy or available, maintaining only one or the other of the two states during SU frame transmission. An investigation in [24] proposed an analytical model wherein one transition from OFF to ON was considered, based on PU throughput. Researchers did not consider, however, the effect of a changing SU frame size.

In [25], the effect of PU changing its state during an OFF period was also analyzed. In [26], the possibility of PU changing states one time during the OFF stage was investigated. CR throughput was maximized based on frame size, assuming that ON/OFF durations and sensing time maintain an exponential distribution. Work presented in [27] developed an analytical model to describe and maximize SU throughput based on optimizing SU frame size and sensing period. The analytical model accounted for up to two PU traffic state transitions, although this assumption might not be true, depending on PU frame duration (i.e., acknowledgement—ACK or data). Authors of [28] implemented a sensing scheme to estimate the distribution of PU ON/OFF durations and decide whether or not to sense a channel. PU traffic ON/OFF durations were assumed to have a Gaussian distribution.

Frame aggregation techniques

Frame aggregation has been researched extensively in literature. The research led eventually to the technology implementation in 802.11n standard's MAC layer. Earlier studies investigating frame aggregation and adaptive frame size are discussed below. This portion of the literature review will facilitate a better understanding of the frame aggregation technology in 802.11n networks. Also, it highlights possibilities of implementing similar approaches for CTs in the ISM band.

Adaptive frame aggregation is investigated in [29] [30] [31] [32] [33] [34] [35] [36]. Research in [29] investigated optimal frame size based on Bit Error Rate (BER) estimated from SNR. The paper assumes saturated nodes with only RTS/CTS scheme. Also, existence of a feedback mechanism that reports SNR to transmitter is assumed.

[30] introduces an algorithm that dynamically chooses the aggregation scheme to be used in 802.11s mesh networks. Algorithm uses BER, quantity, and distribution of frame arrival to the transmitter queue for making a choice regarding the aggregation scheme. This technique assumes that BER is measured from received frames. Authors of [31] develop an analytical model to describe impact of frame aggregation on saturation throughput. Frame error rate is calculated from received block ACK to adaptively change sub-frame size.

A joint data rate and fragment size adaption based on error probability is investigated in [32]. In this context, the probability of error is estimated by the transmitter by counting the number of unsuccessfully received fragments using block ACK whilst not relying on SNR. Authors of [33] propose a frame size estimation technique based on frame error rate (FER). Kalman filter is used to estimate optimal frame size using FER.

In [34], an analytical model to optimize frame size based on delay constraints of the node is proposed. It assumes that the network is in saturated condition. This method also assumes that all nodes in the network broadcast their delay information wherein delay is defined as the time required by a node to successfully access the channel. It is assumed that a node can acquire information about number of transmitting nodes by observing the network without specifying the mechanism.

An algorithm that adaptively changes the aggregated frame size is proposed in [35]. The algorithm aims at maintaining delay below a specific maximum boundary. In [36] a dynamic frame aggregation scheme based on channel conditions in 802.11a network is investigated. The algorithm estimates the probability of error using received ACK signal strength, and then utilizes a lookup table to adjust the data rate and frame size.

A study presented in [37] precedes frame aggregation technology. Different from aforementioned studies, researchers investigate variable frame size in terms of performance of saturated 802.11 DCF in terms of packet size, contending nodes, and packet error probability. An analytical framework was developed to determine optimal frame size for maximizing throughput based on BER.

Other research activities studied channel state estimation or frame size change for other purposes, such as scheduling and technology interoperability (e.g., [38] [39]). Experimental evaluation of increasing 802.11 frame payload size to 4KB was presented in [38]. The main contribution of that study was providing a software interface to enable Linux host to send/receive a frame larger than the Ethernet standard of 1500 Bytes. However no adaptive frame size variation was presented in the paper. Authors of [39] propose a scheduling mechanism that takes into account channel state and transmitter queue size. In this context, access point (AP) is assumed to schedule the user with good channel state and long queue time to optimize throughput. No variation of frame size was presented.

Wireless technology and MAC method identification

To the best of the author's knowledge, no previous work has been published that identifies various 802.11 standards by way of observing power measurements from a medium where

standards are operational. Unlike research detailed below, the newly developed method does not require demodulating the received signal, nor is it necessary to successfully perform accurate identification based only on raw power measurements.

Bayesian machine learning method and independent component analysis technique have been employed in [40] and [41] respectively for clustering 2.4 ISM band wireless networks. These methods investigate blind technology identification (BTI) approach to group wireless transmissions with similar behavior. Such techniques are useful for identifying number of wireless transmissions with distinct behavior using the spectrum band with no prior knowledge about these wireless technologies. Nevertheless, additional information about the underlying wireless technologies being used by such transmissions cannot be deduced without a prior knowledge of the corresponding wireless technologies characteristics.

Authors in [42] aimed at detecting Classic Bluetooth (BT) piconets and Wi-Fi 802.11g networks. The researchers developed a method using Universal Software Radio Peripheral (USRP) to collect (4 MHz) bandwidth power measurements in the ISM band. Classic BT piconets were identified through a time-binning mechanism, which demonstrated that power bursts falling in the same time bin are originated from a single piconet. An alternative suggested method requires demodulating sensed bursts, and then obtaining the 72-bit Channel Access Code, which is unique to each piconet. The presence of Wi-Fi access points is determined by examining distinct equalization sequences included in AP beacons, and then cross-correlating observations within a beacon time period.

Fingerprinting is also heavily studied in literature. In contrast to [42], [43] exploits specific emitter identification (SEI) second-order cyclic OFDM features for identifying different hardware emitting 802.11a/g signals. The experiment output is a wireless card model as opposed to counting the number of nodes or networks existing on the medium. Other similarly targeted sources in literature can be found by investigating means to identify a used wireless network card, such as [44] that identifies specific Network Interface Cards (NICs) among a group of identical NICs. Likewise, [45] promotes the use of transient features that are manifested when a wireless transmitter is switched on as means for transmitter identification. The study presented in [46] relies on frame inter-arrival time as a parameter toward determining a distinct device fingerprint.

Authors of [47] presented a method in which a cognitive radio node identifies the MAC protocol of other nodes (e.g., primary users of spectrum or other cognitive nodes) among four types of MACs: TDMA, CSMA/CA, pure ALOHA, and slotted ALOHA. The method relies on extracting two power features, namely received power mean and variance, and six time features, including minimum, median, and maximum of both channel idle and busy durations. This work relies on simulation to generate fictitious date, which is then input into Support Vector Machine learning-algorithm for identifying a MAC protocol.

Comparison with previous research

This section provides a detailed comparison between work presented in this dissertation and the most relevant studies presented in the previous sections. Earlier studies on spectrum temporal patterns modelling focused on idle time distributions in licensed bands. These studies were expected to be the impetus for a cognitive network solution in which a secondary user would be privileged to use the spectrum whenever the primary

user was inactive. However, several issues were found when employing cognitive radio in a licensed band (e.g., hidden transmitter problem).

Such problems have spawned alternative solutions to spectrum sensing, such as centralized databases providing information about primary user activity in licensed bands. Notably, due to the complexity and heterogeneous nature of this problem, limited work has investigated spectrum occupancy scanning and modelling of 2.4 GHz ISM band. Furthermore, no agreed-upon definition exists for an ISM band primary user.

Work presented in this dissertation is focused on overcoming these issues by detailing temporal distributions modelling in the ISM band. The following assumptions have been made:

- 802.11 networks are the main interferer in the ISM band as a results of their high power and their use as a large data transfer solution, as demonstrated and proven in earlier literature (e.g. [7][8][48]).
- Providing a comprehensive set of experiments to describe 802.11 networks is important for identifying: 1) Homogeneous and heterogeneous network combinations; 2) Varying throughput levels from low throughput to saturation; and 3) Varying number of transmitting terminals. Uncontrolled spectrum measurements are subjective, as indicated by variations in results reported in the literature. Controlled spectrum measurement narrows the problem with a limited set of parameters for presenting a reproducible representation of the spectrum.

Of most interest are studies performed by *Lopez-Benitez et. al.* [21][22]. In [21] spectrum measurements were performed for the following bands: TETRA-UL, TETRA-DL, E-

GSM 900 UL, E-GSM 900 DL, DCS 1800 UL, DCS 1800 DL, DECT, and ISM bands. Active time, idle time, and DC results were then presented for TETRA, E-GSM, and DCS bands at a testing site in Barcelona, Spain. Discrete Time Markov-Chain (DTMC)—with two states representing active and idle time—was implemented to model the obtained spectrum measurements for the three aforementioned bands. Notably, the measurements were characteristic of a large time scale in the order of seconds. DTMC models were unable to represent the statistical characteristics of most scanned bands, as these models diverged from their active and idle time distributions. In an effort to enhance these models, transition probabilities between the active and idle states were determined using instantaneous, time variant, DC models rather than total average DC values. In other words, a time-inhomogeneous, rather than time homogenous, DTMC was implemented. Models performed well for cellular bands DCS and E-GSM demonstrating a deterministic DC pattern. TETRA band models did not perform as well, given that this band is more heterogeneous in nature with random DC behavior. Even though performing ISM band measurement was mentioned, no modelling results were provided for this band. Also, time resolution for spectrum measurement activities performed in [21] is very low— in the order of second. As such, the provided measurements fail to capture short-scale timing behavior demonstrated by the MAC layer of the wireless communication technologies operating in the studied bands. Alternatively, the work performed in this dissertation provides a high resolution, extensive spectrum measurement survey for the 2.4GHz ISM band. A systematic experimental evaluation of the homogeneous and heterogeneous 802.11 networks spectrum activity at wide range of throughput values was performed and presented, providing a detailed description of DC, active time, and idle time distributions.

In [22], authors extended their work by performing empirical modelling for their obtained active and idle time distributions. The investigated models were Exponential, Generalized Exponential, Pareto, Generalized Pareto, Log-Normal, Gamma, and Weibull. Short time-scale measurements were performed using a USRP platform. Models were evaluated and presented for the following bands: amateur, paging, PMR/PAMR, cellular mobile communications, and cordless bands. Weibull distribution provided best models for amateur and PMR/PAMR bands. Paging and cellular mobile communication bands, idle-time distributions were best modeled using Pareto and generalized exponential distributions, respectively. However, no short time-scale analysis was performed for the 2.4GHz ISM band. ISM band analysis was only performed for single large-scale measurement result. Such analysis, as discussed previously, fails to represent temporal behavior of wireless technologies using the band which in turn is greatly dictated by the MAC layer implementation. In contrast to previous work, this dissertation provides a comprehensive experimental analysis of the 802.11 networks temporal behavior on the spectrum in the ISM band, including empirical modeling of obtained results. Empirical modeling is performed at a detailed level to capture appropriate distributions and their parameters that best model different 802.11 combinations at various throughput levels. Also, this work is performed at high time resolution for capturing the smallest 802.11 MAC layer time duration of 10μs. Such high time resolution was not implemented in previous work, leading to a deficiency in accurately describing temporal behavior of the 2.4GHz ISM bands.

Regarding previous work investigating the throughput-sensing problem, none of these studies presents a realistic measure of PU activity pattern, due to assumptions regarding

ON/OFF duration and frequency [27][28]. It is possible that modelling the ON/OFF duration with exponential or normal distribution might prove inaccurate, as these distributions change with protocol type, throughput, and number of nodes in the network. Experimental identification of a PU traffic pattern and temporal characteristics, including MAC protocol, can prove useful toward enhancing CT performance. Modelling of this traffic pattern can then be performed using supporting empirical results. Work presented in Chapter 5 of this dissertation aims at finding empirical time distribution of homogeneous and heterogeneous 802.11 networks in the ISM band. Chapter 6 presents a detailed empirical modelling of idle time distributions in an effort to provide a more accurate representation of these time distributions—beyond normal distribution assumptions made in previous literature.

Regarding adaptive frame size, most aforementioned studies focus on 802.11 networks. Also, many of these assume existence of a feedback mechanism from the receiver to the transmitter, which in fact might not exist. On the other hand, variable frame size for CTs with 802.11 using spectrum temporal pattern provides an opportunity to enhance CTs performance. CTs with 802.11 networks in the ISM band suffer great degradation in performance at 802.11 high throughput values (e.g., ZigBee). Temporal characterization of 802.11 DC and idle time distribution help CTs select a frame size to statistically minimize frame error rate (FER). For example, [31] presents a technique to change MPDU size based on the maximum tolerable FER. In that study, FER is estimated from Block ACK to implement the algorithm. A Bianchi analytical model was constructed to balance MPDU size based on FER to improve saturation throughput. The model assumes that contending nodes are using RTS/CTS mechanism to access the medium. However,

this assumption might not be realistic, as real networks are heterogeneous and may use different schemes. Likewise, RTS/CTS scheme is rarely used in real world implementation due to its low efficiency [49]. Results of the developed analytical model are depicted in

Figure 2-1. Increasing frame size at low FER value would always result in better throughput. On the contrary, at higher FER, optimal throughput is demonstrated by a particular frame size. Increasing frame size beyond that optimal value results in throughput degradation. Choosing optimal frame size relies heavily on the availability of a feedback mechanism to obtain an accurate FER estimation. Also, [49] developed an analytical model for optimizing saturation throughput only while assuming utilization of RTS/CTS mechanism by all contending transmitters. In comparison, work proposed in this dissertation uses an empirically found idle time distribution to adaptively regulate coexisting technology transmitter's frame sizes. An extensive experimental campaign is used to obtain and construct active and idle time distribution for 802.11 networks acting as an interferer degrading coexisting network performance. Such empirical distribution provides an accurate representation of medium availability state for both homogeneous and heterogeneous 802.11 networks. Another advantage of the work presented in this dissertation is that it does not require a feedback mechanism to obtain Packet Error Rate (PER) for implementing the adaptive packet size method. Rather, it directly uses statistical parameters of the obtained idle time distributions to regulate the transmitter's packet size. Nevertheless, PER is acquired and logged for this work to perform analysis on the obtained results. Idle time distributions themselves can be constructed by any radio interface measuring received signal strength (RSSI) by simple energy detection method,

as will be explained further in the following chapters. Adaptive packet size results provided in Chapter 8 of this dissertation show a similar trend when compared to

Figure 2-1. Packet size saturates at a specific level for very low spectrum occupancy, corresponding to low PER, and is limited by the implemented standard, ZigBee, maximum packet size. This maximum packet size provides highest throughput compared to smaller packet sizes. Nonetheless, smaller packet sizes demonstrate an improved throughput compared to larger ones at higher spectrum occupancy levels, corresponding to higher PER.

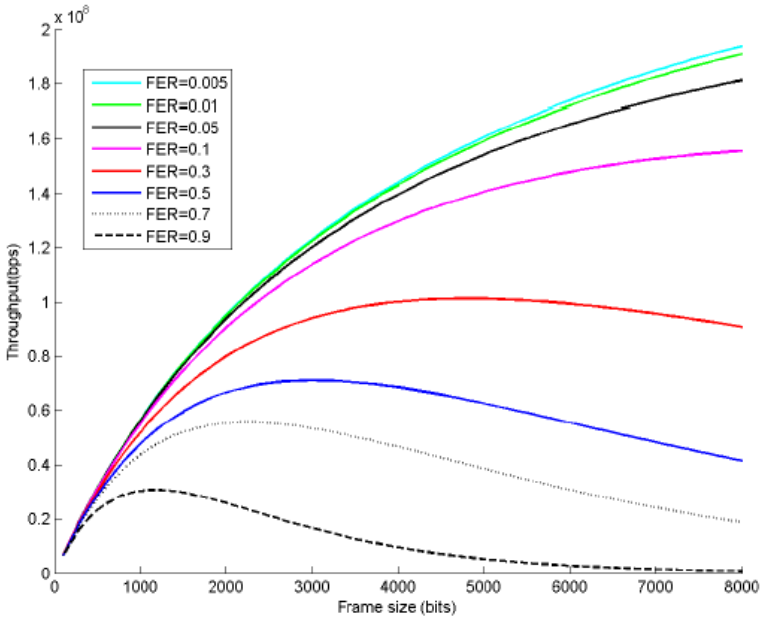

Figure 2-1. Saturation throughput vs. frame size for different FER values [31]

Finally, when considering wireless technology identification, work presented in this dissertation is unique in that it provides a simple, yet effective, time-based feature detection technique for wireless technology identification. A practical example of this

method is presented and validated in chapters that follow. Previous research presented in [47] is of most interest when compared to the work presented herein, as it relies on features extracted from spectrum power measurement to perform identification. Authors in [47] used simulation to identify MAC layer implementation for transmitters using the spectrum. Support Vector Machine (SVM) algorithm is used to perform the identification process. Two power features—received power mean and variance—and six time features, namely minimum, median and maximum idle time, and busy time durations, were used. Notably, time duration vary considerably in actual implementation based on throughput, number of transmitters using the spectrum, and the PHY and MAC layers implementation for these transmitters. As such, time durations obtained from simple MAC technique implementation, with the assumption of fixed active durations, would not accurately represent real world implementations. To calculate received power, implemented simulation assumes a simple Rayleigh fading channel. This assumption constitutes a simplification that does not represent real world environments with multi-path fading. The results show the possibility of performing MAC layers identification, Aloha, Slotted Aloha, CSMA/CA, and TDMA when using the aforementioned features and assuming a single technology is using the spectrum. Wireless technology identification work presented in this dissertation is based on extensive experimental results from 802.11 homogeneous and heterogeneous measurements at varying spectrum occupancy/throughout levels. A set of temporal features extracted from active and idle time distributions. Compared to previously discussed research, this dissertation presents and validates a wireless technology identification method, not only MAC layer implementation, but also using a comprehensive experimental campaign. Notably,

temporal-based features are used only to avoid uncertainty associated with power related features resulting from power fluctuations dependent upon the communication environment. Wireless technology identification, presented in Chapter 8, demonstrates identification accuracies of 96.9% and 85.9% were achieved for homogeneous and heterogeneous 802.11 networks, respectively. Also, number of transmitter identification was investigated with satisfactory result. Details of the conducted study are offered in Chapter 8.

2.4 GHz ISM band spectrum overview

The ISM band, spanning over 80 MHz from 2.4 GHz to 2.48 GHz, is the home for many popular wireless technologies (e.g., Wi-Fi 802.11b/g/n, ZigBee, Bluetooth, Bluetooth Low Energy (BLE), and others). These technologies share the same spectrum with overlapping frequency channels. See Figure 2-2 for a visual approximation of frequency channels belonging to different ISM band technologies.

802.11Wi-Fi has the widest frequency channel size—22 MHz, with 11 overlapping channels, of which 1, 6, and 11 are non-overlapping. 802.15.4 ZigBee has a more limited frequency channel width of 2 MHz with frequency span of 5 MHz between center frequencies of adjacent channels. 802.15.4 ZigBee has 16 non-overlapping in the ISM band. Classic Bluetooth, on the other hand, uses a frequency hopping spread spectrum access with 79 non-overlapping, 1 MHz channels. Finally, Bluetooth Low Energy (BLE) has 40 channels, each 2 MHz wide.

802.11 networks, and to some extent 802.15.4 ZigBee, are under investigation in this work. Consequently, more details on the MAC and physical layers of 802.11b/g/n and

802.15.4 ZigBee are provided in the following subsections. A thorough understanding of these standards will aid in interpreting results in following chapters.

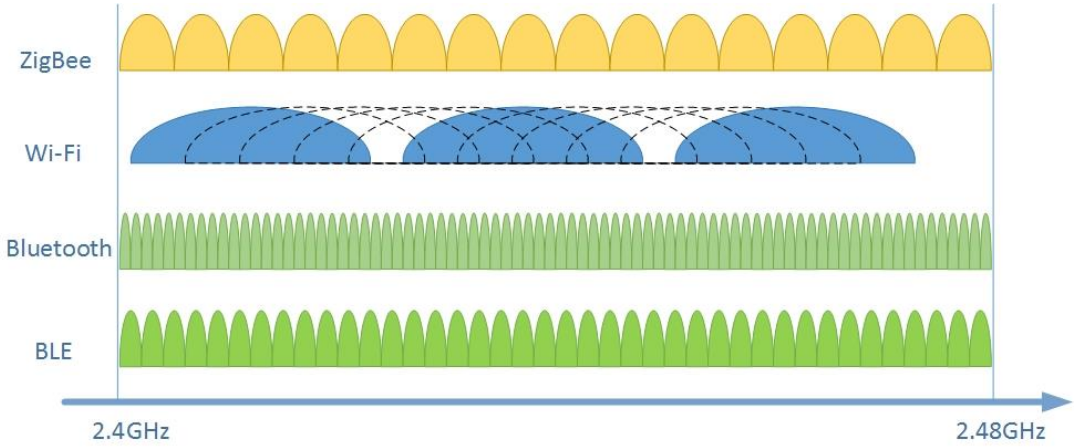

Figure 2-2. 2.4GHz ISM band frequency channels.

802.11b

802.11b was published in 1999 as an amendment to the original 802.11 standard [50]. The standard supports data rates of up to 11Mbps. This subsection provides information on 802.11b Physical (PHY) and Medium Access Control (MAC) layers. Both have a direct effect on spectrum temporal characteristics of transceivers implementing the standard.

Distributed coordination function (DCF)

IEEE 802.11b implements Distributed Coordination Function (DCF) as its MAC technique for which a transmitter follows carrier sense multiple access/collision avoidance (CSMA/CA) scheme. CSMA/CA uses a technique known as Clear Channel Assessment (CCA) to ensure that the medium is vacant prior to performing a frame transmission. The purpose of this procedure is avoiding collisions with other transmitters.

Figure 2-3 illustrates functionality of DCF. A transmitter with a frame in its queue choses a random back-off value from a specific minimum contention window and continuously

senses the medium until it becomes idle. If the medium is occupied, transmitter freezes its back-off counter. Once the medium becomes idle, transmitter starts decrementing its back-off counter. This process is repeated until the back-off counter expires (i.e., reaches a value of 0.) The transmitter then proceeds with frame transmission. Receiver replies with an Acknowledgment (ACK) after short inter-frame spacing (SIFS) waiting time, provided the frame was received correctly. Other transmitters should wait for distributed inter-frame spacing (DIFS) waiting time after transmission ends before continuing to decrement their back-off counters. If two transmitting nodes choose the same back-off value at the same time, a collision will occur, and packet transmission will be rendered unsuccessful. Colliding nodes will then move to a higher back-off stage wherein back-off window is binary exponentially larger. Details of 802.11b MAC timing parameters can be found in Table **1**.

Notably, a transmitter using DCF will hold off frame transmission until its back-off counter expires even if the medium remains idle during the entire process. This behavior results in a low temporal efficiency whenever a single transmitter is attempting to access the medium. Nevertheless, DCF provides a better chance of coexistence (between 802.11 transmitters strictly) when a large number of these transmitters are using the medium at the same time.

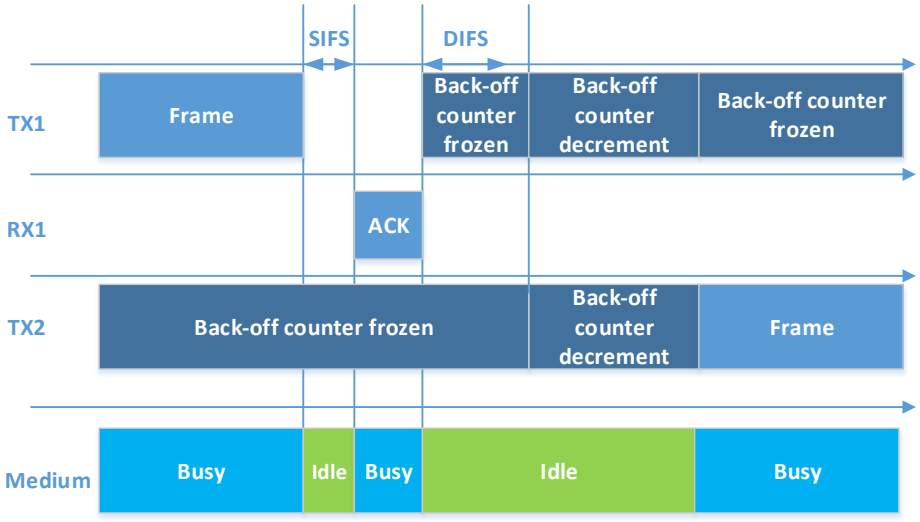

Figure 2-3. DCF functionality

Two CCA modes are generally used in wide band networks (e.g., 802.11 and 802.15.4 ZigBee) [51][52]:

1. Non-coherent carrier sensing: This method uses a fixed CCA power threshold to detect spectrum occupancy. It is fast and low power, but prone to errors.
2. Coherent carrier sensing (preamble detection): This method demodulates the signal and detects the preamble before backing off. It is slower and consumes more power, but less prone to errors.

Commercially available 802.11 chipsets commonly implement coherent carrier sensing to take advantage of its robustness. 802.15.4 ZigBee chipsets implement a non-coherent carrier sensing method to conserve energy. Narrow band networks use energy detection only.

Table 1. 802.11b timing parameters

Parameter	***Value***
SIFS	10 μs
DIFS	50 μs
ACK	202 μs
MPDU size	1500 Byte
frame duration	1220 μs

Complimentary Code Keying (CCK)

802.11b PHY layer supports data rates of 1, 2, 5.5 and 11Mbps. The higher data rates of 5.5 and 11Mbps, which are of interest in this work, use CCK modulation wherein data ready for transmission is grouped in 8-bits sequences. Each sequence is then used to find an 8-chips spreading code. Spreading codes are modulated using Differential Quadrature Phase Shift Keying (DQPSK) and sent over the air at a rate of 11Mchip/s. An 11Mbps data rate is then achieved, given that an 8-bits sequence was used to find the 8-chip symbols [53][54].

CCK modulation works by using the aforementioned 8-bits data sequence to choose one of 64 orthogonal code words. The 8-bits sequence is divided into 2-bits pairs known as dibits (d0, d1, d2, d3), where d0 represents the two least-significant bits. These dibits are then used to find phase parameters φ1 to φ4, as specified in Table 2.

Table 2. CCK phase parameters

Dibit	***Phase parameter***
00	0
01	π/2
10	π
11	3π/2

The phase parameters are then substituted in (1) to find the code word to be transmitted. CCK functionality is depicted in Figure 2-4.

$$c = \left\{ \begin{matrix} e^{j(\varphi_1+\varphi_2+\varphi_3+\varphi_4)}, e^{j(\varphi_1+\varphi_3+\varphi_4)}, e^{j(\varphi_1+\varphi_2+\varphi_4)}, \\ -e^{j(\varphi_1+\varphi_4)}, e^{j(\varphi_1+\varphi_2+\varphi_3)}, e^{j(\varphi_1+\varphi_3)}, -e^{j(\varphi_1+\varphi_2)}, e^{j(\varphi_1)} \end{matrix} \right\} \quad (1)$$

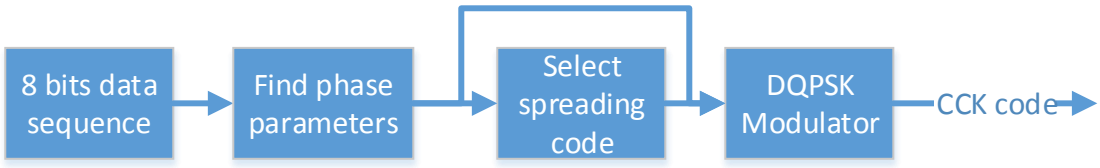

Figure 2-4. CCK functionality

802.11g

802.11g standard was published in 2003 [55]. The primary difference between 802.11b and g resides in the PHY layer. 802.11g supports peak data rate of up to 54Mbps with Orthogonal frequency-division multiplexing (OFDM) and 64-QAM modulation. Similar to its 802.11b predecessor, 802.11g implements DCF for its MAC layer with few differences in timing parameters. Nevertheless, the temporal efficiency effect of DCF is more pronounced in 802.11g, resulting in average data rates much lower than the standard's peak data rate. This behavior results from the shorter frame duration of 802.11g, compared to 802.11b due to its higher data rate. Temporal efficiency of the various standards is discussed in greater details in the following chapters.

Table 3. 802.11g timing parameters

Parameter	Value
SIFS	10 µs
DIFS	28µs
ACK	30 µs
MPDU size	1500 Byte
Frame duration	253 µs

Orthogonal Frequency Division Multiplexing (OFDM)

OFDM works by modulating data into multiple narrowband adjacent subcarriers, which are orthogonal in nature. Consequently, sidebands of each subcarrier has limited interference effect on the other subcarrier. OFDM is characterized by its immunity to frequency selective fading, as the channel is divided into narrowband subcarriers that are affected individually[56].

In 802.11g, the 20MHz channel is divided into 52 subcarriers with 312.5 KHz carrier spacing. Four subcarriers are used as pilot carriers while the remaining 48 are used as data subcarriers. Data subcarriers are then modulated using 64-Quadrature Amplitude Modulation (64-QAM) modulation resulting in peak data rate of 54 Mbps when using a single spatial stream. OFDM functionality is depicted in Figure 2-5 [57]. The scrambler is used to randomize bit streams to eliminate long strings of '1' and '0'. Such long sequences negatively affect time synchronization at the receiver. The sequences also prevent power concentration in a particular narrow frequency band. Convolutional encoding is a type of error-correcting code used in the scheme. Inverse Fast Fourier Transform (IFFT) is intended to distribute data into different subcarriers. Finally, 64-QAM is a used as a digital modulation scheme.

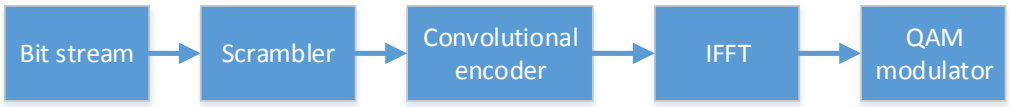

Figure 2-5. OFDM functionality

802.11n

802.11n was introduced in 2009 and enabled data rates of up to 600Mbps [58]. The standard implements several enhancements in both PHY and MAC layer. PHY layer enhancements include beamforming, channel aggregation, and Multi-Input Multi-Output (MIMO) data streams. Beamforming provides the transmitter with the capability of tracking a particular receiver by changing the radiated beam shape, thus taking advantage of multiple transmitter antennas. This functionality is limited by radio interface capabilities, number of antennas, and 802.11n radio chip. Most of today's common 802.11n transmitters lack the latter functionality with number of antennas limited to two for a transceiver.

Channel aggregation allows the choice of either 20 MHz or 40 MHz channel. A channel of 20MHz is generally chosen in the 2.4 GHz ISM band due to its limited bandwidth of 80 MHz. MIMO allows for up to 4X4 antennas on the transmitter and receiver sides, enabling higher data rates.

802.11n uses DCF as its MAC layer protocol. Nevertheless, the standard introduces frame aggregation as MAC layer enhancements. This functionality leads to the foremost effects on spectrum temporal characteristics.

For testing reported in this work, A-MPDU was used for 802.11n. This enabled a peak data rate of 65Mbps for a single spatial stream and 64-QAM modulation type. See Table 4 for 802.11n timing parameters in the 2.4 GHz ISM band.

Table 4. 802.11n timing parameters.

Parameter	Value
SIFS	10 μs
DIFS	28μs
RIFS	2 μs
Block ACK	36 μs
MPDU size	1500 Byte
Frame duration	Variable depending on A-MPDU size (189 μs – 8.9ms)

Frame aggregation

Frame aggregation is introduced in 802.11n, wherein multiple sub-frames can be aggregated into one large aggregated frame [59]. The result is a considerable improvement in temporal efficiency when compared to earlier standards. However, frame aggregation increases the likelihood of interference with other non-802.11 CTs. Also, 802.11-b and -g terminals sharing the medium could suffer from performance degradation resulting from extended 802.11n spectrum occupancy.

Two types of aggregation schemes are defined in 802.11n: 1) aggregated MAC service data unit (A-MSDU) and 2) aggregated MAC protocol data unit (A-MPDU). A-MSDU works by aggregating several MSDUs with a single MAC header, a PHY header, and frame check sequence (FCS). See Figure 2-6.

A-MPDU is formed from multiple MPDUs, each having its own MAC header and FCS. Each sub-frame has its own FCS and can be retransmitted independently. See Figure 2-7. A-MSDU is more efficient, as it is characterized with a lower header-to-payload ratio. However, it is also more prone to erroneous environments. 802.11n introduces block ACK,

as well, wherein each sub-frame can be acknowledged individually. This allows independent retransmission of corrupted frames.

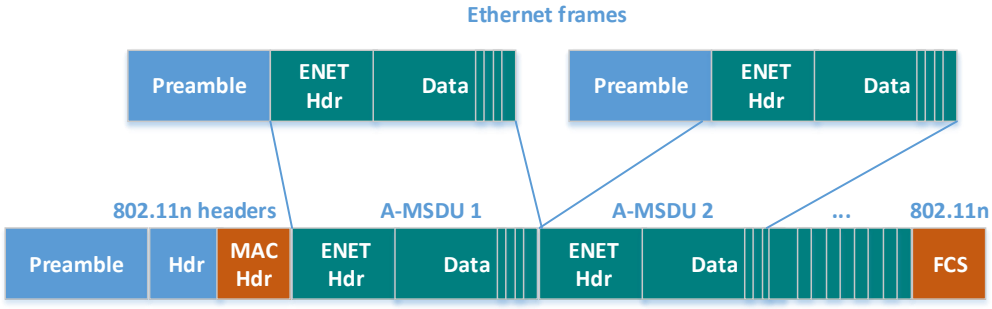

Figure 2-6. Aggregated MAC service data unit

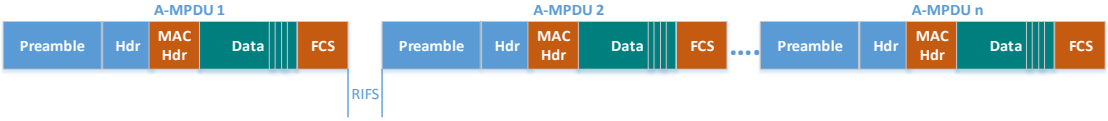

Figure 2-7. Aggregated MAC protocol data unit

802.15.4 ZigBee

802.15.4 ZigBee is designed as a low power, low data rate technology, making it suitable for wireless sensor network (WSN) and wireless medical devices applications [60]. The standard supports a data rate of 250 kbps in the ISM band by implementing Direct-Sequence Spread Spectrum (DSSS) coding and Orthogonal Quadrature Phase-Shift Keying (OQPSK) digital modulation. ZigBee technology has a maximum packet size of 127 bytes, including header, and uses a CSMA/CA for regulating medium access while operating in ad hoc mode [61].

A simulation using 802.11g/n and 802.15.4 heterogeneous networks MAC layer was developed in Matlab. The simulation was intended to validate experimental results presented herein. The setup supported multiple nodes so that each node can be configured with its own 802.11 or 802.15.4 standard, frame size, and number of aggregated frames.

The same simulation was used for a ZigBee adaptive packet size case study, which is presented later in this dissertation.

Chapter3: Experimental and Simulation Setup

This chapter provides a detailed description of both experimental and simulation setups implemented in this work. For the experimental setup, 802.11 networks, including their equipment and setup, are first described. Second, measurement equipment and their tasks are presented. Finally, a description of algorithms implemented to analyze collected data is provided. For computer simulation setup, simulation approach and parameters are described for both 802.11 and 802.15.4 networks.

Experimental setup

The spectrum temporal characterization, empirical modelling and wireless technology identification work presented in this dissertation was performed using a proper experiments campaign that implemented an energy detection technique. This method can be easily applied to any radio interface measuring received signal strength (RSS) values. Power measurements were first performed on 802.11 networks using external measurement devices. Detected signal was then processed to extract DC values and temporal distributions. Next, this data was used to perform empirical modelling of 802.11 idle time distributions. Extracted distributions were also used in wireless technology identification using machine-learning methods. The following subsections detail network and measurement equipment and their layout.

Networks under test

The experimental setup utilized one-, two-, or three-pair 802.11 networks, each with an access point acting as a transmitter (TX) and a station acting as a receiver (RX) positioned

at a prefixed separation distance of one meter. Equipment was deployed on wooden tables at an elevation of one meter. See Figure 3-1.

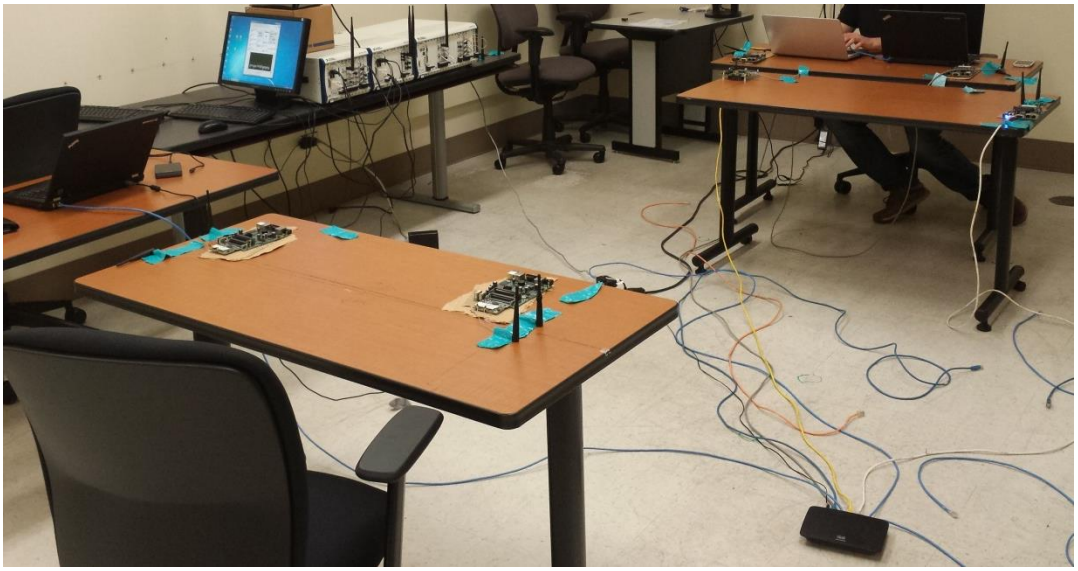

Figure 3-1. Example of 802.11 test setup

Tests were conducted at the University of Oklahoma-Tulsa Wireless and Electromagnetic Compliance and Designer (WECAD) center. 802.11 nodes were Mikrotik router boards 433UAH [62] that were interfaced with a "R52Hn" miniPCI network adapter supporting 802.11b/g/n networks using Atheros chipsets. See Figure 3-2.

Figure 3-2. Mikrotik 802.11 router boards and miniPCI network adapters

802.11 networks were each configured to operate using the standards under investigation (i.e., 802.11b, 802.11g, and 802.11n). 802.11 transmitters operated using a Unix-based

operating system with a graphical user interface capable of controlling all of the 802.11 chip functionalities. The operating system included test software that was used for generating traffic at a particular throughput [63]. Requested throughput values were incremented for consecutive tests, starting from low throughput to saturation. Throughput increment values were varied based on the 802.11 standard used, number of pairs, and the standards combination under test.

A one-pair 802.11 network was used for first testing stage. Another pair was added to second testing stage, and a third pair was included for third testing stage. All pairs were configured to use the same 802.11 standard for each homogeneous networks test. The following combinations were used for both 2-pair and 3-pair heterogeneous tests: 1) 802.11_b-g, b-n, and g-n; and 2) 802.11_b-b-g, b-b-n, b-g-g, g-g-n, b-g-n, b-n-n, and g-n-n. Achieved throughput values and other 802.11 configuration parameters were logged for each test.

Terminals were set to maintain a transmit power of 16dBm for homogeneous networks tests. Such transmission power proved to be high, as 802.11 receiver RF front end might be saturated and cause instability in the recorded throughput. Consequently, some of the homogeneous network tests were repeated until stable throughput was achieved to ensure consistent output. To avoid this problem in heterogeneous networks tests, transmission power was dropped to 8dBm. This transmission power still ensures a signal to noise ratio (SNR) high enough for distances considered in the test setup, making noise effect negligible.

Measurement setup

Two NI Vector Signal Analyzers (VSAs) were configured to collect time and frequency domain measurements [64]. The used devices are VSA are PXIe-5644R and PXIe-5663 for time domain and frequency domain measurements, respectively. Both devices were running NI LabVIEW software. For frequency domain measurements, a channel width of BW=20MHz and resolution bandwidth of RBW=400 kHz was used. Notably, frequency domain measurements were used merely for DC comparison and validation of the time domain measurements.

For time domain measurements, the VSA's local oscillator was pre-tuned to the center frequency of channel in use. The selected I/Q rate determine the sampling rate for this channel. A 10MS/s rate was used for measurement, and a moving average—served as a low pass filter—was implemented to smooth instantaneous power values. Note that the smallest time parameter defined in all 802.11b, g and n standards MAC layers is the Short Inter-Frame Spacing (SIFS). SIFS for 802.11b, g and n in the 2.4 GHz ISM band is 10μs. Assuming a sampling rate four times the Nyquist rate of (2*f), f being the highest frequency component in the message signal, a sampling rate of 0.8 MS/s should suffice for providing a satisfactory representation of the sampled signal. Time domain measurements were used for all analysis and modelling work presented in this dissertation.

VSAs were used to perform spectrum activity measurements of 802.11 networks using energy detection method. Two VSAs were deployed adjacent to one another at a prefixed distance from 802.11 transmitters. Distance between 802.11 transmitters and VSAs was

calibrated so that average power received from all transmitters was equal. Figure 3-3 shows a graphical representation of the test setup, including separation distances.

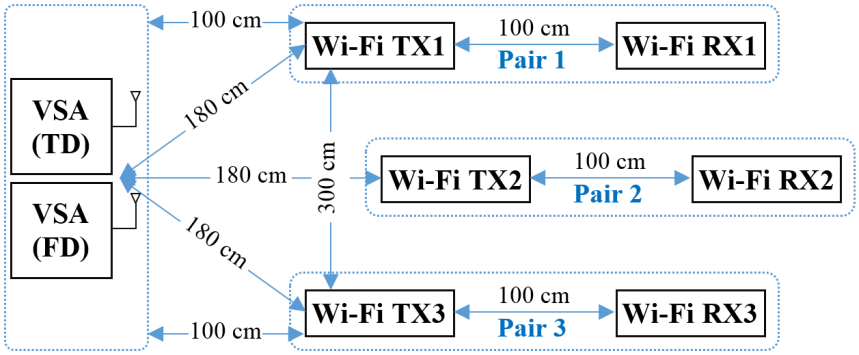

Figure 3-3. Graphical representation of test setup with separation dimensions

Energy detection algorithms

Two different measurement methods were employed in this research: time domain (TD) and frequency domain (FD) [65]. In TD measurement, received power values from a specific frequency band were recorded continuously at a predetermined sampling rate. VSA swept a set of frequencies, collecting and storing received power values in FD measurements.

Time domain algorithm

Time domain measurements were conducted at two phases. In phase 1, a VSA was tuned to the center frequency of the 802.11 channel under use (e.g., channel 6, 2.437GHz). Amplitude values were streamed as data file-to-disk during testing at a sampling rate of 10MS/s. In phase 2, a time domain algorithm processed collected data to extract DC values, active time distributions, and idle time distributions.

The algorithm commences by extracting the power threshold separating channel active and idle times. Next, the program analyzes the entire recording and compares power

averages with the found threshold. Power values above the threshold are assigned a ‘1’, representing activity; power values below the threshold are assigned a ‘0’, representing an inactive channel. Strings of consecutive ‘1’s and ‘0’s are then used to build active and idle time distributions. These strings are also used test data to determine duty cycle.

The time domain analysis algorithm process is depicted in Figure 3-4. The following provides a step-by-step description of the algorithm’s process:

1) Calculate the instantaneous power values.

2) Smooth the signal, using a moving average algorithm that serves as a low pass filter.

3) Calculate the power signal threshold by i) determining the power histogram for a set of the data recordings, ii) fitting a Gaussian distribution to the lowest power hill in the histogram, and iii) setting the threshold to five standard deviations from the peak of the lowest power hill to ensure ample separation between 802.11 signal and noise floor [66].

4) Analyze entire data recording by comparing calculated power averages to calculated threshold (i.e., ‘1’ represents channel activity and is assigned if the average power value is above the threshold; ‘0’ represents channel idle state and is assigned in case average power values is below the threshold). As such, data recording is converted to ‘1’s and ‘0’s, representing active and idle periods.

6) Calculate consecutive active and idle time durations.

5) Calculate and save DC value.

TD measurement Algorithm

Input: *frequency channel, sampling rate*
Output: *Duty-cycle, Activity and Idle time distributions*
Initialization:
1: *frequency = 2.437GHz*
2: *IQ rate = 10MS/s*
3: *Set number of samples to be read*

do:
1: Stream IQ data to disk
2: Calculate *Power-value for all IQ data*
3: Smooth signal using LPF
4: Find power histogram
5: Fit lowest peak in power histogram to Gaussian
6: Set *Threshold* = 5*Gaussian standard deviation
7: for each *Power-value*
    if *Power-value* >= *Threshold*
        Activity-state(*State-number*) = 1
    else *Activity-state*(*State-number*) = 0
    end if
    State-number=+1
  end for
8: Histogram active and idle durations
9: *Duty-cycle = Activity-state/ State-number*

Figure 3-4. Time domain (TD) algorithm pseudo-code.

Frequency domain algorithm

For frequency domain measurements, VSA first scans the medium and measures the noise floor. A threshold value at least 5dB above the noise floor is set. VSA then samples 802.11 frequency channel. Average power value is constantly compared with the reference threshold. Given that average power value is above threshold, an activity state '1' is logged, meaning the channel is occupied/utilized for this particular sample. Conversely, if average power value is below threshold, logging a '0' indicates an idle time state. Duty cycle indicates the level of channel utilization and is calculated by taking the number of '1's over the total number of logged '0s' and '1's (e.g., DC = ['1s' / ('1s' + '0s')]) for both time and frequency domain measurements [65]. Frequency domain measurements aim solely at validating time domain duty cycle readings.

Frequency domain DC measurements were conducted in real-time. The algorithm process included the following steps:

1) Set a VSA to sweep the 802.11 frequency channel bandwidth (e.g., 22MHz) under test (e.g., channel 6).

2) Scan the medium and calculate the noise-floor peak power value.

3) Set the threshold value at least 5dB above the noise-floor to minimize false detection and to distinguish signal from noise.

4) Run the VSA to sweep the selected 802.11 frequency channel.

5) Compare each power value in every sweep with the reference threshold.

6) Calculate DC, indicating the level of channel utilization in frequency domain [65] by calculating the number of '1s' over the total number of combined '0s' and '1s'.

7) Use cumulative moving average to assimilate DC values calculated in each sweep.

Figure 3-5 illustrates a pseudo-code of the used frequency domain algorithm.

FD measurements Algorithm

Input: *Spectrum, Bandwidth, Channel-Band, Bin-Size*
Output: *Duty-cycle*
Initialization:
1: *Spectrum*=2.40~2.48GHz; *Bandwidth*=80MHz;
Bin-Size = 100KHz; *Channel-Band* = 22MHz
2: Read *Power Spectrum*
3: CALC/Set *Threshold* value

Duty-Cycle:
1: Read *Power Spectrum*
2: **for** each *Power-value* in a *Channel-Band* **do**
if *Power-value* >= *Threshold* **then**
Activity-States = +1
end if
States-Number = +1
end for
3: *Duty-cycle* = *Activity-States* / *States-Number*
4: **do** *Moving Average Duty-cycle*

Figure 3-5. Frequency domain algorithm pseudo-code.

Test methodology

The following steps describe the testing protocol implemented to collect aforementioned measurements of 802.11 networks:

- A pre-scan for the medium was conducted prior to testing to ensure no interference from adjacent buildings in the ISM band and to measure noise floor. Noise floor was measured less than -105dBm. An example of measured noise floor is depicted in Figure 3-6.
- 802.11 network terminals were configured on the standard under study (802.11b, 802.11g and 802.11n), and 802.11 channel 6 was chosen as transmit channel.
- Starting from low throughput to saturation, pre-defined throughput values were incremented in steps for consecutive tests. The increment step was defined based on the 802.11 protocol under test. Figure 3-7 and Figure 3-8 depict examples of spectrograms for 802.11g 25Mbps and 5Mbps throughputs, respectively. These figures illustrate the effect of high throughput vs. low throughput on the spectrum occupancy at a high level. As expected, higher throughput leads to higher detected power levels for longer times on the spectrum. This results in higher measured DC values. A detailed analysis investigating DC levels corresponding to various 802.11 networks and varying throughput levels is presented in the following chapters.

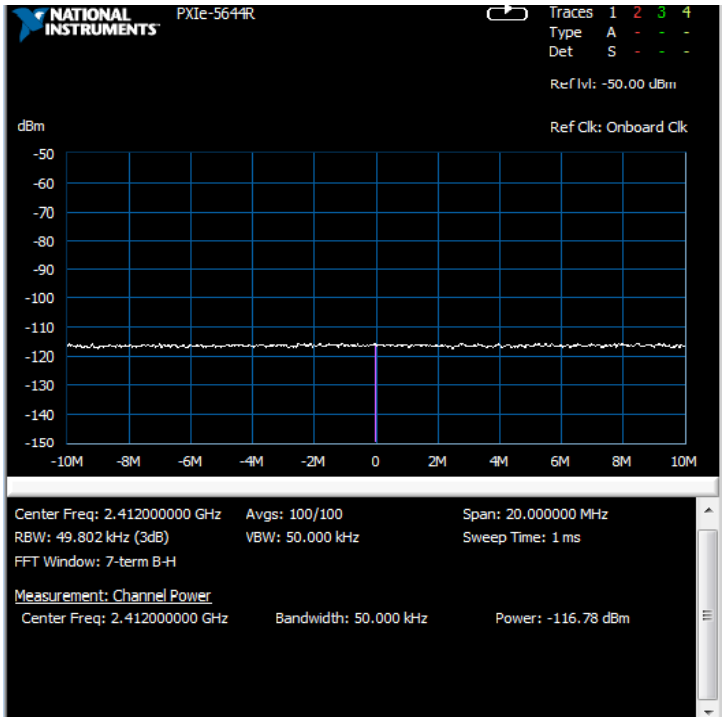

Figure 3-6. Noise floor lab measurement.

- Achieved throughput values and other 802.11 configuration parameters were logged for each test.
- Two NI VSAs were configured to collect and log time-domain and frequency-domain measurements, as described in previous sections.

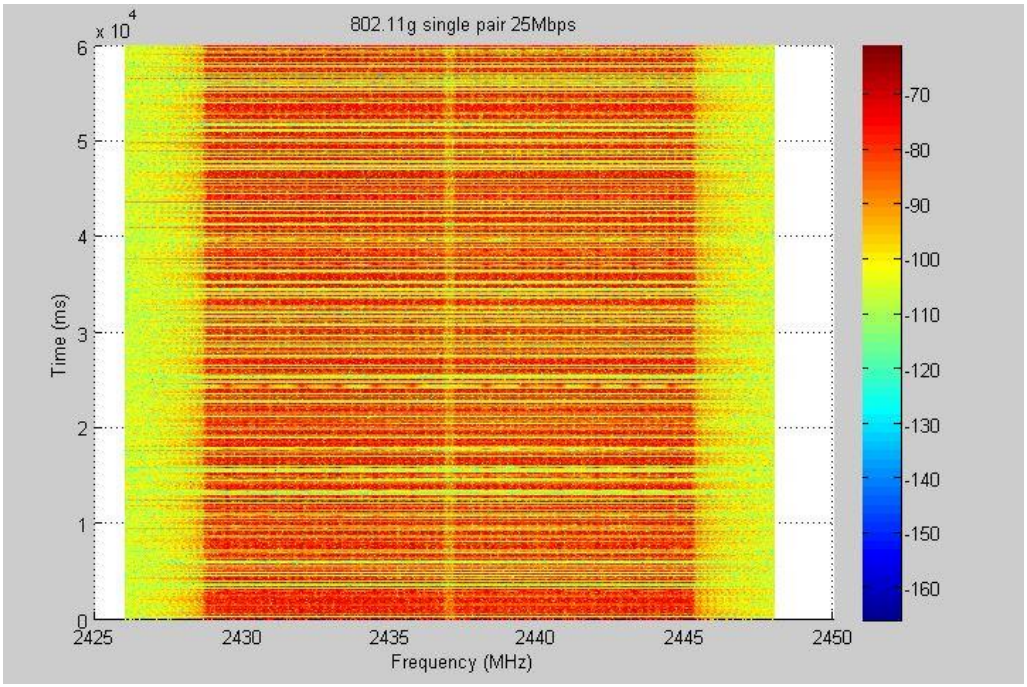

Figure 3-7. Spectrogram for 802.11g at 25Mbps.

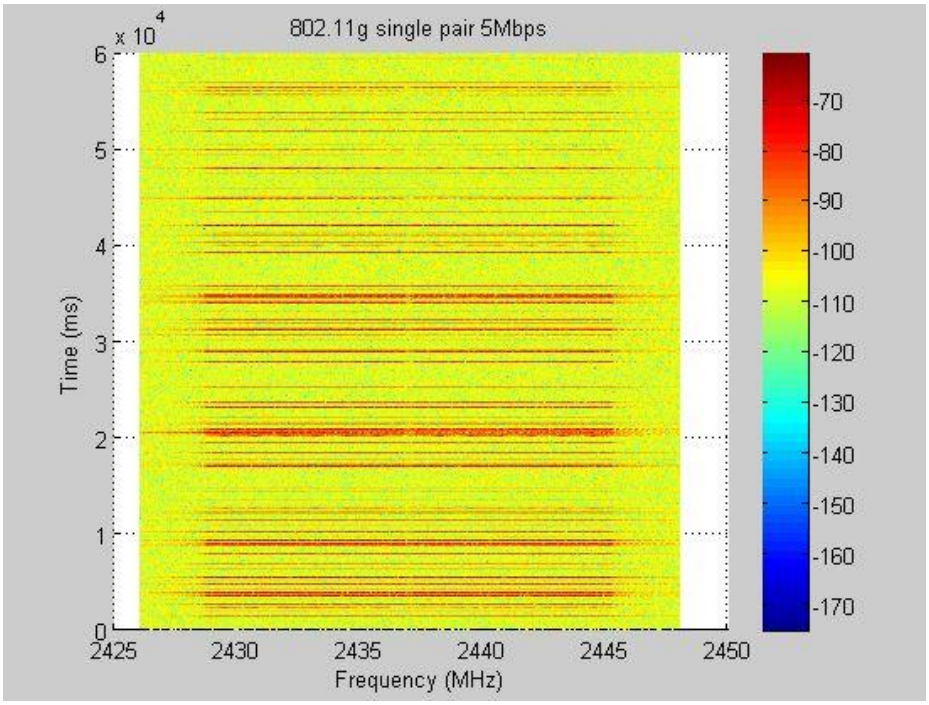

Figure 3-8. Spectrogram for 802.11g at 5Mbps.

Simulation setup

MATLAB simulation was developed for both 802.11g and 802.15.4 ZigBee MAC layer transmission. The purpose of these simulations is threefold:

1) Comparing simulation and experimental measurements achieved DC and inactivity distributions for 802.11g networks, as well as highlighting some behavior of large 802.11 networks that might be difficult to investigate through experimental effort.
2) Creating an interfering medium to test for 802.15.4 ZigBee packet error rate (PER) variation based on 802.11g traffic, highlighting sever effect of 802.11 networks on CTs in the ISM band.
3) Assessing 802.15.4 ZigBee throughput enhancement when implementing variable frame size based on 802.11g idle time distributions, which demonstrates possible enhancements to CTs performance that might be obtained by 802.11 temporal characterization.

802.11g simulation

Simulation implements the 802.11 MAC layer, DCF (Distributed Coordination Function), in a MATLAB® environment and defines multiple 802.11g nodes that can contend over the medium. A node can be either saturated or Poisson. A saturated node has a full frame queue at all times, as the name implies. In a Poisson node, frames arrive to the transmission queue following a Poisson distribution with average arrival rate of λ. Varying λ results in variable achieved throughput values. The following parameters can be controlled in the

developed simulation: number of transmitters, frame size, minimum contention window, number of back-off stages, and average arrival rate.

According to current configuration, simulation provides total network throughput, channel utilization, idle distribution, probability of collision, per transmitter back-off value, and per transmitter back-off stages. Comparing simulation and experimental results is beneficial for validating both approaches.

The following steps describe the 802.11g simulation process:

- Number of nodes and their types are selected (e.g., Poisson, saturated), and the simulation parameters are chosen (e.g., arrival rates for Poisson nodes, contention windows sizes).
- Simulation duration, including warm-up duration, is chosen.
- The simulation commences. 802.11 measurements are not logged during the warm-up period.
- A node with a packet in its queue attempts to access the medium using DCF functionality, described in Chapter 2, with the following three results:
    - Successfully access the medium and perform transmission after waiting for randomly selected back-off time and Distributed Inter Frame Spacing (DIFS) value. 802.11g first back-off stage consists of 16 values ranging from 0 to 15 time slots, where each time slot is 9μs. A transmitting node will wait for a DIFS value after an end-of-transmission prior to choosing a random back-off value, where DIFS value is 28μs.
    - If the medium becomes occupied with other 802.11 transmissions during the back-off period, the 802.11 transmitter waits for those to finish.

- If two transmitting nodes choose the same back-off value, a collision will occur and packet transmission is rendered unsuccessful. Colliding nodes will jump to a higher back-off stage for which the back-off window is exponentially larger.

- The following data is logged for the post warm-up simulation duration, based on the 802.11g transmission:
  - Achieved throughput, which might be different from requested throughput due to possible medium congestion and collisions, based on the number of simulated nodes.
  - Duty cycle.
  - Active and idle time distributions.
  - Medium occupancy durations, which are an array of durations at which the medium was occupied with 802.11g transmission for later use in the 802.15.4 ZigBee simulation.

Table 5 provides timing parameters used in 802.11g simulation.

Table 5. 802.11g simulation parameters values

Parameter	***Value***
SIFS	10 µs
DIFS	28 µs
Minimum contention window	0 – 144 µs
ACK	30 µs
802.11 MPDU size	1500 Byte

The following equations provide parameters contributing to calculated simulation timing output. Note that timing outputs apply for both 802.11g and 802.15.4 simulations:

- Transmission time = PHY header + MAC header + packet payload + SIFS + 2*propagation delay + ACK + DIFS
- Channel utilization time during Tx = PHY header + MAC header + packet payload + ACK
- Collision time = PHY header + MAC header + packet payload + DIFS + propagation delay
- Channel utilization time during collision = PHY header + MAC header + packet payload

802.15.4 ZigBee simulation

802.15.4 ZigBee simulation implements 802.15.4 ZigBee MAC mechanism. ZigBee uses DCF for distributed medium access with several variations from 802.11. To save energy, ZigBee transmitter does not perform carrier sensing while decrementing its back-off counter. Thus, it does not freeze the back-off counter in the event of a busy medium. Rather, back-off counter is decremented until it reaches the penultimate back-off slot where carrier is sensed for the last two time slots. In the event of occupied medium, transmission is deferred and ZigBee terminal jumps to a higher back-off stage. In this simulation a node can either have frame arrival resulting in a saturated queue or Poisson-distributed frame arrival with average arrival rate of λ. Note that ZigBee has data rate of 250Kbps and time slot duration of 320μs.

Notably, 802.11 nodes perform coherent clear channel assessment wherein they back off only to other 802.11 transmitters. 802.15.4 ZigBee nodes perform non-coherent clear channel assessment wherein they perform back off merely based on the Received Signal

Strength (RSS) value. The purpose of this behavior is to conserve energy. Both coherent and non-coherent clear channel assessment methods are described in Chapter 2.

Developed simulation assesses 802.15.4 ZigBee coexistence in the presence of interfering transmission on the same frequency channel (e.g. 802.11 transmissions). The simulation utilizes medium occupancy information, which can be obtained from 802.11g simulation to determine 802.15.4 ZigBee throughput and probability of collision. It is assumed that 802.11g is using coherent carrier sensing and, thus, does not back off for ZigBee transmission [67]. Also, any collision between ZigBee and 802.11g transmission results in a corrupted ZigBee packet.

The following parameters can be controlled in the developed simulation:

- Number of transmitters.
- Minimum contention window.
- Number of back-off stages.
- Packet size.
- Frame arrival rate.
- Medium occupancy durations.

Simulation output includes total network throughput, channel utilization, and packet error rate. Simulation provides several other parameters unrelated to this work, thus, are not described.

Chapter 4: Spectrum Characterization – 802.11 Throughput and Duty Cycle

This chapter presents experimental spectrum occupancy results obtained in this research, including DC and throughput for single-pair and multi-pair homogeneous and heterogeneous 802.11 networks [68][69]. Experimental and simulation results are compared, and then presented in an effort to provide a more detailed analysis of DC results and to extrapolate for a higher number of communicating 802.11 terminals. DC measurements are validated by comparing time-domain and frequency-domain spectrum occupancy results.

Homogeneous networks DC

Each of the three standards was assessed individually for a single-pair network. In this configuration, an access point acts as a transmitter by sending UDP data at multiple throughput values to a station that acts as a receiver.

Throughput and duty cycle results for one-pair networks

DC results per throughput for single-pair 802.11b, g, and n networks are shown in Figure 4-1.

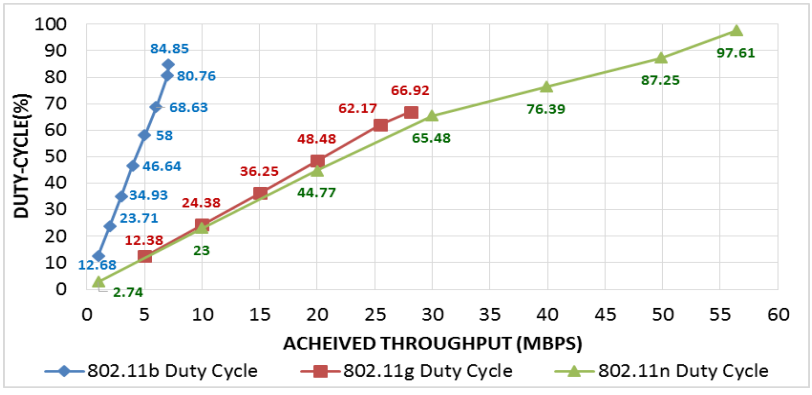

Figure 4-1. 802.11b/g/n single-pair DC vs. throughput.

802.11g achieved maximum DC of 67.29% at throughput of 28.1 Mbps. The relatively low DC observed for 802.11g results from overhead imposed by DCF standard. In this scenario, the transmitter must perform a back-off at each single-data frame transmission.

802.11b achieves a higher maximum DC of 84.95%, at throughput of 7.1 Mbps. Although both 802.11 b and g have similar back-off functionality, 802.11b transmits at the lower data rate of 11Mbps, which results in a longer frame duration. Consequently, 802.11b records higher DC for a much lower throughput.

802.11n achieves the highest DC of 97.97% with throughput reaching 56.4 Mbps. High DC demonstrated by 802.11n is a direct result of the frame aggregation mechanism implemented in the standard, rendering it an extremely time-efficient technology.

Throughput and duty cycle results for two-pairs networks

Spectrum occupancy for multiple pairs was investigated next. Figure 4-2 and Figure 4-3 depict throughput and DC for two-pair 802.11b. Test number labeling used in this chapter refers to the standard being investigated, as well as the throughput value (e.g., G05N10 refers to two pairs: 802.11g with set throughput value of 5Mbit/s and 802.11n with set throughput value of 10Mbit/s). Figure 4-2 shows that achieved throughput is divided equally among contending pairs when offered traffic for both pairs reaches saturation point.

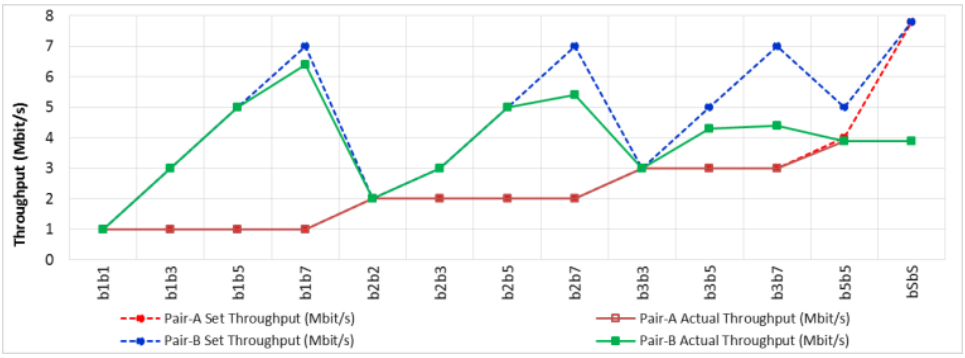

Figure 4-2. Set throughput vs. achieved throughput for 802.11b two-pair network.

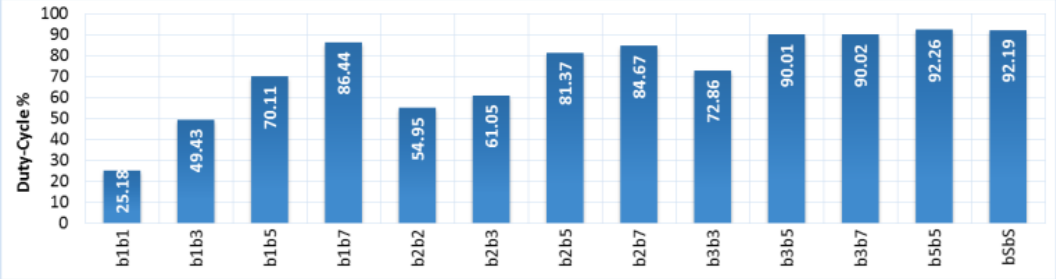

Figure 4-3. DC results for 802.11b two-pair network.

Total network throughput reaches 7.8Mbps at saturation, which is slightly higher than the one-pair scenario. Recorded DC for two pairs reaches up to 92.26% for saturation. This phenomenon is a consequence of a more efficient spectrum use for two pairs. Whenever a one-pair transmitter is performing back-off, the second pair has a chance to proceed with transmission.

Results for two-pair 802.11g, including throughput and DC, are shown in Figure 4-4 and Figure 4-5. Similar to 802.11b, saturation DC and total achieved throughput recorded an increase for two-pair 802.11g. Saturation DC was 77.86%, indicating a 10% increase over the single pair.

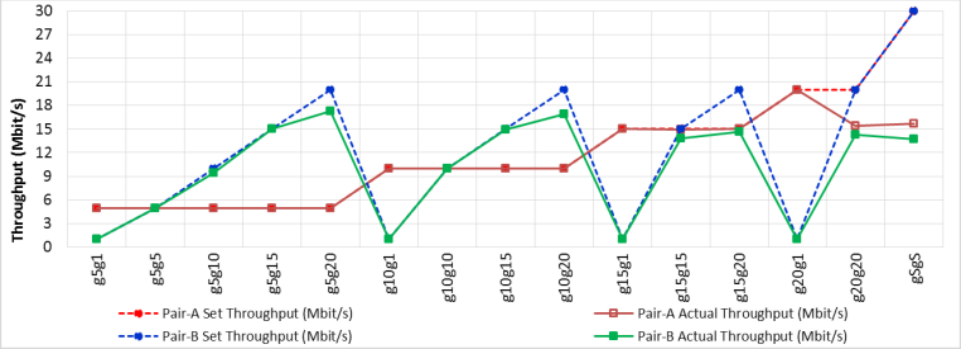

Figure 4-4. Set throughput vs. achieved throughput for 802.11g two-pair network.

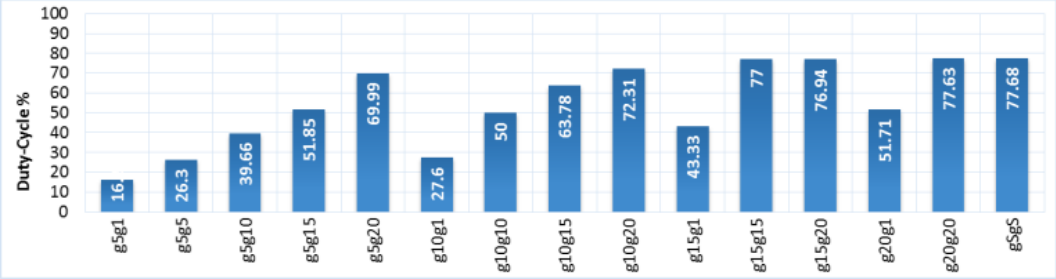

Figure 4-5. DC results for 802.11g two-pair network.

Two-pair spectrum occupancy results for 802.11n are presented in Figure 4-6 and Figure 4-7. A marginal increase of less than 1% in DC saturation is observed for two pair when compared to a single pair. However, saturation aggregate throughput dropped to 52.2Mbps. 802.11n initially achieves DC of more than 97% for single-pair scenario. Adding more transmitters did not significantly impact temporal efficiency. Nevertheless, additional transmitters increased the chances of erroneous transmissions, which in turn led to a decrease in total achieved throughput.

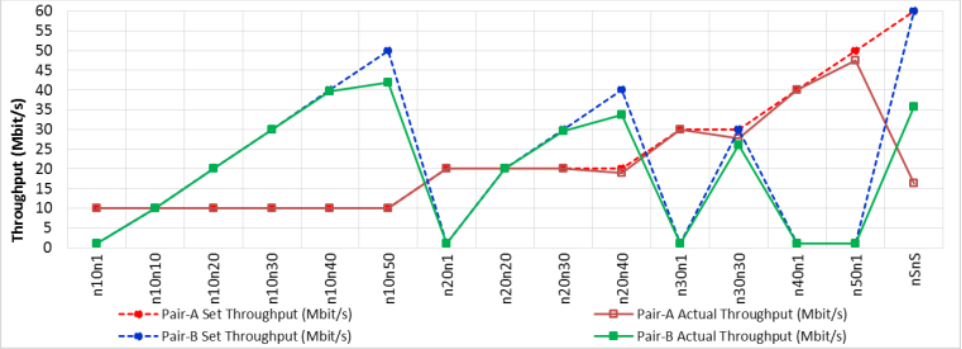

Figure 4-6. Set throughput vs. achieved throughput for 802.11n two-pair network.

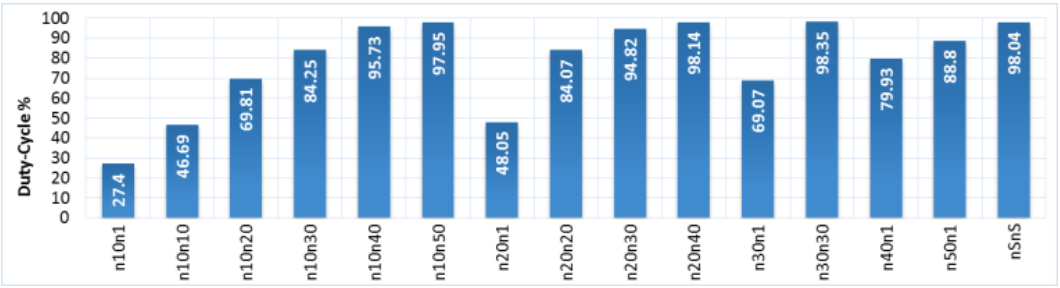

Figure 4-7. DC results for 802.11n two-pair network.

Throughput and duty cycle results for three-pair networks

802.11 b, g, and n three-pair spectrum occupancy results are depicted in Figure 4-8 through Figure 4-13. Figure 4-9 shows that maximum achievable DC of 92.48% was recorded for 802.11b, which is comparable to results for two pair. Maximum saturation aggregate throughput drops to 7.6Mbps when compared to 7.8Mbps achieved for two pair as can be seen in Figure 4-8.

802.11g three pair achieves maximum DC saturation of 80.65%. The highest aggregate throughput for 802.11g was comparable to two pair. 802.11n three-pair DC remains at approximately 98% and demonstrates a marginal increase over two pair. Maximum achieved throughput dropped to 51.5Mbps.

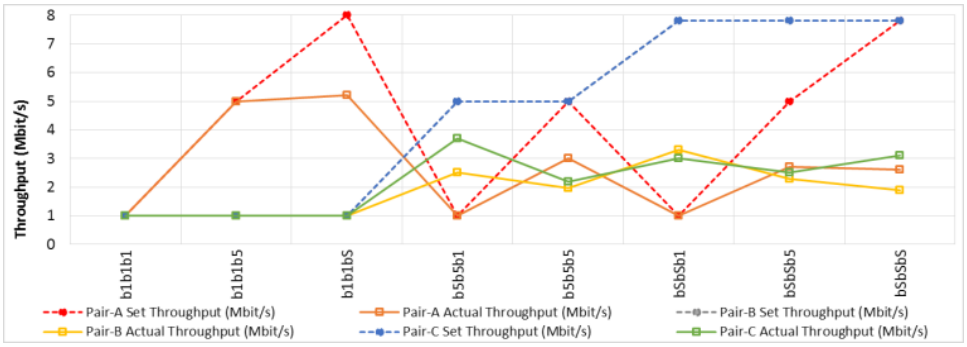

Figure 4-8. Set throughput vs. achieved throughput for 802.11b three-pair network.

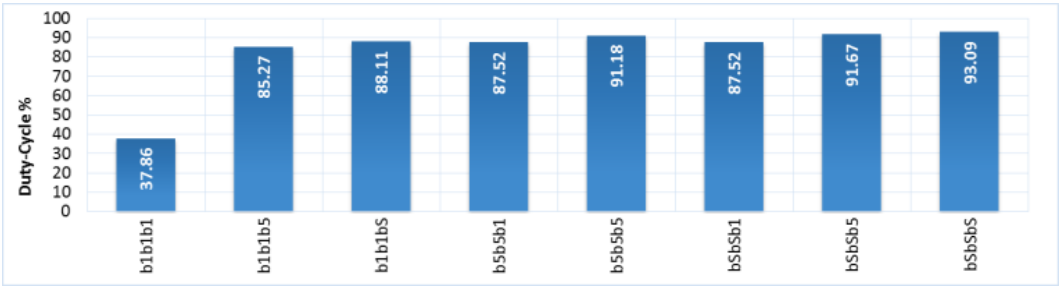

Figure 4-9. DC results for 802.11b three-pair network.

All transmitters achieved their requested throughput for tests characterized as below saturation. DC for two pair with a specific aggregate throughput is comparable to DC value at the same throughput level for single pair at a difference not exceeding 4%, in most scenarios. For example, 802.11g two-pair test with 10Mbps throughput for both pair-A and pair-B yielded a DC of 50%, which is comparable to DC of 48.48% achieved for single pair with 20Mbps achieved throughput. Another example is 802.11n two pair with achieved throughput of 10Mbps for pair-A and 20Mbps for pair-B. This test recorded a DC of 69.81%, which is comparable to DC of 65.48% achieved for single pair with 30Mbps throughput. Similar observations apply when comparing three-pair DC to two-pair.

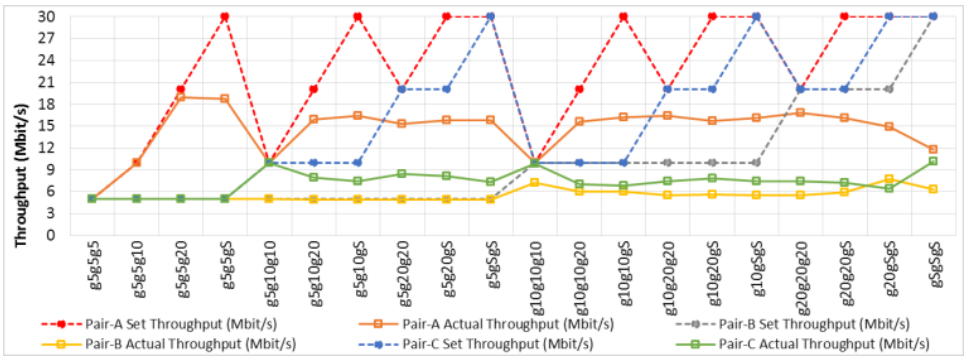

Figure 4-10. Set throughput vs. achieved throughput for 802.11g three-pair network.

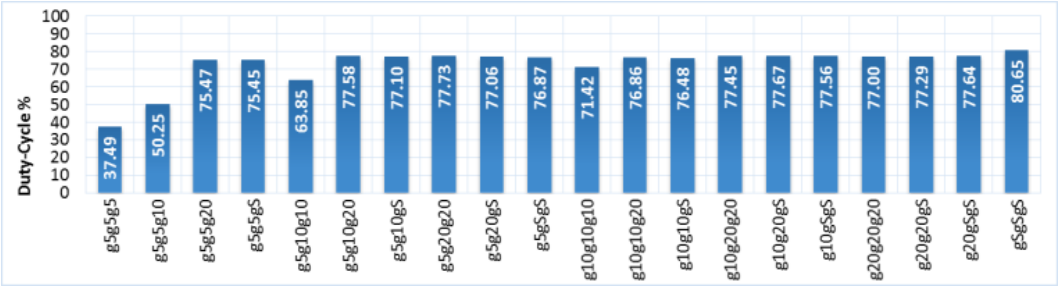

Figure 4-11. DC results for 802.11g three-pair network.

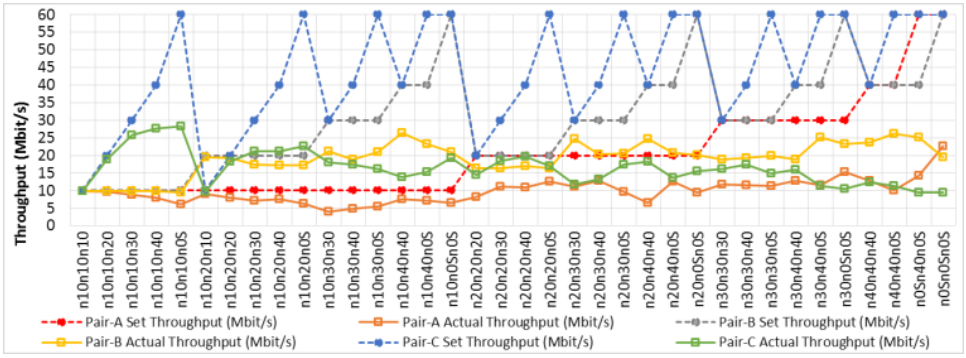

Figure 4-12. Set throughput vs. achieved throughput for 802.11n three-pair network.

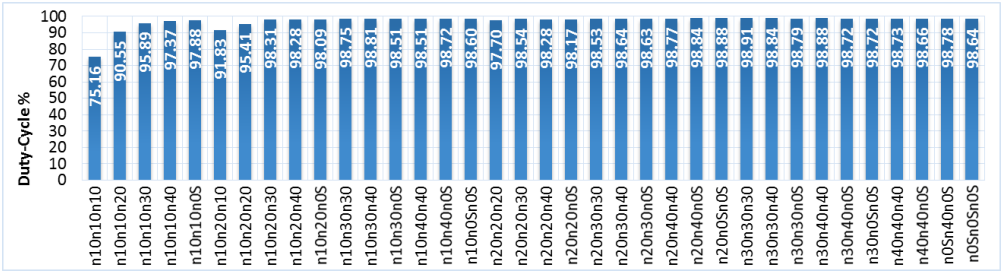

Figure 4-13. Set throughput vs. achieved throughput for 802.11n three-pair network.

Duty cycle error analysis

This subsection provides error analysis for DC results obtained from time-domain and frequency-domain measurements. Error analysis aims at validating both DC measurement techniques. Time-domain DC measurements were obtained via offline analysis, while frequency-domain DC measurements were calculated in real-time. Hence, this analysis allows the flexibility to choose the technique that provides the best results given resources available. Two 6.6 GHz VSAs (NI PXIe-5663E) were tested side by side. The primary difference in measurements was an algorithm running on VSA-1 for calculating DC in time domain and an algorithm running on VSA-2 for calculating DC in frequency domain. Three validation methods were conducted to compare DC measurements obtained from each VSA.

Comparing the mean and Standard Deviation:

Comparing standard deviation and mean values of time domain and frequency domain measurement groups demonstrated identical variation from the mean, which indicates statistical confirmation for both groups. See Table 6. Figure 4-14 details a test-by-test comparison between DC measurements obtained in time domain and frequency domain. Clearly, both approaches achieved similar results.

Table 6. Comparison between DC Statistics in time domain and frequency domain

Methodology	Number of tests	Mean	Standard Deviation
DC- time domain	128	75.282	24.462
DC- frequency domain	128	74.983	24.223
Differences		0.299	0.239

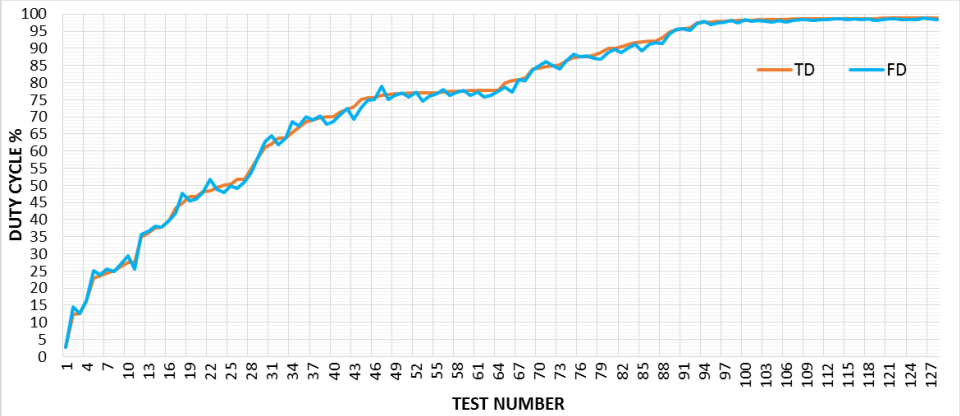

Figure 4-14. Comparison between DC measurements in time domain and frequency domain.

Linear Regression Analysis (LRA):

Linear Regression Analysis (LRA) was used to model the relationship and correlation between TD and FD measurements, as shown in Figure 4-15. Given two equal size sets of values; X and Y, LRA fits the group of observations to a line. This line represents the "best-fit" line in a sense that the error between real Y values and corresponding predicted values using fitted line equation is minimized [70]. Then a value r2 is calculated as a measure of linear relationship between X and Y. The r2 is a fraction that assumes a value between 0 and 1. It is computed using the following equation:

$$r^2 = 1 - \frac{SS_{reg}}{SS_{tot}} \qquad (2)$$

Where SS_{reg} represents the sum of deviations between fitted line and (x, y) observations and SS_{tot} is the sum of deviations between null hypothesis and (x, y) observations [71]. Null hypothesis is a horizontal line that passes through the mean of all Y observations. An r2 value of 0 means that X provides no information on Y whereas a value of 1 means that all (x, y) observations lie on the fitted line perfectly. An r^2 of 0.9979 was calculated for

homogeneous DC tests representing a strong correlation between the two datasets of measurements and confirming a trivial difference between the two groups.

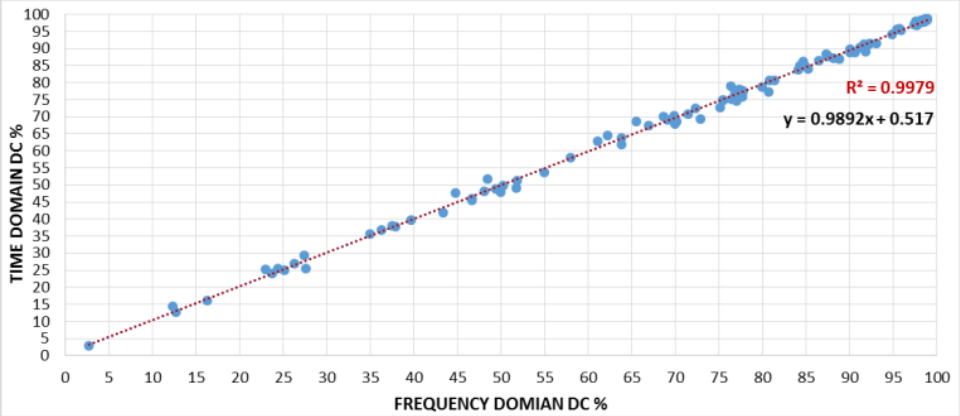

Figure 4-15. Linear regression calculated between time domain and frequency domain.

Root Mean Square Deviation (RMSD):

Root Mean Square Deviation (RMSD), in other words Root Mean Square Error (RMSE), was adopted to find the average difference between the two DC measurement datasets. See (3).

$$\text{RMSD} = \sqrt{\frac{\sum_{i=1}^{n}(X_{obs,i} - X_{model,i})^2}{n}} \qquad (3)$$

X_{obs} is the observed value and X_{model} is the modelled value at time/place i. Results indicated RMSD = 1.18219, which represents the mean deviation between time-domain and frequency-domain DC measurements in terms of percentage (i.e., 1.18219%), which is negligible.

Heterogeneous networks DC

This section provides spectrum occupancy results, including DC and throughput for mutli-pair heterogeneous 802.11 networks in the 2.4 GHz ISM band.

Throughput and duty cycle results for two-pairs

The setup included two access points, transmitters (TX),sending UDP data to two stations acting as receivers (RX). Various throughput values were set for each node in the network, ranging from low throughput to saturation.

Figure 4-16 depicts set throughput vs. achieved throughput for two heterogeneous pairs. One pair was setup as 802.11g, and the other as 802.11n. The figure demonstrates that 802.11n dominates 802.11g and achieves a much higher percentage of peak data rate than 802.11g in the scenario of saturation. This behavior is a result of frame aggregation implemented in 802.11n. Thus, an 802.11n device will transmit multiple frames after accessing the medium, whereas 802.11g releases frequency channel after each single-frame transmission. Both 802.11 g and n achieve desired throughput when below saturation. Figure 4-17 shows measured DC for 802.11gn combination. A maximum DC of 97.88% was recorded, which compares to results obtained from 802.11n single pair. In addition, total achieved DC for below saturation is comparable to aggregate DC of corresponding single pair tests with the same throughput. For example, two-pair tests using 10Mbps achieved throughput for both 802.11g, and 802.11n recorded a DC of 47.1%. This compares to 47.38% aggregate DC for both 802.11g and n single-pair tests with 10Mbps achievable throughput.

Figure 4-18 demonstrates set vs. achieved throughput for 802.11bn. Similar to 802.11gn, the transmitter using 802.11n dominates the spectrum, leaving little chance for 802.11b communication. Figure 4-19 depicts DC results with maximum achievable DC of 98.06%. Results are similar to 802.11g-n for below saturation in that measured DC is

comparable to single-pair aggregate DC resulting from the two corresponding tests with achieved throughput values equal to the two-pair scenario.

Set throughput vs. achieved throughput results for 802.11g-b tests are shown in Figure 4-20. 802.11b achieved a higher percentage of its peak data rate when compared to 802.11g under saturation. Because of 802.11b lower data rate, its frame duration is much longer than that of 802.11g. Consequently, 802.11b occupies the medium for much longer durations compared to 802.11g, thus resulting in the higher percentage of achieved throughput to peak data rate. Figure 4-21 depicts achieved DC for 802.11g-b test. Maximum achieved DC reached 88.17%. This constitutes a slight increase over the 802.11b single-pair scenario.

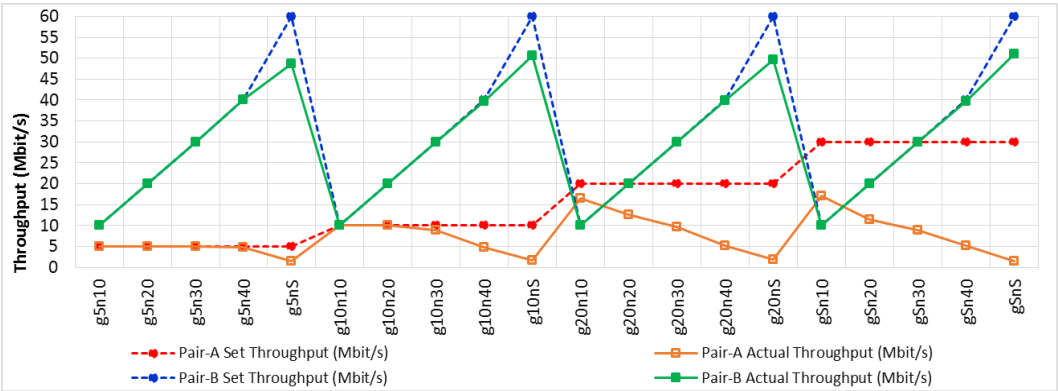

Figure 4-16. Set throughput vs. achieved throughput for two heterogeneous pairs: 802.11gn (GN).

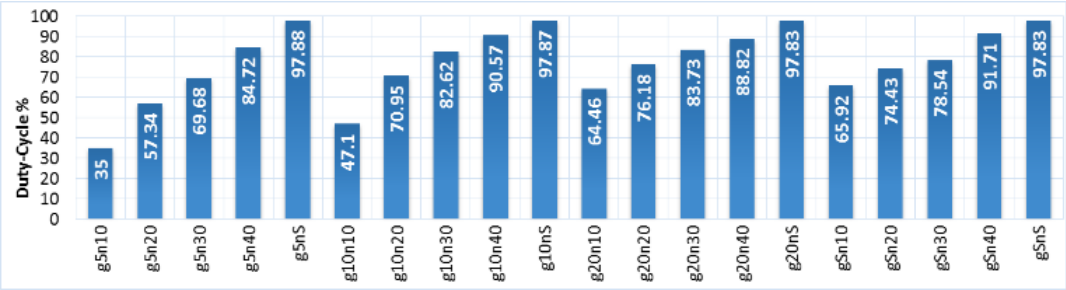

Figure 4-17. DC value for two heterogeneous pairs: 802.11gn.

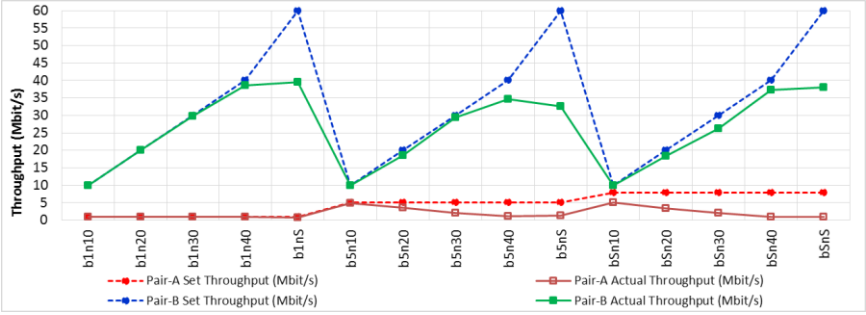

Figure 4-18. Set throughput vs. achieved throughput for two heterogeneous pairs: 802.11bn (BN).

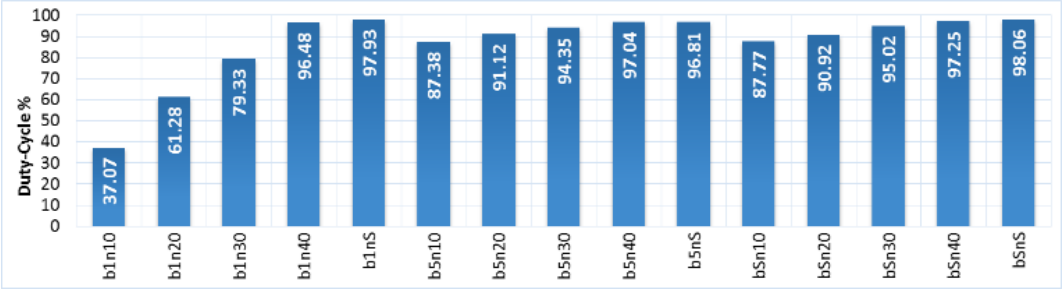

Figure 4-19. DC value for two heterogeneous pairs: 802.11bn.

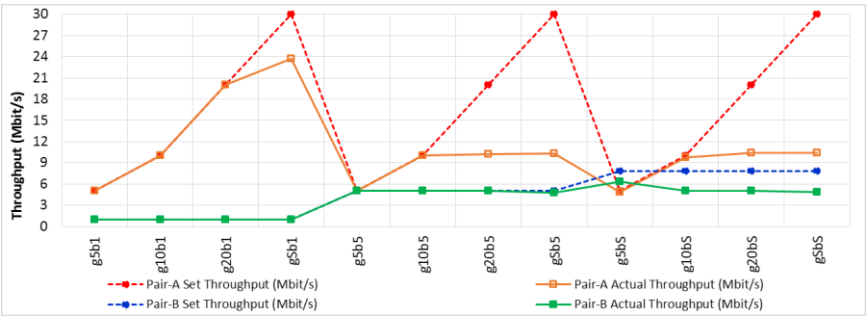

Figure 4-20. Set throughput vs. achieved throughput for two heterogeneous pairs: 802.11bg (BG).

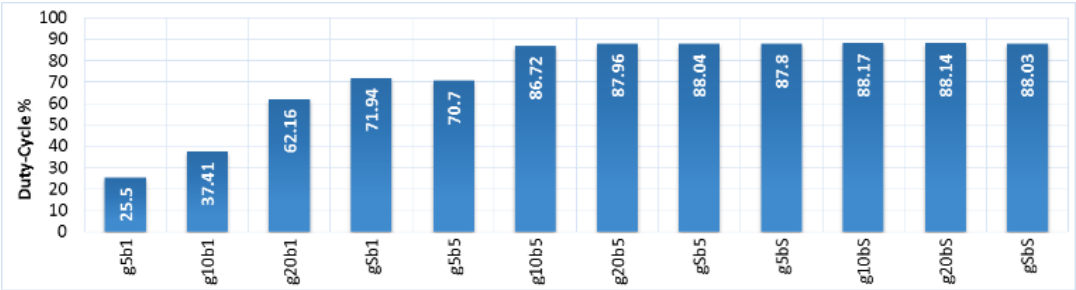

Figure 4-21. DC value for two heterogeneous pairs: 802.11bg.

Throughput and duty cycle results for three-pairs

In this subsection, spectrum utilization for 802.11b, g, and n three-pair heterogeneous networks combinations were investigated. Figure 4-22 and Figure 4-23 depict achieved

throughput and measured DC for 802.11b-b-g combination. Pairs A and B operated on 802.11b, whereas pair C operated on 802.11g. The effect of 802.11b for three pairs on 802.11g transmitter was similar to two-pair scenario where 802.11g pair achieved only 5Mbps of the approximately 30Mbps maximum achievable throughput. Two 802.11b pairs achieved analogous throughput values of 3.3 and 2.9Mbps. Maximum saturation DC of 87.89% was recorded, which is comparable to 802.11bg two-pair scenario. Achieved throughput and DC for 802.11g-g-b combination are shown in Figure 4-24 and Figure 4-25. Although three-pair combinations achieved similar throughput values, 802.11g has a peak data rate five times greater than 802.11b. Maximum saturation DC of 87.94% was recorded.

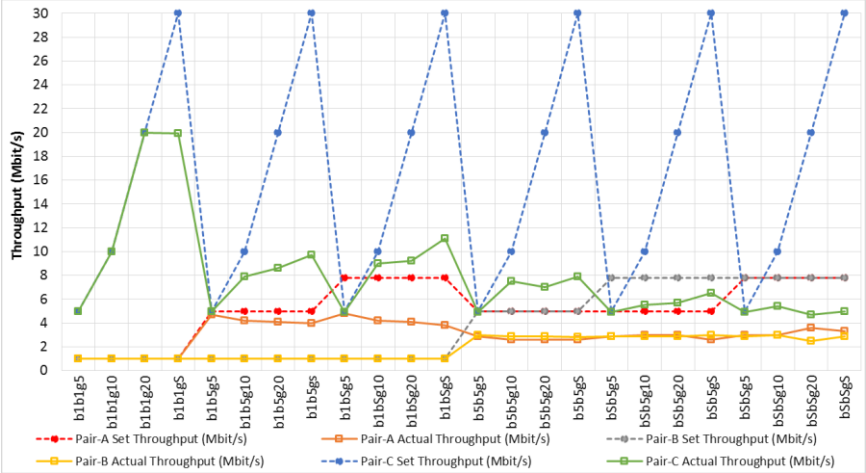

Figure 4-22. Set throughput vs. achieved throughput for three heterogeneous pairs: 802.11bbg (BBG).

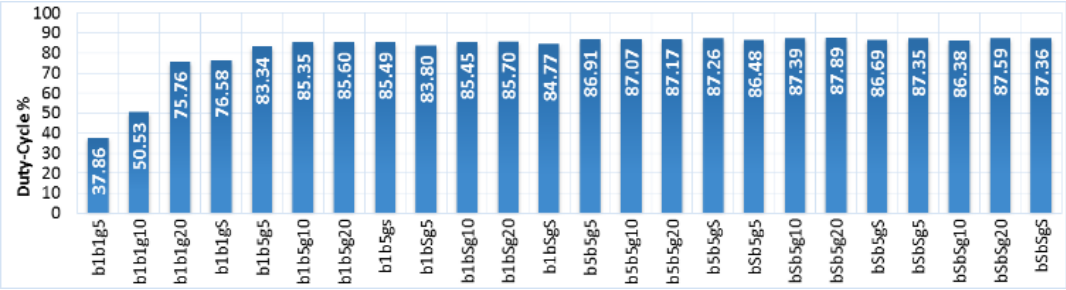

Figure 4-23. DC value for three heterogeneous pairs, 802.11bbg.

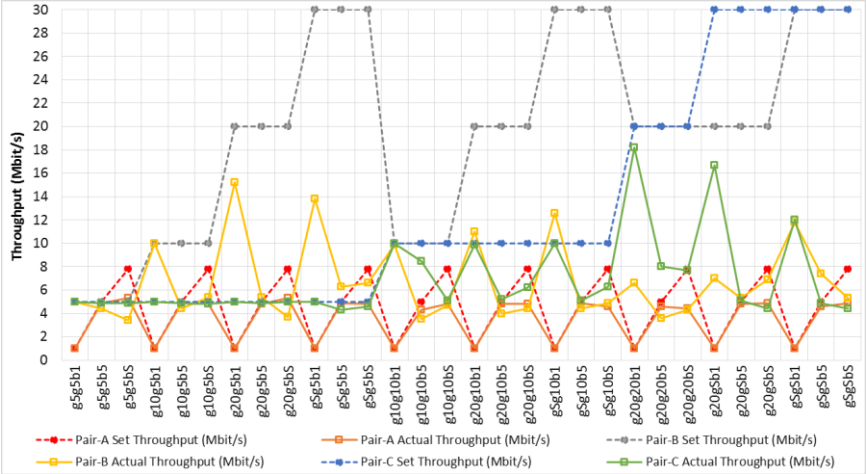

Figure 4-24. Set throughput vs. achieved throughput for three heterogeneous pairs: 802.11ggb (GGB).

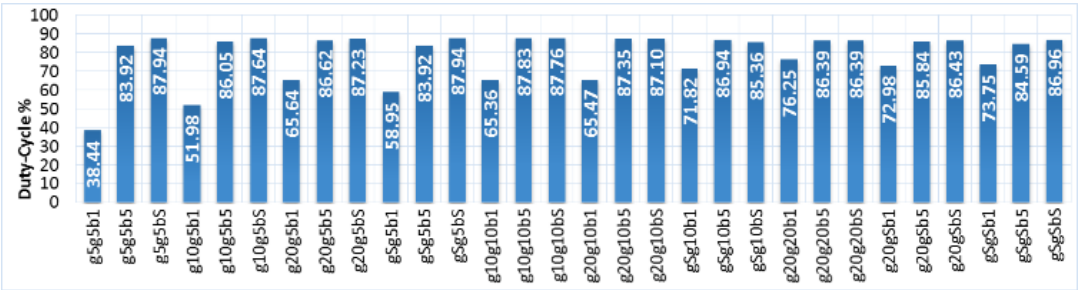

Figure 4-25. DC value for three heterogeneous pairs: 802.11ggb (GGB).

Figure 4-26 through Figure 4-29 depict achieved throughput and DC for 802.11bbn and 802.11nnb combinations. Examining 802.11b and n three-pair combinations, it can be seen that 802.11n pairs dominate the spectrum with higher achieved throughput to peak data rate. 802.11b pairs were unable to achieve throughput higher than 1.2Mbps for either one of the two combinations at saturation. Saturation DC reached 96.21% and 98.65% for 802.11bbn and 802.11nnb, respectively.

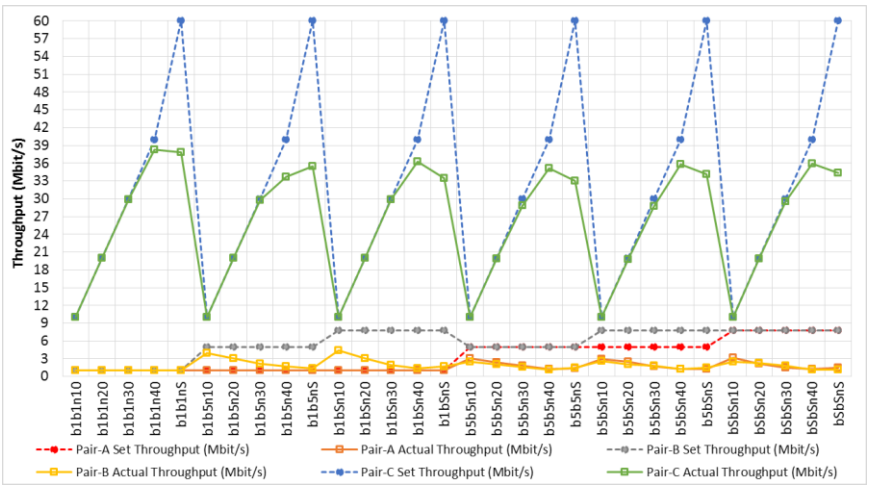

Figure 4-26. Set throughput vs. achieved throughput for three heterogeneous pairs: 802.11bbn (BBN).

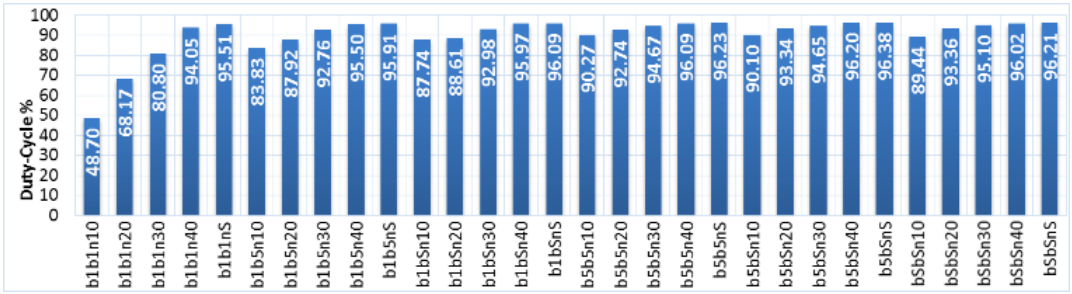

Figure 4-27. DC value for three heterogeneous pairs: 802.11bbn (BBN).

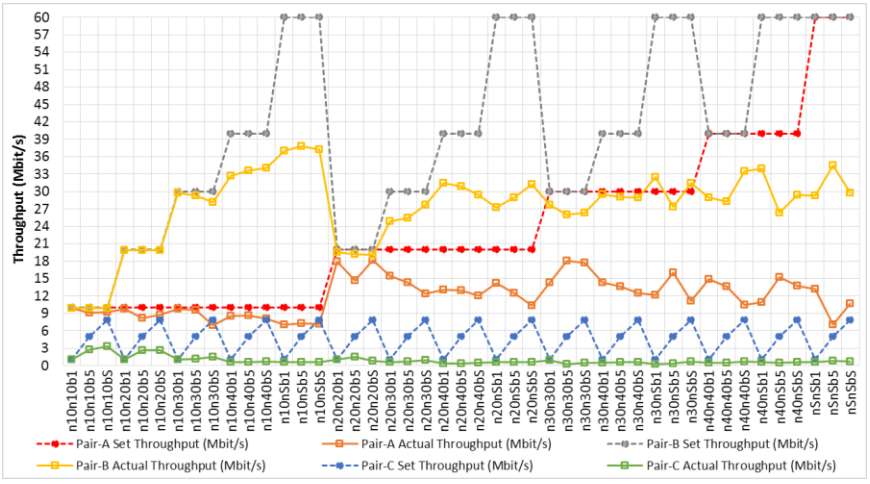

Figure 4-28. Set throughput vs. achieved throughput for three heterogeneous pairs: 802.11nnb (NNB).

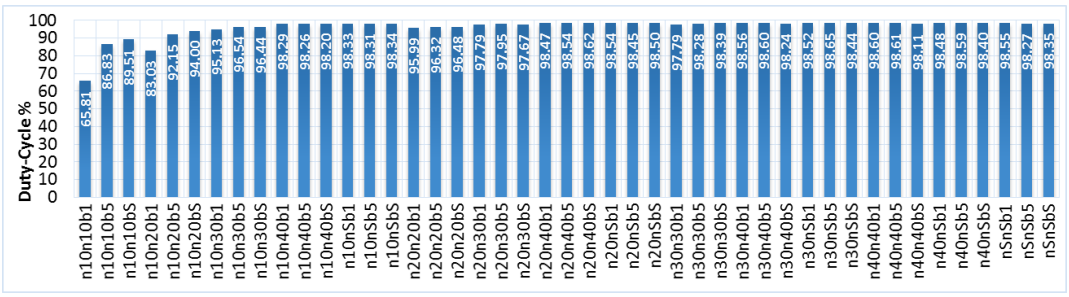

Figure 4-29. DC value for two heterogeneous pairs: 802.11nnb (NNB).

Set throughput vs. achieved throughput and DC results for 802.11ggn and 802.11nng combinations are shown in Figure 4-30 through Figure 4-33. 802.11g performed poorly in both combinations, which is a similar behavior to 802.11gn two-pair scenario. This is a result of 802.11n frame aggregation depriving 802.11g transmitters from frequently accessing the medium. This is reflected in achieved DC, which reached up to 97.2%, primarily for 802.11n transmissions.

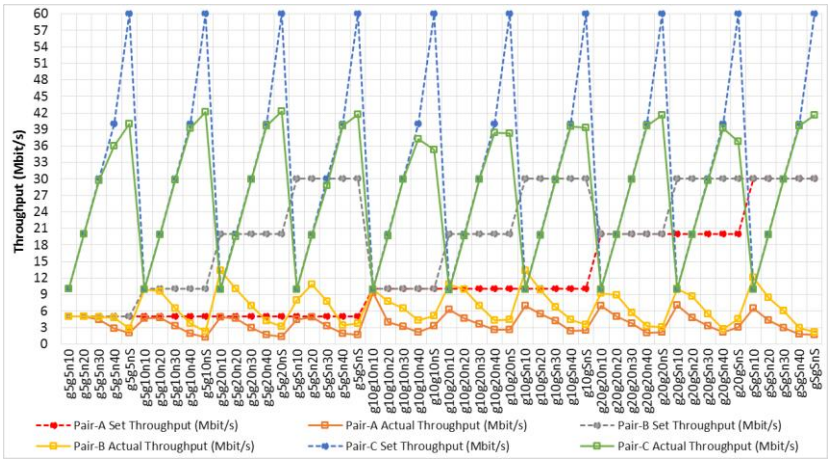

Figure 4-30. Set throughput vs. achieved throughput for three heterogeneous pairs: 802.11ggn (GGN).

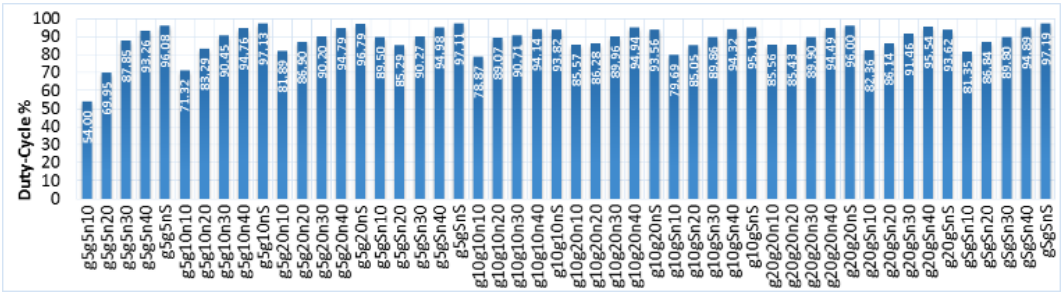

Figure 4-31. DC value for three heterogeneous pairs: 802.11ggn (GGN).

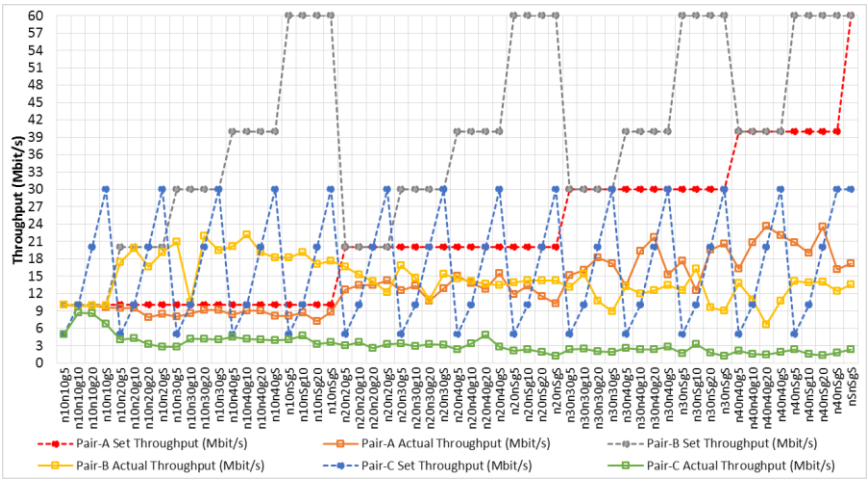

Figure 4-32. Set throughput vs. achieved throughput for three heterogeneous pairs, 802.11nng (NNG).

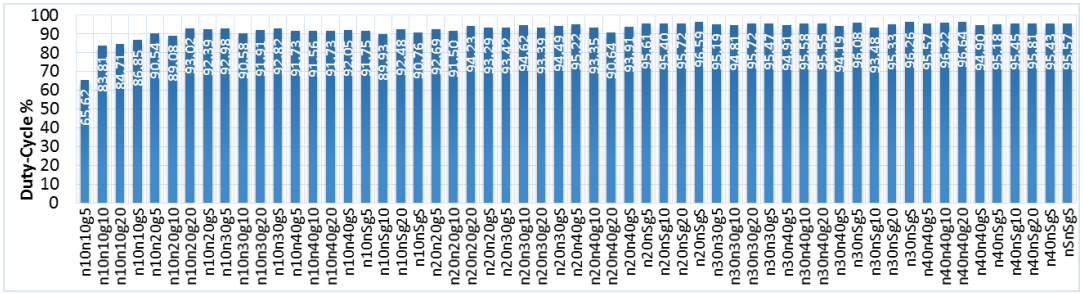

Figure 4-33. DC value for three heterogeneous pairs, 802.11nng (NNG).

Results of 802.11b-g-n combination are presented in Figure 4-34 and Figure 4-35 and confirm previous findings. At saturation throughput, 802.11n transmitter scored the highest percentage of achieved throughput-to-peak data rate, achieving 60.46% of its peak data rate. 802.11b and 802.11g achieved 7.81% and 3.89%, respectively, of their peak data rates.

Duty cycle error analysis

This subsection provides error analysis for DC results obtained from time-domain and frequency-domain measurements. The two aforementioned VSAs were used to collect time-domain and frequency-domain measurements. Similar to the homogeneous scenario,

the algorithm operating on VSA-1 calculated DC in time domain, and the algorithm operating on VSA-2 calculated DC in frequency domain. Three validation methods were conducted to compare DC measurements obtained from each VSA.

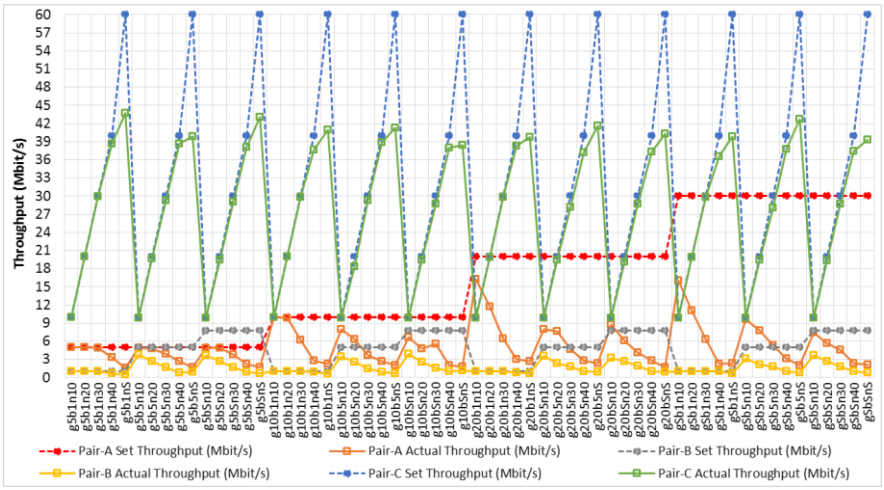

Figure 4-34. Set throughput vs. achieved throughput for three heterogeneous pairs: 802.11g, 802.11b, and 802.11n (GBN).

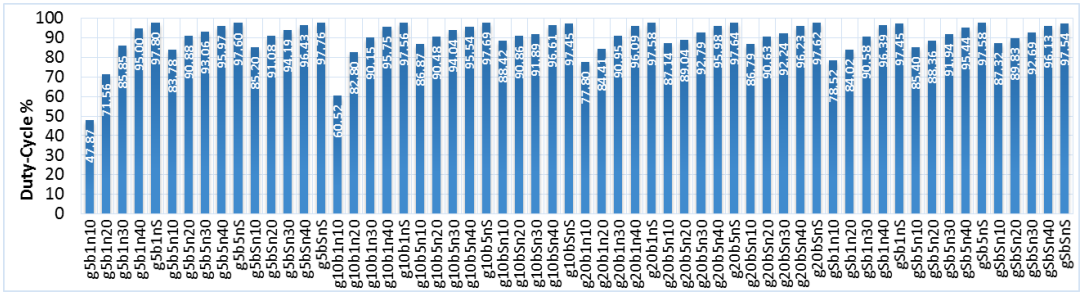

Figure 4-35. DC value for three heterogeneous pairs: 802.11g, 802.11b, and 802.11n (GBN).

Comparing the mean and Standard Deviation:

Standard deviation and mean values of time-domain and frequency-domain measurement groups show similar values, as shown in Table 7. This suggests that statistically both groups have similar distributions.

Table 7. Comparison between DC Statistics in time domain and frequency domain

Methodology	Number of tests	Mean	Standard Deviation
DC- time domain	343	88.3162	11.97395
DC- frequency domain	343	87.5784	11.92431
Differences		0.7378	0.04964

Figure 4-36 depicts a test-by-test comparison between DC measurements obtained in time domain and frequency domain. Both methods achieved similar results.

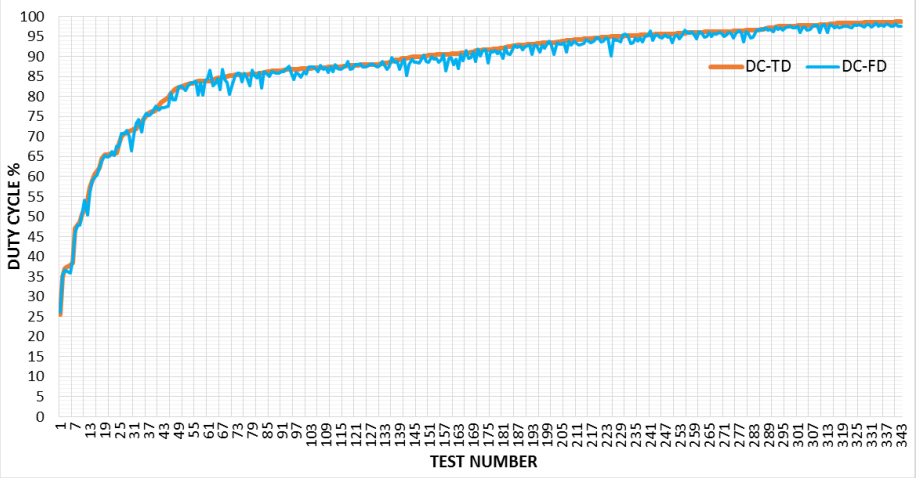

Figure 4-36. Comparison between DC measurements in time domain and frequency domain.

Linear Regression Analysis (LRA):

LRA was also used to model the relationship and estimate the correlation between time-domain and frequency-domain 802.11 heterogeneous networks measurements, as shown in Figure 4-37. The value R^2=0.9925 was calculated and represents strong goodness of fit (i.e., correlation) between the two dataset measurements. This result confirms a negligible difference between the two groups.

Root Mean Square Deviation (RMSD):

RMSD was also used to find the average difference between the two time-domain and frequency-domain DC measurements for the heterogeneous 802.11 networks. Results provided an RMSD value of 1.37717. As explained earlier, this value represents the mean deviation between the measurement sets in percentage. This value is negligible.

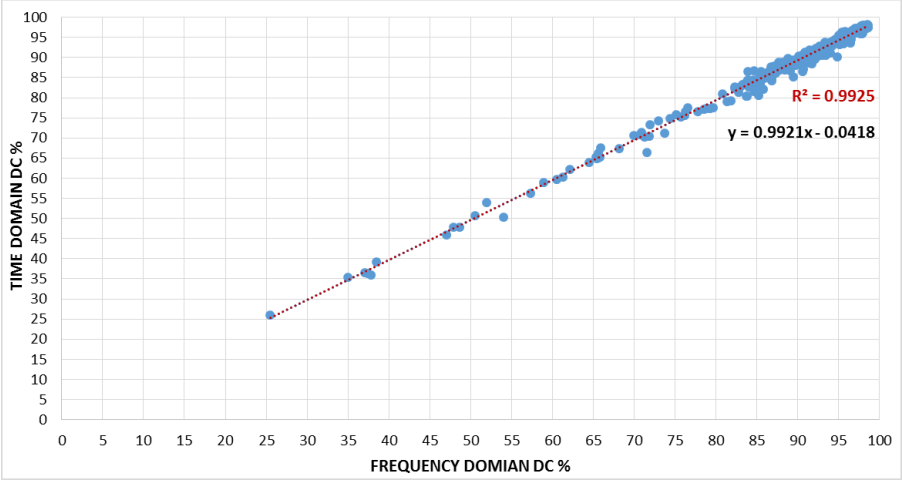

Figure 4-37. Linear Regression time domain vs. frequency domain for heterogeneous network.

Simulation results

This subsection provides a comparison for DC and throughput results between simulation and experimental tests. Figure 4-38 shows DC at incrementing throughput values for a single 802.11g node. Although results are nearly identical, experimental measurements achieved slightly higher DC than simulation for all throughput values.

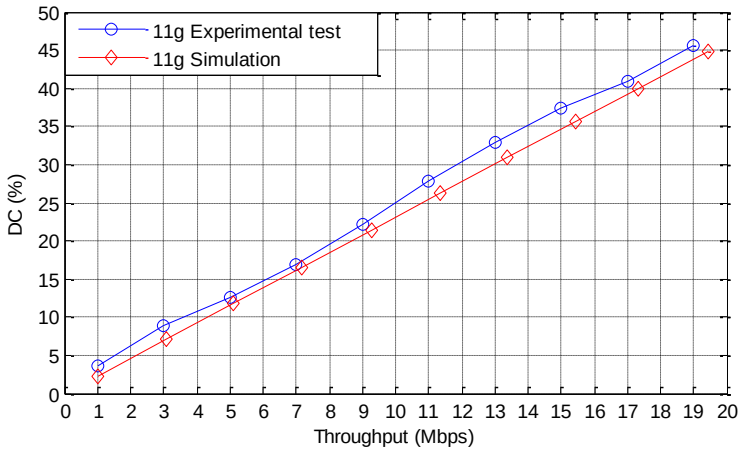

Figure 4-38. Simulation and experimental DC and throughput comparison for a below saturation 802.11g one-pair network.

Figure 4-39 compares maximum achieved DC and throughput for one, two, and three 802.11g nodes. Contrary to the "below saturation scenario," simulation DC for the "saturation scenario" was slightly higher than the experimentally measured DC. The most significant difference for a single-pair saturation test was 5.63%. Differences did not exceed 2.08% for all other saturation and below-saturation tests. All experimental and simulation results followed the same trend.

Saturation results for both experimental and simulation showed that as the number of transmitter increases, DC increases. Notably, the rate of DC increase is lower for three pair when compared to two pair. Total network throughput increased for two pair, and then dropped for three pair and resulted from an increased number of collisions reported in the simulation.

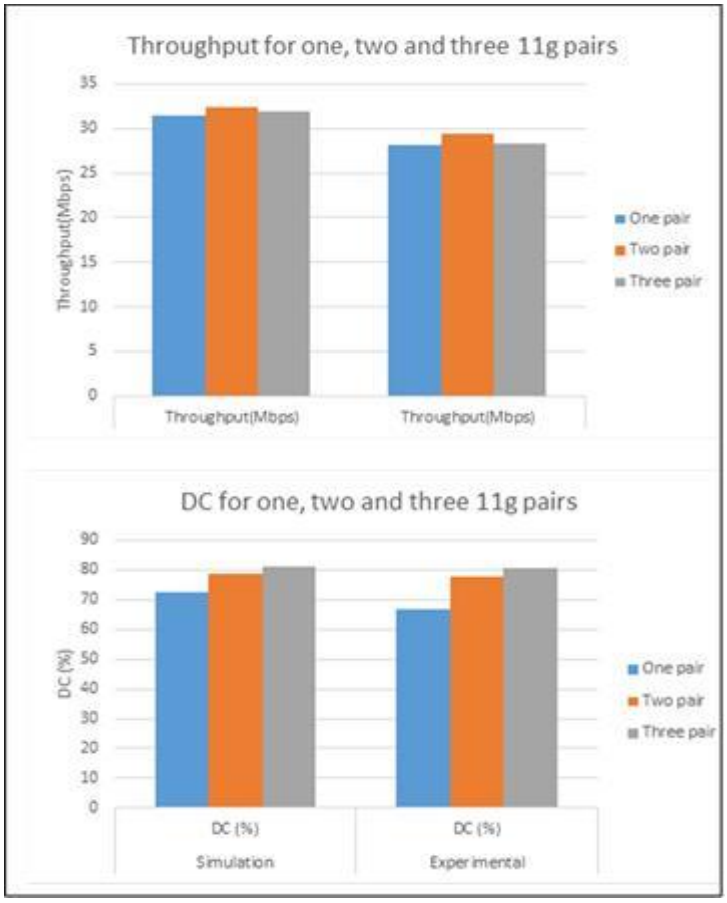

Figure 4-39. Simulation and experimental DC and throughput comparison for 802.11g one-, two- and three- pair saturated networks.

Figure 4-40 presents extrapolated throughput and DC results for a large number of transmitters using 802.11g simulation. Highest achieved throughput was recorded for two transmitters. Total throughput starts dropping after populating the network with three or more transmitters. Nevertheless, DC continues to increase as the network is populated with more transmitters. Rate of increase becomes low when populating the network with more transmitters.

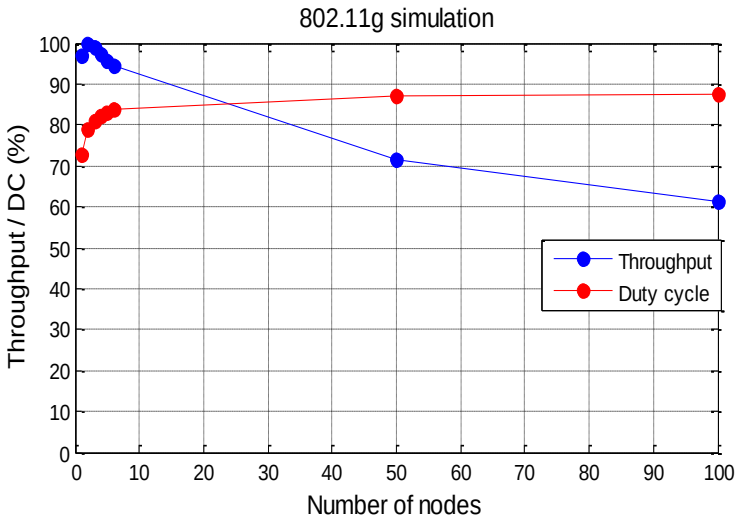

Figure 4-40. 802.11g simulation extrapolated throughput and DC values for a large number of transmitters

Aggregated frame size has a significant effect on heterogeneous 802.11 network throughput and wireless coexistence, as has been discussed earlier. An experiment was conducted using simulation where one 802.11g node was coexisting with nine 802.11n nodes. Two 802.11n aggregated frame sizes were used—10 aggregated frames and 42 aggregated frames.

Figure 4-41 shows achieved per node throughput. 802.11g node achieves lower throughput as the number of 802.11n aggregated frames increases. Nonetheless, all nodes, including the nine 802.11n and one 802.11g nodes, have uniform medium access, as can be seen in Figure 4-42. Even though the opportunity for medium access is fairly distributed, 802.11g nodes send only one frame per medium access whereas 802.11n nodes send multiple frames per medium access. This phenomenon deprives 802.11g from medium access for longer periods of time and causes sever degradation in 802.11g node performance when coexisting in the same vicinity with 802.11n nodes.

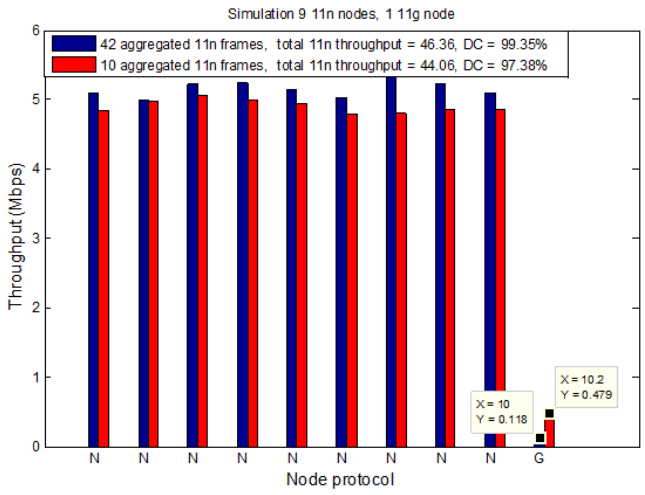

Figure 4-41. Per transmitter throughput for 802.11g/n shared medium for various numbers of 802.11n aggregated frames.

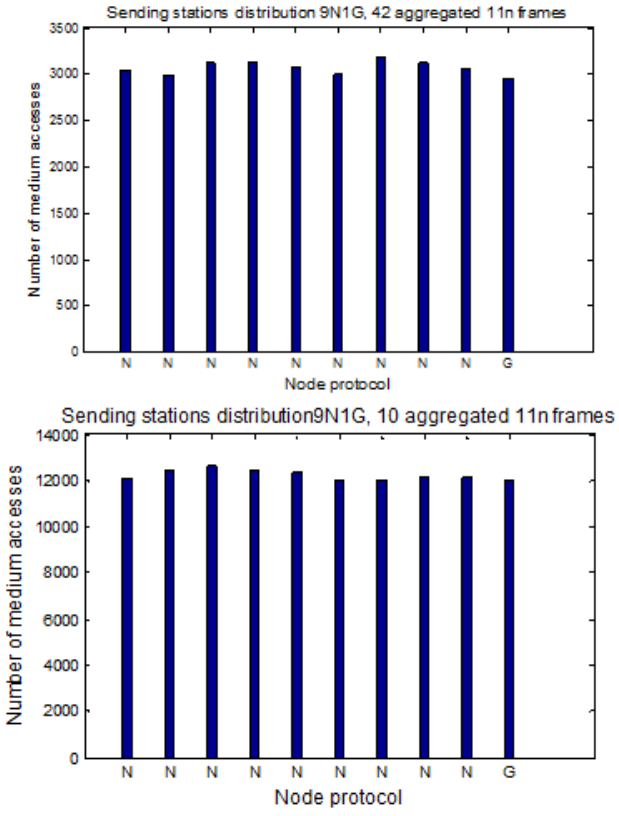

Figure 4-42. Medium access distributions for 802.11g/n shared medium at various numbers of 802.11n aggregated frames

Conclusion

This chapter presented a comprehensive study of 802.11b, g and n spectrum occupancy. DC and throughput levels were presented and discussed for one, two, and three communicating pairs. Both 802.11 homogeneous and heterogeneous networks were investigated. Tools developed for time domain and frequency domain were used to obtain DC measurements. Error analysis between time domain and frequency domain DC measurements was presented, as well. Analyses included four statistical methods for confirming equivalence between two methods for obtaining DC measurements.

Chapter 5: Spectrum Characterization – 802.11 Experimental Time Distributions

This chapter provides 802.11 time distribution results obtained from test performed for the work presented in this dissertation. Results detail activity and idle time distributions for both homogeneous and heterogeneous 802.11 networks in the 2.4 GHz ISM band. Distributions were obtained from time domain measurements and represent time fragment distributions for active and inactive periods during a specific test. Active periods are times during which a channel is occupied with a transmission; idle periods are times during which the channel is available. Along with duty cycle (DC) values, these distributions provide a detailed analysis of channel traffic patterns. Results for one-, two-, and three-pair 802.11 networks are presented and discussed below. Details in this chapter highlight temporal efficiency of various 802.11 standards, as well as their aggressiveness towards other 802.11 standards. Idle time distribution simulation results for an 802.11g network are also presented and compared with empirical distribution results.

Homogeneous networks

This section offers results obtained from homogeneous experimental tests. The 802.11 channel was populated with networks composed of one-, two-, or three-transceiver pairs. Networks were configured to operate on 802.11b, g, or n for any given test.

Idle time distributions

Idle time distribution provides valuable information on channel availability to the CT, which can be used to estimate appropriate frame size and time of channel access. The aim is to minimize the probability of collision with 802.11 transmissions.

Various behaviors can be observed in three distinct idle-time duration regions for all idle time distributions presented in this work. The first region represents idle-time fragment durations equal to or below the SIFS value and corresponds with up to 50% of total idle-time fragments. They represent inter-frame spacing before ACK transmission. The second idle-time region represents the DCF standard minimum contention window. Distribution in this region depends on the number of transmitters and offered traffic. It also assumes an exponential shape when more than one transmitter utilizes the network. Idle-time fragment distribution is uniform when the network is populated with only one saturated transmitter. The third idle-time region includes idle-time fragments with duration longer than the minimum contention window. Distribution in this region depends mainly on offered traffic and throughput distribution between contending transmitters, as discussed below.

Figure 5-1 illustrates one pair idle-time CDFs for 802.11b, g and n. SIFSs account for approximately 50% of total idle-time fragments presented. Remaining time fragments are distributed between DCF minimum contention window (i.e., second region) and higher idle-time durations (i.e., third region), depending on throughput. Time fragments resulting from minimum contention window account for a higher percentage of the total

idle time for higher throughput. Figure 5-1 also indicates that idle-time fragments in the second region are uniformly distributed. This is a direct result of the DCF functionality, as discussed earlier. Notably, the second idle-time region for 802.11b is larger than that of 802.11g/n, primarily due to the wider minimum contention window of 802.11b with 32 time slots as compared to 802.11g and n with 16 time slots.

Regarding the third region, idle-time distribution is primarily dependent on frame arrival rate and transmitter queue state. Figure 5-1 shows that 802.11g and n 10Mbps are nearly the same for idle-time CDFs, duty cycle, and exhibited behavior. 802.11g and n 20Mbps distributions exhibit similar behavior. The reason for the observed similarity is that peak data rate for 802.11n is 65Mbps whereas peak data rate for 802.11g is 54Mbps, thus both standards will have comparable frame arrival rate for throughput values much lower than saturation. CDFs for the two standards diverge at higher throughput values.

Figure 5-1 also shows that 802.11g saturates at 67% DC at the point where nearly 99% of idle-time fragments are either SIFS or back-off values resulting from minimum contention window. This means that even with a saturated queue, channel is available almost 33% of the time when a single 802.11g pair is occupying the medium. However, 802.11n saturates at 98% DC resulting from frame aggregation. Hence, the standard is extremely time efficient. Time fragments resulting from SIFSs and minimum contention window equal approximately 95% of total idle time fragments, given 802.11n saturation. 802.11b saturates at DC of 85%.

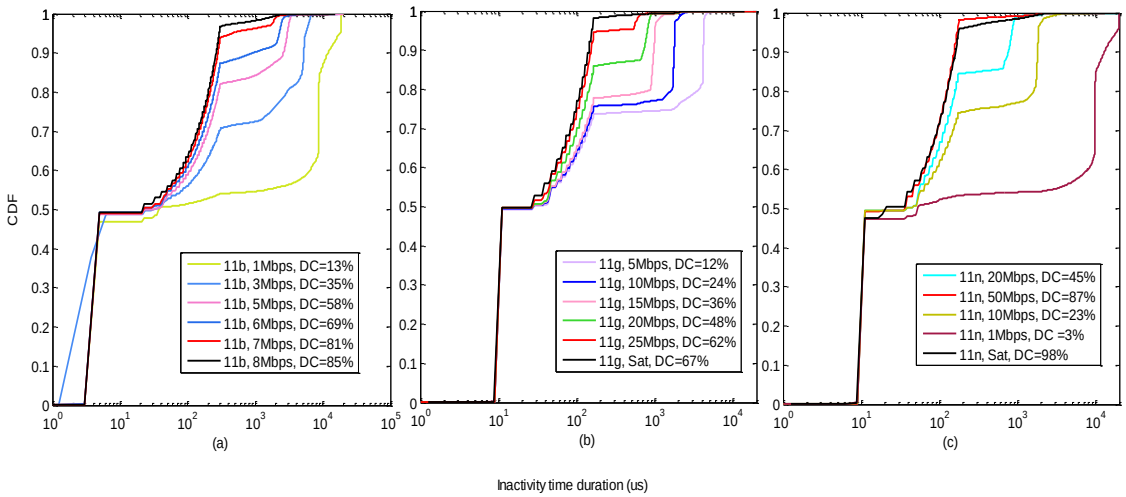

Figure 5-1. Idle-time distributions for: a) 802.11b, b) 802.11n and c) 802.11g one pair

Figure 5-2, Figure 5-3, and Figure 5-4 depict two- and three-pair idle-time CDFs for 802.11b, g and -n, respectively. Test runs for identical standards with comparable throughput were shown to have similar DC. However, idle-time CDFs had dissimilar third region patterns, depending on throughput distribution among transmitters. Idle-time fragments were found to spread over a wide range of time durations when throughput was distributed more equally among transmitters. Nevertheless, idle-time fragments become more concentrated around a certain value whenever one transmitter dominates network throughput. See dashed curves in the figures below. Idle-time fragments in the second region have an exponential distribution when two or more pairs at high throughput value occupy the medium when compared with uniform distribution observed for one-pair scenario. This scenario is a direct result of the transmitter back-off counter freezing when the medium is sensed busy during the transmission of another node. This leads to further fragmentation of second region idle-time intervals.

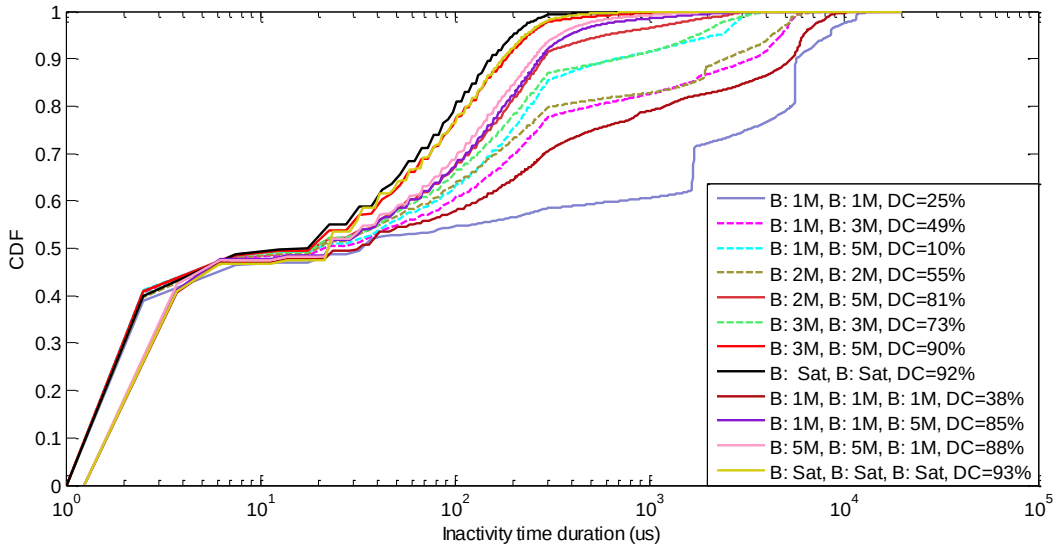

Figure 5-2. 802.11b idle time distributions for two and three pairs

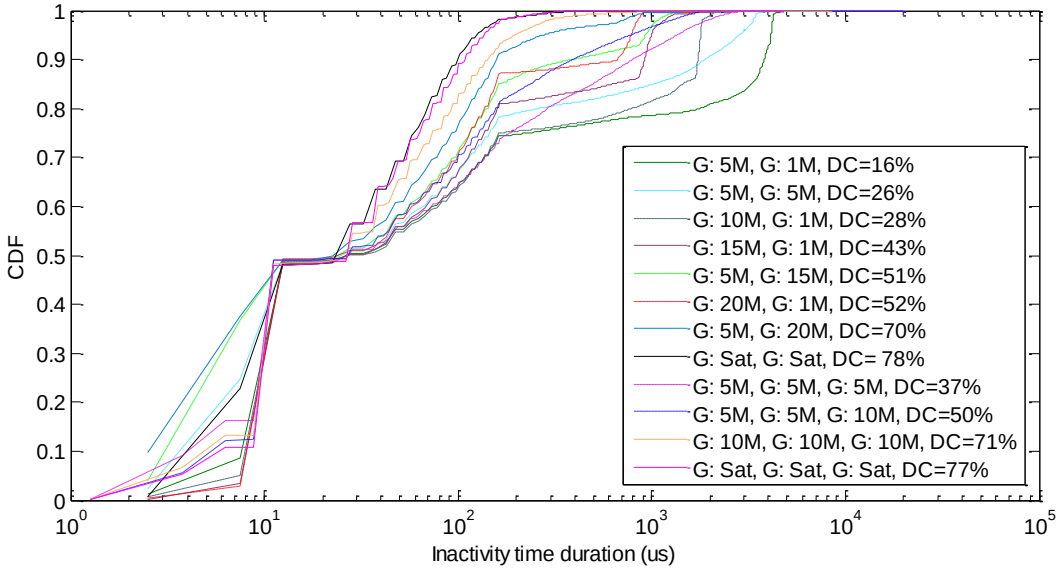

Figure 5-3. 802.11g idle time distributions for two and three pairs

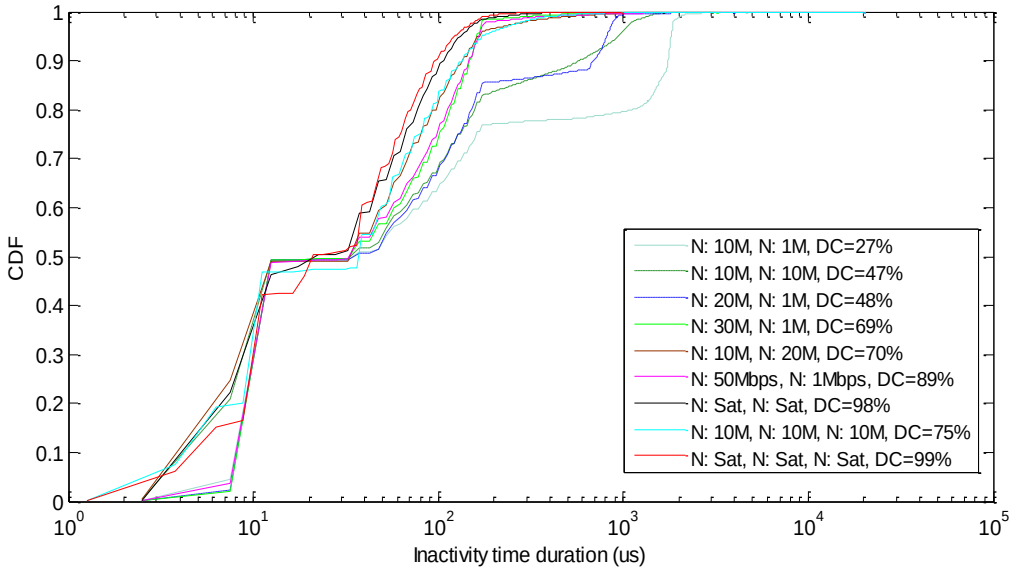

Figure 5-4. 802.11n idle time distributions for two and three pairs

Activity distributions

802.11b, g and n activity distributions for one-, two-, and three-saturation tests are depicted in Figure 5-5, Figure 5-6 and Figure 5-7, respectively. Note that these distributions are not normalized and that they represent time duration, count of ACK frames, and count of data frames. The resulting frame and ACK durations are straightforward for both 802.11b and g, as frame size is fixed. Thus, most frame durations are fixed around a certain value because they primarily depend on data rate. As for 802.11n, activity distribution depends on the number of aggregated frames, which is in turn is affected by offered traffic, assuming a large enough queue. This behavior is clearly demonstrated from activity distributions as 802.11n throughput is increased. See Figure 5-8 for 802.11n one-pair activity distributions.

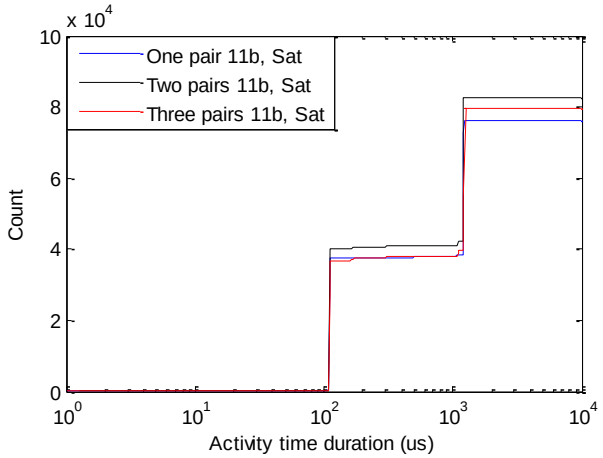

Figure 5-5. 802.11b saturation activity distributions for one- two- and three pairs

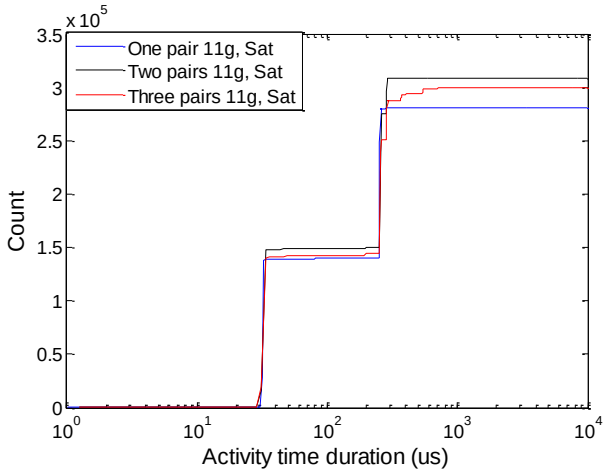

Figure 5-6. 802.11g saturation activity distributions for one- two- and three pairs

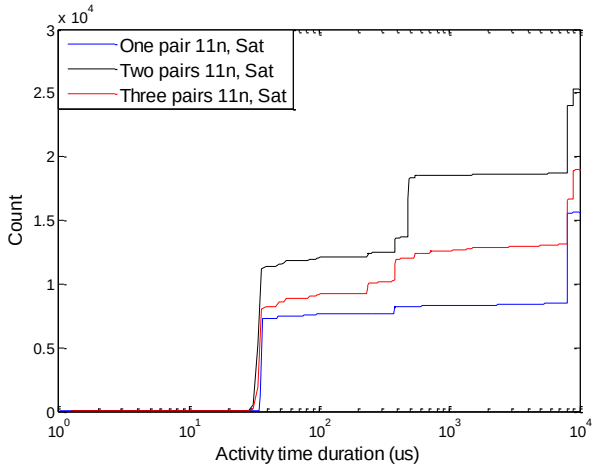

Figure 5-7. 802.11n saturation activity distributions for one- two- and three pairs

An interesting observation for all three standards is that the number of detected frames and ACKs were larger for two pairs when compared with both the one-pair and the three-pair cases. The reason for this behavior is the following: 1) for the one-pair case, requested throughput is achieved without any risk of collision. However, the spectrum resource is not fully utilized due to the DCF procedure; 2) transmitters achieve a more efficient use of the frequency spectrum when more data frames are sent with a very low potential probability of collision in the two-pair case; 3) given three pair scenario, transmitters occasionally send frames at lower data rate due to the increased number of errors when compared with two- and one-pair cases. This in turn results in fewer transmitted frames per unit time. See table IV for 802.11g/n saturation achieved throughput.

Table 8. 802.11n/g saturation throughput

standard	***Number of pairs***	***Achieved Throughput (Mbps)***
802.11g	One	28.1
	Two	29.4
	Three	28.3
802.11n	One	56.4
	Two	52.2
	Three	51.5

802.11n one-pair activity CDFs while increasing throughput from 1Mbps to saturation are depicted in Figure 5-8. Clearly, the size of aggregated frames becomes larger as throughput increases. This in turn leads to a lower number of aggregated frames transmitted on the channel after a certain throughput level is achieved. As a result, the transmitted frames become larger.

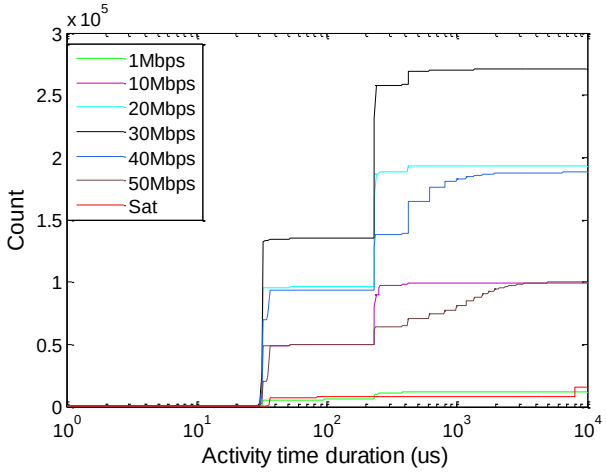

Figure 5-8. 802.11n one pair activity distribution

Heterogeneous networks

This section presents experimental results of heterogeneous networks tests. Distributions include a combination of two- and three-pair tests running different standards where each pair can be 802.11b, g or n. Results aid in understanding temporal behavior of mixed environments that contain multiple networks operating on different 802.11 standards (e.g., apartment buildings and complexes, shopping areas, downtown buildings, and other like settings).

Idle time distributions

Two- and three-pair heterogeneous idle-time distributions for 802.11g and n (and not 802.11b) are presented in this chapter to avoid redundancies. 802.11bgn three-pair combination results are presented as well. Figure 5-9 shows idle-time CDF for two-pair heterogeneous network tests, including an 802.11gn combination. Throughput for each transmitter was incremented from low values to saturation. Select representative tests are shown in Figure 5-9. Results for two-pair heterogeneous networks idle-time distribution were similar to homogeneous networks in that idle-time distributions are divided into

three regions. Two tests (see dashed curves in Figure 5-9) demonstrated variable behavior when SIFS accounted for less than 50% of total idle-time count. The decrease in SIFS percentage resulted from missing ACKs, as indicated by dashed curves in Figure 5-12 below—802.11g/n activity distributions.

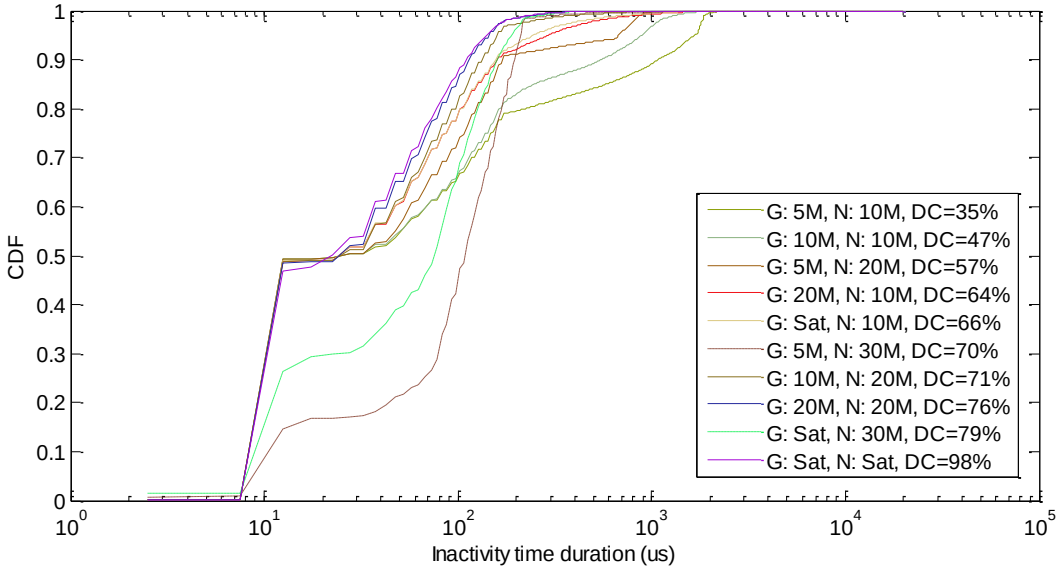

Figure 5-9. Two pairs heterogeneous networks idle time distribution

Figure 5-10 depicts idle-time CDFs for three pair 802.11g and n heterogeneous networks, including ggn and gnn combinations. Second and third regions merge when there is no clear separating margin observed between the two regions. This results from further fragmentation of idle-time durations in both regions.

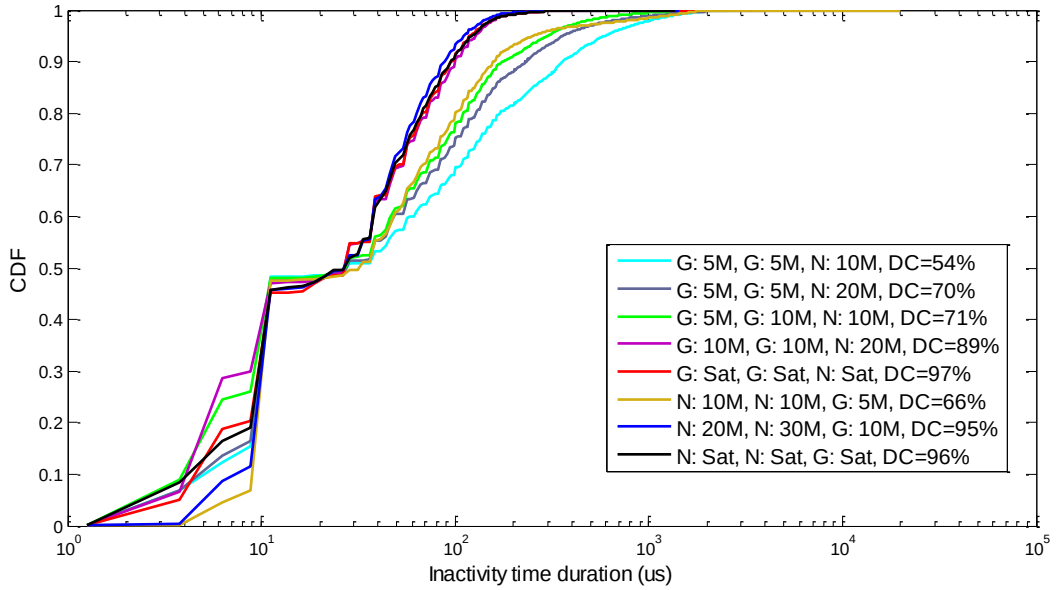

Figure 5-10. Three pairs heterogeneous networks idle time distribution

Figure 5-11 depicts idle time-CDFs for three-pair 802.11bgn combination. The effect of 802.11b on idle-time distribution is minimal, as both 802.11g and n have smaller minimum contention window that results in significantly more frequent medium access. Consequently, the second idle-time region appears to be similar to that of 802.11gn two-pair CDFs. The third-idle time region did not exceed 2000μs of idle time-fragment for offered throughput values. This behavior is an outcome of extended spectrum occupancy resulting from 802.11b and n traffic. Also, 802.11b and g, lacking frame aggregation capability, would likely attempt to access the spectrum at a higher frequency to achieve their requested throughput when compared with 802.11n.

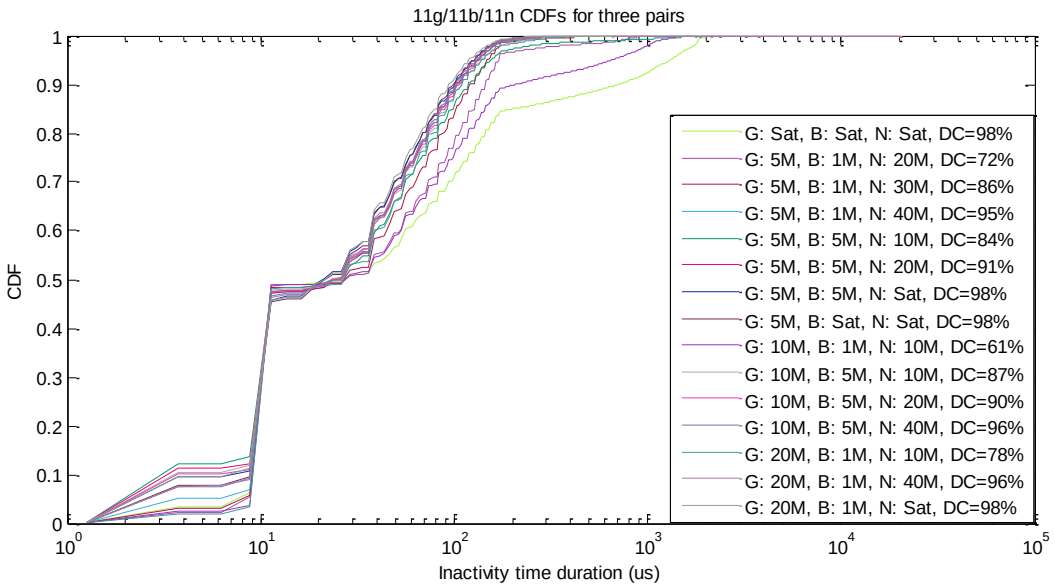

Figure 5-11. Three pairs bgn heterogeneous networks idle time distribution

Activity distributions

Activity-time fragment distributions for heterogeneous networks are of interest, as they aid in standard identification through energy detection, which is presented as an application in Chapter 8 of this document. Time duration of activity fragments represents transmitted frame duration, which is related to frame size, data rate, and frame aggregation. Detecting frame duration through energy detection provides an effective way for standard identification primarily because it does not require demodulation of received frames.

Figure 5-12 depicts 802.11g/n two-pairs heterogeneous networks activity CDFs for select tests. Frames belonging to the two standards can be distinguished by their time duration. 802.11b and g frame durations are generally fixed due to fixed frame size. A small number of these frames might have a specifically longer duration when an 802.11g terminal transmits at certain data rate that is lower than 54Mbps.

802.11n frame durations are variable and result from frame aggregation, which depends upon offered traffic, number of datagrams in the transmitter queue, and queue size. Similar behavior can be observed in Figure 5-13 for three pair 802.11b/g/n combination.

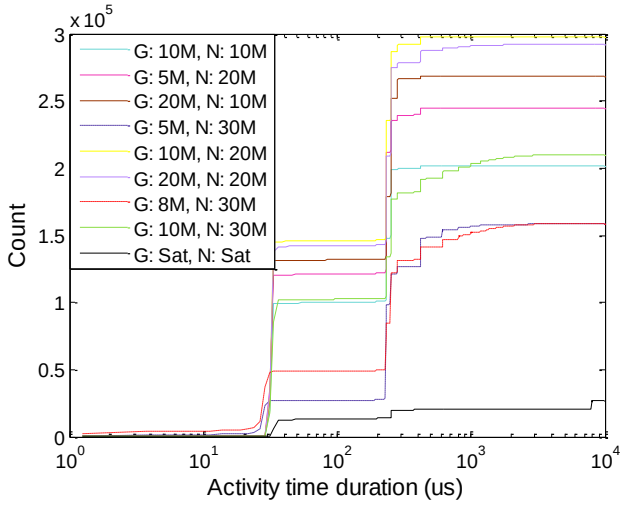

Figure 5-12. Two pairs heterogeneous networks activity distribution

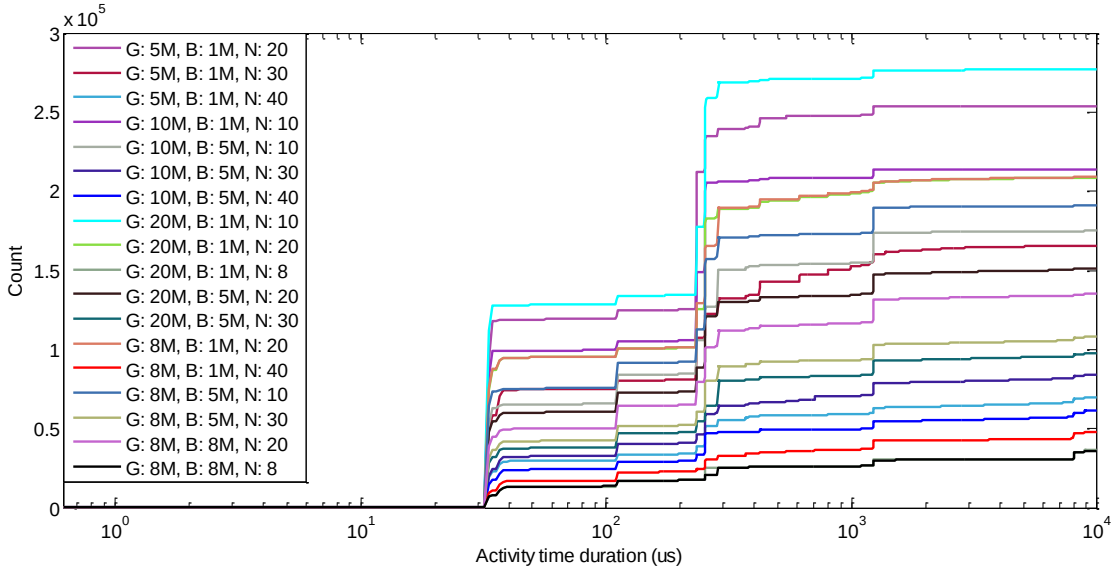

Figure 5-13. Three pairs heterogeneous networks activity distribution

Simulation results

This section discusses results obtained from simulation for 802.11g and compares them with experimental results. As previously discussed, simulation for an 802.11g network was developed for time distribution and DC comparison purposes and to assess possible enhancement to technologies coexisting with 802.11 networks in the ISM band. Figure 5-14 demonstrates similarities between experimental and simulation DC for 802.11g in both unsaturated and saturated network.

By examining CDF idle time in Figure 5-14, one can observe that idle-time distributions obtained from the experimental study and the simulation are comparable for saturated networks. Notably, dissimilarity becomes evident at time durations equal to or higher than the first back-off stage for unsaturated network. This results from the assumption of Poisson distributed frame arrival in the simulation, which is explained in more detail below. Saturation idle-time fragments result primarily from SIFS and DCF back-off durations because the transmitter queue is always saturated. Nevertheless, frame arrival to the transmitter queue had a higher impact on idle-time distribution at lower traffic.

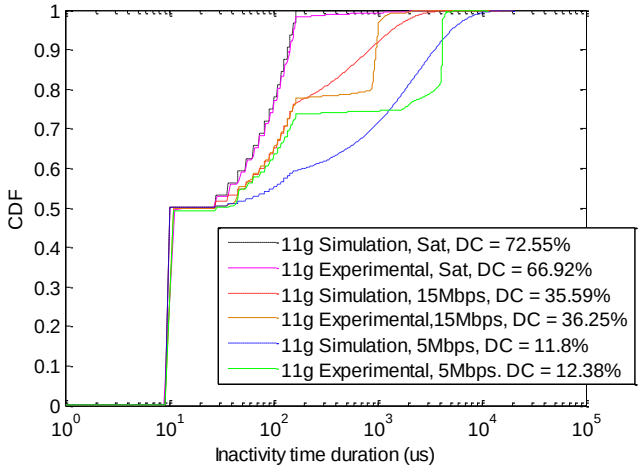

Figure 5-14. Simulation vs. experimental idle time distributions

In the simulation, frame arrival is modeled using a Poisson distribution, which is a popular and typical mathematical tool for modeling frame arrival into queue.

In presented experiments, Poisson distribution provided accurate results for modeling DC experimental measurement, as observed in Chapter 4. Given idle-time distribution, the simulation shows a steady increase in frequency for periods longer than the minimum contention window. Experimental idle-time distribution exhibits a sudden rise in percent of idle time fragments for the aforementioned idle-time region. This rise indicates that the specific transmitter application provided a deterministic frame arrival rate at a specific value. This phenomenon explains dissimilarity observed in Figure 5-14. Hence, 802.11 channel traffic patterns in an idle-time region higher than the minimum contention window is directly impacted by frame arrival to the queue.

In summary, traffic patterns are directly affected by both MAC layer standard and the queue frame arrival. Results demonstrated that an applied method for assessing traffic patterns on a wireless channel is necessary for both wireless coexistence and cognitive radio applications. An empirical modelling of 802.11 time distributions would provide a mathematical approach to capture realistic 802.11 networks temporal behavior.

Conclusion

This chapter presented an extensive temporal characterization of 802.11b, g and n traffic patterns. Presented results provided information about active and idle time distribution. These distribution illustrated behavior of 802.11 homogeneous and heterogeneous networks for one-, two- and pairs. Investigation were performed for throughput ranging

from low values to saturation and delivered critical information regarding wireless coexistence potential with 802.11 networks in the 2.4GHz ISM band.

Chapter 6: 802.11 Time Distributions Empirical Modeling

This chapter presents empirical modeling methodology and results for 802.11 homogeneous and heterogeneous networks. Empirical idle-time distributions obtained and discussed in previous chapters were used as a basis for this study. Modeling analysis was performed to accurately describe best-fit models for 802.11 empirical idle-time distributions. Doing so is essential for determining the appropriate design of wireless technologies able to coexist with 802.11 networks. Furthermore, the models serve as a foundation for enabling cognitive transmission on the ISM band. Idle-time distributions are of special interest, as they can be used to design a superior wireless network and improve performance of other coexisting wireless devices. Several approaches can be utilized to model idle-time distributions.

Earlier research focused on passive energy scanning of activity in various bands to build traffic pattern distribution and model idle-time distributions. Though this approach is valid for licensed bands, such practice is inadequate for the unsilenced ISM band. Traffic patterns in the heterogeneous ISM band are random in nature, as they depend on multiple parameters such as desired throughput, 802.11 networks combination, and number of transmitters in the network. To overcome this limitation, a comprehensive set of experiments was designed to encompass a wide variety of 802.11 combinations and traffic levels. The experimental setup was presented in Chapter 3 described in earlier chapters. Energy detection method was used to sense 802.11 activity and construct idle-time distributions. Later, idle-time distributions were modeled based on a number of mathematical distributions. Two metrics are used to evaluate constructed models. Figure 6-1 provides an overview of the work flow. A detailed description of the process is

provided in the following subsections to help the research community 1) reproduce the experiment; and 2) accurately utilize models in future research.

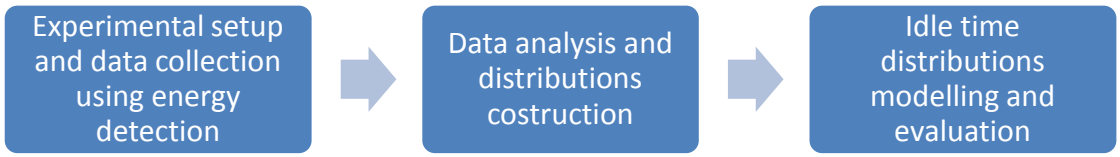

Figure 6-1. Process for analyzing 1.4GHz ISM band 802.11 idle time distributions

A number of candidate distributions (Exponential, Weibull, Log-Normal, Generalized Pareto, and Gamma) are selected and described based on previous literature work [22][20][72][19]. These candidate distributions are used as a starting point for deriving empirical 802.11 network idle-time Cumulative Distribution Functions (CDF). Two metrics, namely Kullback-Leibler divergence (D_{KL}) and Bhattacharyya distance, are described and discussed in the following section. These metrics are used to evaluate models with various distributions against 802.11 empirical idle-time distributions. Empirical modelling results for a variety of 802.11 combinations are then presented and evaluated. Finally, a set of best performing models that describe 802.11 combinations are presented.

Candidate distribution for 802.11 modelling

This section describes candidate distributions that were identified in a comprehensive search of the literature and utilized for empirical modeling reported in this chapter. The distributions serve as preliminary candidates to model 802.11 idle-time distributions in the ISM band. Table 9 provides notations used for distribution employed in this work.

Table 9. Notations

Notation	Description
$1/a$	Exponential distribution rate parameter
c	Scale
k	Shape
m	Log mean
s	Log standard deviation
θ	Threshold parameter

The following provides a description of corresponding distributions [73]:

Exponential distribution

The commonly known Exponential distribution has been widely used for modeling various physical phenomena, especially in networking applications. Exponential distribution describes the time between consecutive events (i.e., packet arrivals) in a Poisson process. Probability Density Function (PDF) and Cumulative Density Function (CDF) are given in (4) and (5):

$$f_E(t;a) = \frac{1}{a} e^{\frac{-t}{a}} \quad (4)$$

$$F_E(t;a) = 1 - e^{\frac{-t}{a}} \quad (5)$$

The following equations provide moments of the Exponential distribution:

$$E_E(t) = a \quad (6)$$

$$V_E(t) = a^2 \quad (7)$$

Weibull distribution

Weibull distribution is extensively used in reliability engineering, as well as other applications, given its simplicity and adaptability. The distribution is drastically affected

by its scale and shape parameters, c and k respectively. The flexibility of Weibull distribution is a primary reason for implementation in this investigation, as well as in other time-dimension spectrum modeling research reported in literature. The following equations provide PDF and CDF of Weibull distribution:

$$f_W(t;k,c) = \frac{k}{c}\left(\frac{t}{c}\right)^{k-1} e^{-\left(\frac{t}{c}\right)^k} \qquad (8)$$

$$F_W(t;k,c) = 1 - e^{-\left(\frac{t}{c}\right)^k} \qquad (9)$$

Moments of Weibull distributions are provided in (10) and (11):

$$E_W(t) = c.\Gamma\left(\frac{1}{k}+1\right) \qquad (10)$$

$$V_W(t) = c^2\left\{\Gamma\left(\frac{2}{k}+1\right) - \Gamma\left(\frac{1}{k}+1\right)^2\right\} \qquad (11)$$

where $\Gamma(.)$ is the complete Gamma function.

Log-normal distribution

Log-normal distribution corresponding variable is the product of a large number of independent and identically distributed (i.i.d), variables. Log-normal distribution is often used in wireless communications to describe received power fluctuations around a mean value. It has also been used for modelling spectrum occupancy CDFs for various licensed frequency bands. The following equations provide PDF and CDF of log-normal distribution:

$$f_{LN}(t;m,s) = \frac{1}{ts\sqrt{2\pi}} e^{-\frac{1}{2}\left(\frac{\ln t - m}{s}\right)^2} \qquad (12)$$

$$F_{LN}(t;m,s) = \frac{1}{2} + \frac{1}{2}\, erf\left(\frac{ln\, t - m}{s.\sqrt{2}}\right) \qquad (13)$$

Moments of Log-normal distribution provided in (14) and (15):

$$E_{LN}(t) = e^{m+\frac{s^2}{2}} \tag{14}$$

$$V_{LN}(t) = e^{2m+s^2}\left(e^{s^2} - 1\right) \tag{15}$$

Generalized Pareto distribution

Generalized Pareto distribution is often used to model tails of other distributions. This particular distribution is of special interest as it has shown plausible results when used in studies reported in literature for spectrum temporal distributions modeling. PDF and CDF of Generalized Pareto distribution are provided in the following:

$$f_{GP}(t; k, c, \theta) = \frac{1}{c}\left(1 + k\frac{(t-\theta)}{c}\right)^{-1-\frac{1}{k}} \tag{16}$$

$$F_{GP}(t; k, c, \theta) = 1 - \left(1 + k\frac{(t-\theta)}{c}\right)^{-\frac{1}{k}} \tag{17}$$

Equations 18 and 19 describe moments of Generalized Pareto distribution:

$$E_{GP}(t) = \theta + \frac{c}{1-k} \tag{18}$$

$$V_{GP}(t) = \frac{c^2}{(1-k)^2(1-2k)} \tag{19}$$

Gamma distribution

Gamma distribution is generally used to model the sum of exponentially distributed random variables. As such, it has been included in this work as a candidate distribution. Gamma distribution has shown favorable results for modeling Terrestrial Trunked Radio

(TETRA) idle-time distributions in literature [22]. The following formulas provide PDF and CDF of Gamma distribution:

$$f_G(t;k,c) = \frac{1}{\Gamma(k)c^k} t^{k-1} e^{-\frac{t}{c}} \quad (20)$$

$$F_G(t;k,c) = \frac{1}{\Gamma(k)} \gamma(k, \frac{t}{c}) \quad (21)$$

where; $\gamma(.)$ is the lower incomplete Gamma function.

Moments of Gamma distribution are described in (22) and (23):

$$E_G(t) = k\sigma \quad (22)$$

$$V_G(t) = k\sigma^2 \quad (23)$$

Models evaluation metrics

This section describes the metrics and methods used to evaluate the obtained 802.11 idle-time distribution models. Two metrics, namely Kullback-Leibler divergence and Bhattacharyya distance, were employed in this research to evaluate idle-time distribution models. The following subsections provide a brief description of each metric.

Kullback-Leibler divergence

Kullback-Leibler divergence (D_{KL}) represents the relative entropy between two distributions [74]. D_{KL} is commonly used as a measure to evaluate whether or not a set of data follows a particular model. The symmetric D_{KL} is described in (24):

$$D_{KL}^{sym} = \sum_{n=1}^{N} F(t_n) \ln(\frac{F(t_n)}{G(t_n)}) + \sum_{n=1}^{N} G(t_n) \ln(\frac{G(t_n)}{F(t_n)}) \quad (24)$$

where; $F(t_n)$ is the evaluated model and $G(t_n)$ represents idle-time distribution. The smaller the D_{KL} value is, the more representative the evaluated model of the idle-time distribution.

Bhattacharyya distance

The Bhattacharyya distance (D_B) is used as a measure of divergence between two distributions [75]. D_B is provided in (25):

$$D_B = -\ln\left(\sum_{n=1}^{N}\sqrt{F(t_n).G(t_n)}\right) \qquad (25)$$

In this work, D_B evaluates distribution $F(t_n)$ with mean μ_f and standard deviation σ_f, modeling idle-time distribution $G(t_n)$ with mean μ_g and standard deviation σ_g. D_B can alternatively be described using (26):

$$D_B = \frac{1}{4}\ln\left(\frac{1}{4}\left(\frac{\sigma_f^2}{\sigma_g^2}+\frac{\sigma_g^2}{\sigma_f^2}+2\right)\right)+\frac{1}{4}\left(\frac{\left(\mu_f-\mu_g\right)^2}{\sigma_f^2+\sigma_g^2}\right) \qquad (26)$$

As can be seen from (26), the first term in D_B represents the separation between the two variances belonging to the two distributions $F(t_n)$ and $G(t_n)$. The second term in D_B represents the distance between the mean values of the two distributions.

Generally speaking, D_{KL} provides a stronger measure to assess target models when compared to D_B, as it evaluates information divergence between two distributions, rather than the distance between the two distributions' moments. Therefore, D_{KL} was used to provide conclusions in the following section regarding which models best describe

802.11 empirical distributions. Nevertheless, both D_B and D_{KL} have been implemented in this study for the sake of comparison.

Empirical modelling results

This section presents and evaluates idle-time models when compared with corresponding empirical distributions for 802.11b, g, and n single- and multi-pair transmissions. Minor fluctuation can be observed when examining D_{KL} and D_B for different models at varying throughput values. Given a particular 802.11 combination, a single model was shown to outperform all other investigated models for most throughput value experiments for a corresponding combination.

Furthermore, it is possible that different 802.11 combinations and various number of pairs are best modeled by different distributions. Figure 6-2 to Figure 6-13 provide 802.11n, nn, nnn, gn, bn, and bgn combinations models, along with the results of the models evaluation metrics serving as examples. These include D_B and D_{KL} metrics calculated for different distributions modeling empirical idle time CDFs at different throughput values. Mean D_B and D_{KL} of all throughput values for different 802.11 combinations were shown in the figures to highlight various distribution performances. An optimal match between a particular distribution and its model is achieve when mean D_B and D_{KL} asymptote "0". As mean D_B and D_{KL} increase, the investigated model becomes less representative of the distribution. In this work, mean D_B and D_{KL} are used as relative measures to find particular models that best describe empirical distributions compared to others. The following notations are used to describe the studied distributions—E: Exponential, W: Weibull, LN: Log-Normal, GP: Generalized Pareto, and G: Gamma.

Figure 6-2 indicates that, according to D_{KL} divergence metric, Gamma distribution outperforms others in describing 802.11n idle-time distribution. Gamma distribution ranks second with minimal difference over Log-Normal distribution, according to $D_B$distance. D_{KL} divergence and D_B distance metrics provided comparable conclusions for most 802.11 combinations. Both metrics are shown in the following graph. Notably, the analysis included only D_{KL} divergence to avoid unnecessary reiteration. The reason for adopting D_{KL} divergence was previously discussed in detail.

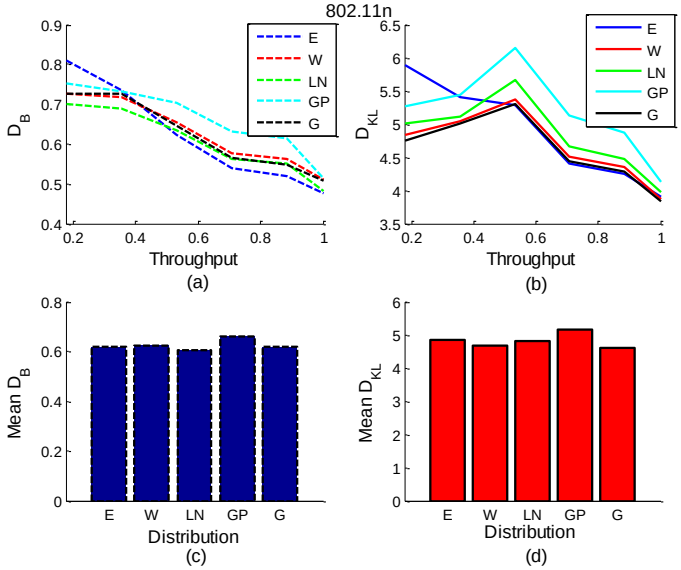

Figure 6-2. 802.11n models evaluation metrics a) D_B for various throughput values a) D_{KL} for various throughput values c) Mean D_B d) Mean D_{KL}

Figure 6-3 depicts 802.11n models overlaying their corresponding empirical distribution. Clearly, all models diverge from the empirical distribution for very low idle-time durations, which correspond to DCF minimum contention window. Note the logarithmic scale for idle-time duration in the presented graphs. Shorter idle-time duration distributions may be better described with discrete geometric distribution. Nevertheless presented models converge to the empirical distribution for higher idle-time duration. A more in-depth discussion of this phenomenon is provided later in this section to highlight

the significance of longer idle-time duration when compared with shorter durations, as well as to emphasize the need for accurate descriptions of their distribution.

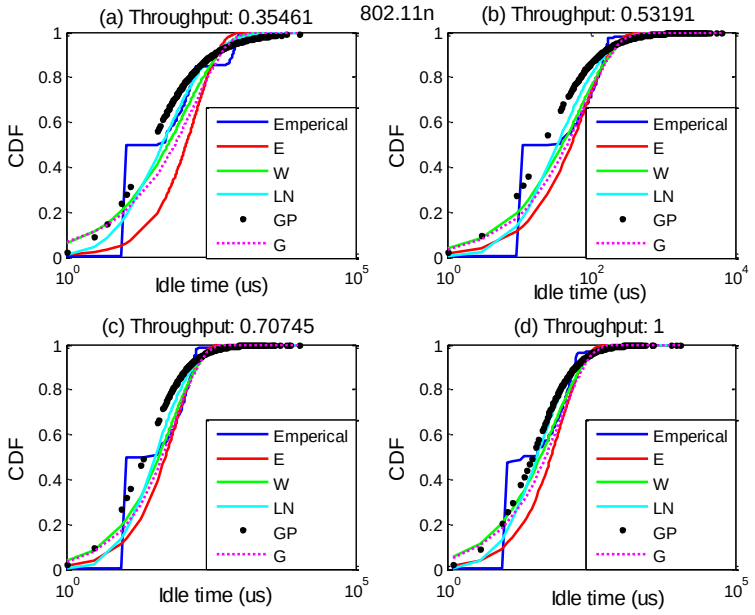

Figure 6-3. 802.11n models vs. empirical distribution for different throughput levels

Figure 6-4 demonstrates that Weibull distribution best describes 802.11nn combination, slightly outperforming Gamma and Generalized Pareto distributions. Figure 6-6 shows that Weibull distribution best describes 802.11nnn combination, as well. Gamma, Generalized Pareto, and Exponential distributions for 802.11nnn combination provided relatively similar results.

Figure 6-5 depicts empirical distribution overlaid with 802.11nn models and shows more satisfactory results for low idle-time duration when compared with the 802.11n combination. Similarly, Figure 6-7, Figure 6-9, Figure 6-11, and Figure 6-13 depict 802.11nnn, gn, bn and gbn combination models, respectively with corresponding empirical distribution. Corresponding D_{KL} and D_B results for these combinations are depicted in Figure 6-6, Figure 6-8, Figure 6-10, and Figure 6-12 Best results were found

for the 802.11nnn combination; poorest results were observed for the 802.11gbn combination.

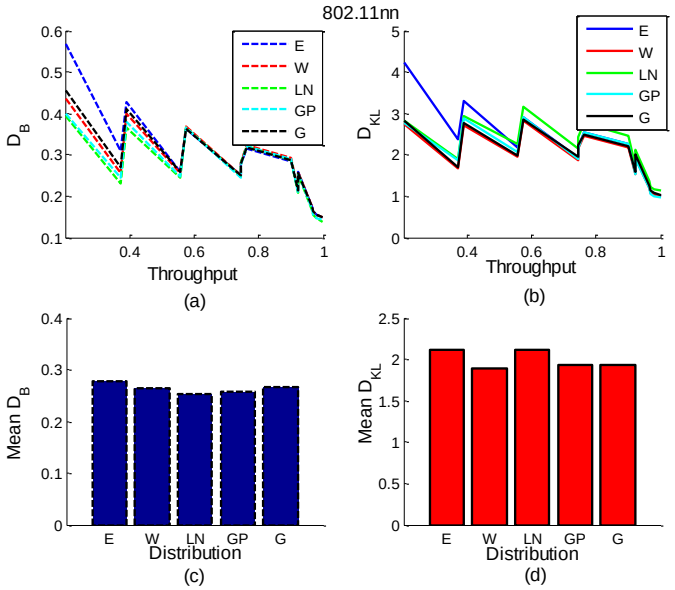

Figure 6-4. 802.11nn models evaluation metrics a) D_B for various throughput values, b) D_{KL} for various throughput values, c) Mean D_B d) Mean D_{KL}

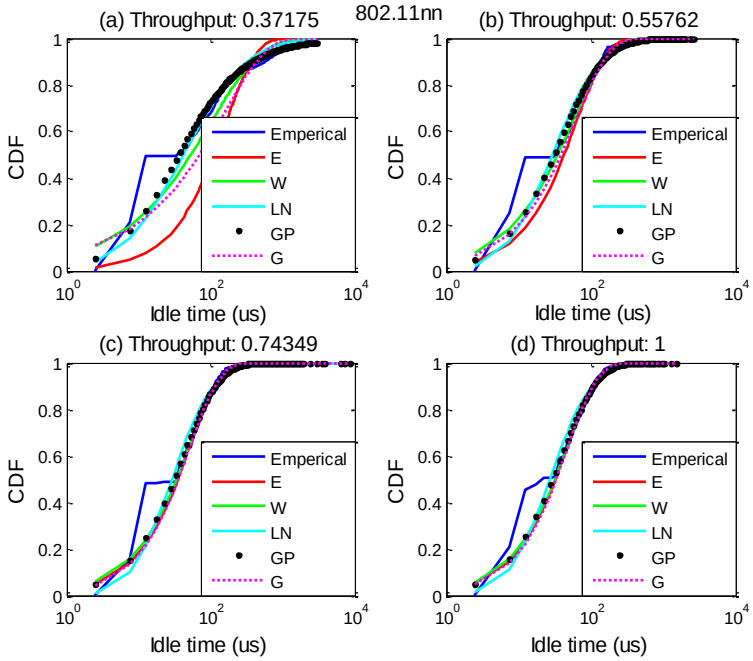

Figure 6-5. 802.11nn models vs. empirical distribution for different throughput levels

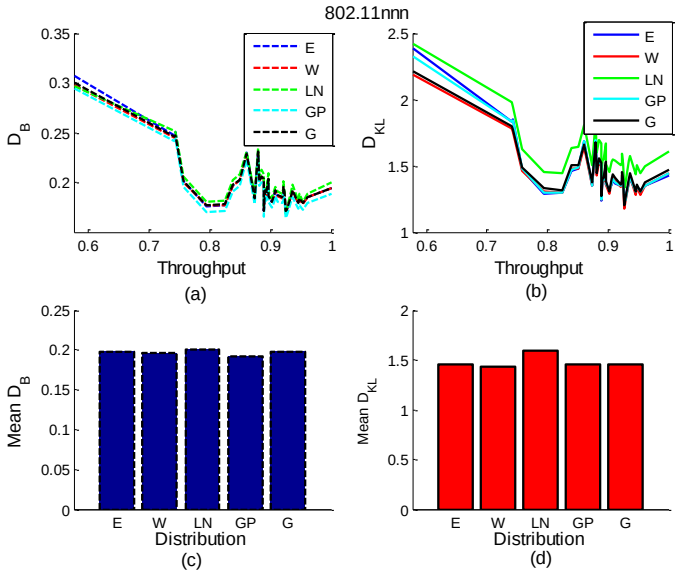

Figure 6-6. 802.11nnn models evaluation metrics a) D_B for various throughput values, b) D_{KL} for various throughput values, c) Mean D_B d) Mean D_{KL}

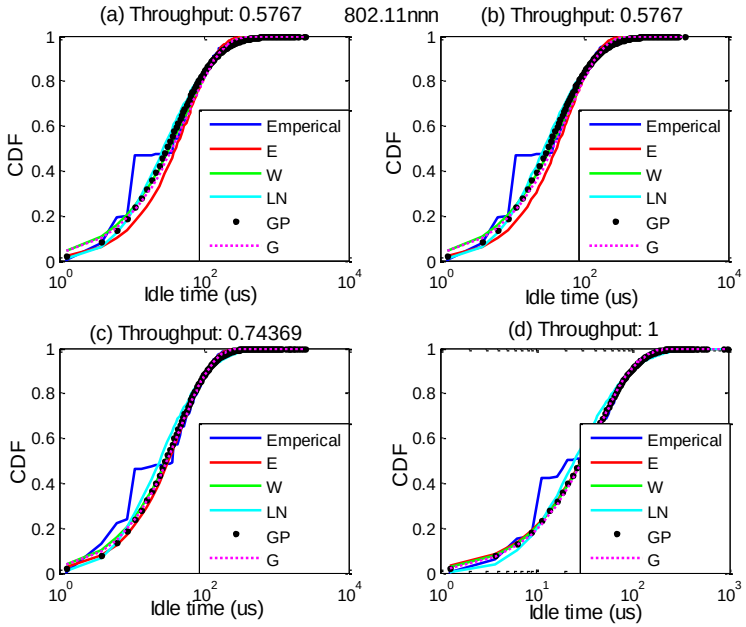

Figure 6-7. 802.11nnn models vs. empirical distribution for different throughput levels

As for heterogeneous 802.11 combinations, Figure 6-8 demonstrates that Generalized Pareto outperforms other distributions for 802.11gn combination. See Figure 6-10 and Figure 6-12 for 802.11 802.11bn and bgn combinations D_{KL} and D_B. Weibull distribution provided best results for 802.11bn combination and 802.11ggn combinations. 802.11bgn

and 802.11nng combinations were best modeled by a Log-normal distribution. Generalized Pareto outperformed the other studied models for all other 802.11 heterogeneous combinations. Table 10 presents mean D_{KL} for complete distribution models corresponding to all studied 802.11 combinations.

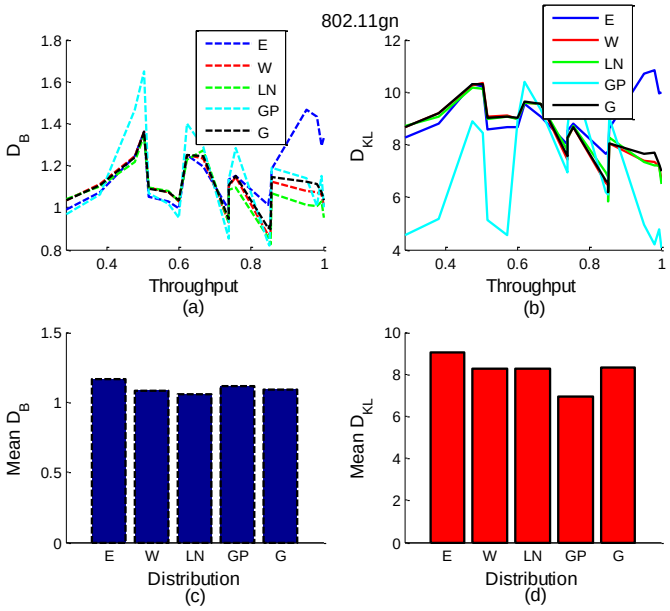

Figure 6-8. 802.11gn models evaluation metrics a) D_B for various throughput values, b) D_{KL} for various throughput values, c) Mean D_B d) Mean D_{KL}

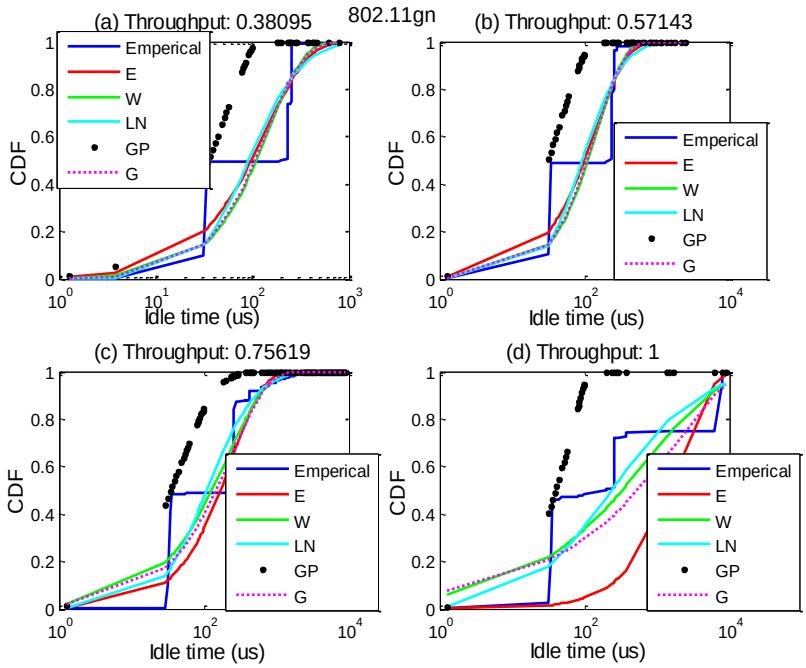

Figure 6-9. 802.11gn models vs. empirical distribution for different throughput levels

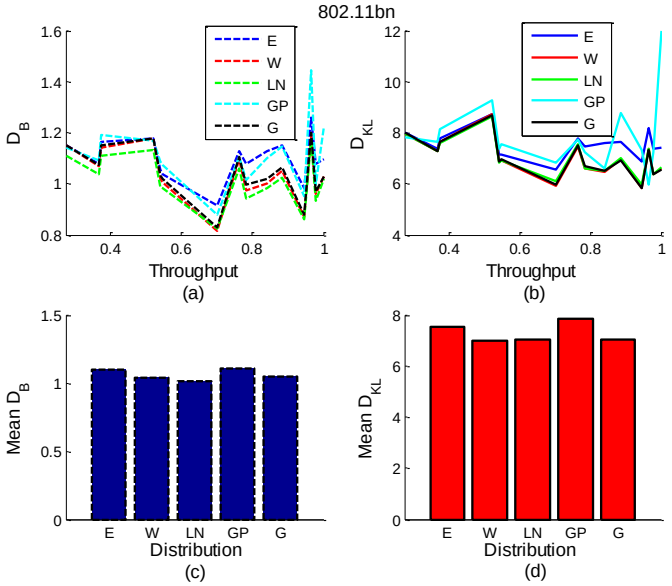

Figure 6-10. 802.11bn models evaluation metrics a) D_B for various throughput values, b) D_{KL} for various throughput values, c) Mean D_B d) Mean D_{KL}

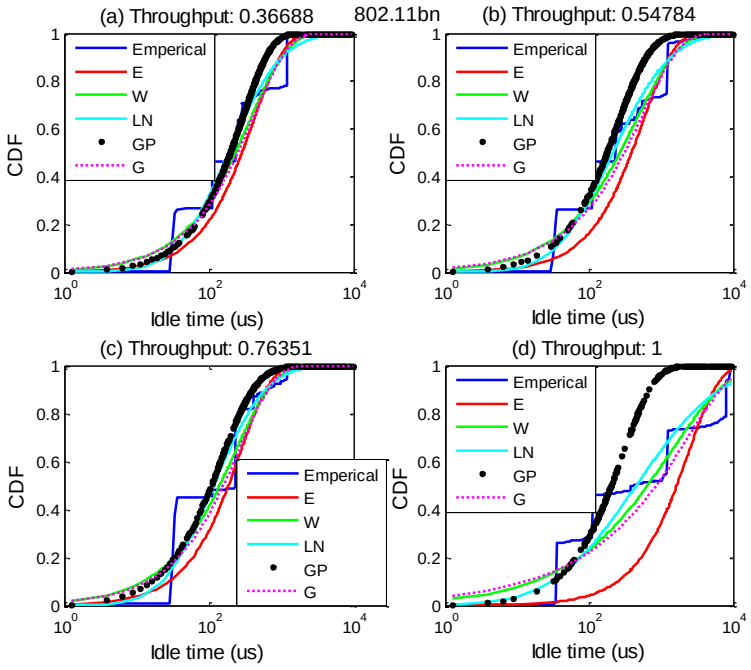

Figure 6-11. 802.11bn models vs. empirical distribution for different throughput levels.

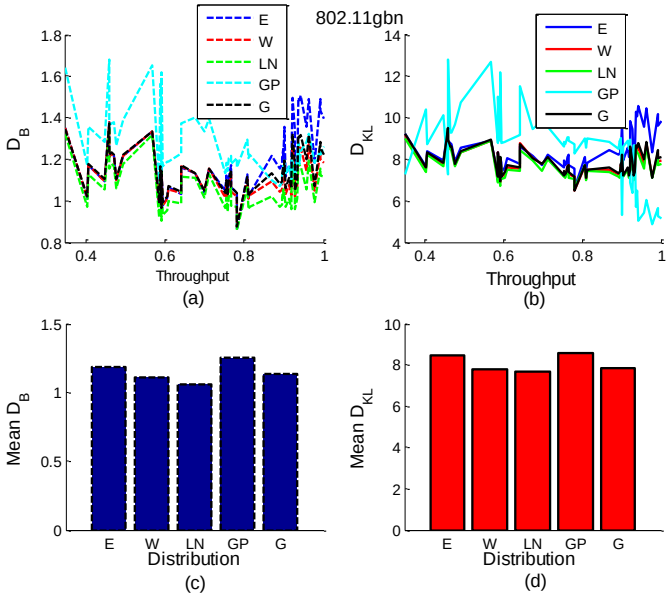

Figure 6-12. 802.11gbn models evaluation metrics a) D_B for various throughput values, b) D_{KL} for various throughput values, c) Mean D_B d) Mean D_{KL}

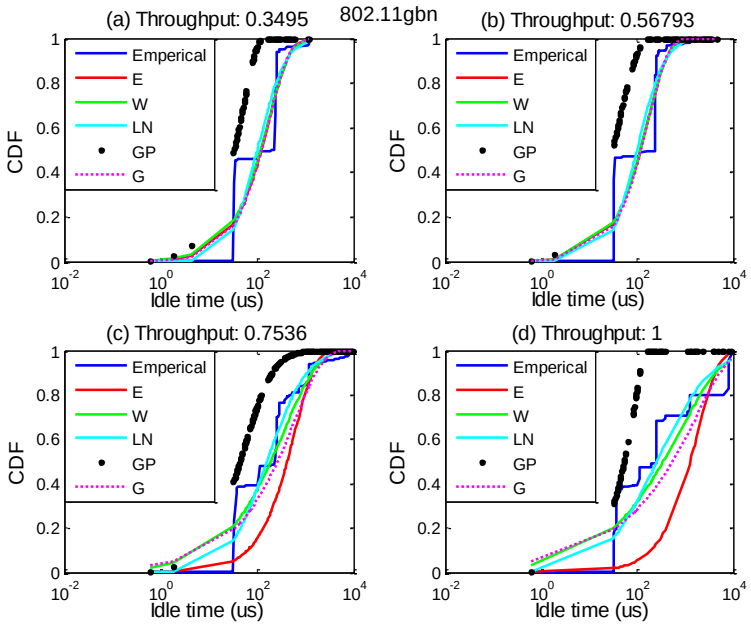

Figure 6-13. 802.11gbn models vs. empirical distribution.

As previously discussed, the models presented were found to diverge from empirical distributions for low idle-time durations (i.e., those below DCF minimum contention window durations). Presented models converged to their corresponding idle-time empirical distributions at durations higher than minimum contention window durations. This work offers more emphasis on larger idle-time durations longer than that of DCF minimum contention window. Such idle-time durations form a more significant part of the distribution for two main reasons:

1. Idle-time durations correspond to the majority of studied distributions, meaning that durations for the contention window are limited to a few hundred *micro*seconds. Nevertheless, an idle-time duration higher than the minimum contention window can extend to several *milli*seconds, an order of magnitude higher.

Table 10. Complete distibutions emperical modelling D_{KL} results for 802.11 networks

	Complete distribution D_{KL}				
	Exponential	Weibull	Log-Normal	Generalized Pareto	Gamma
802.11b	5.47	3.88	4.13	4.37	**3.78**
802.11bb	1.80	1.23	1.44	1.53	**1.16**
802.11bbb	3.26	2.47	2.80	2.85	**2.37**
802.11g	5.94	5.15	5.23	5.40	**5.14**
802.11gg	2.31	**1.59**	1.70	1.61	1.68
802.11ggg	2.85	**2.74**	2.99	2.82	2.78
802.11n	4.85	4.66	4.81	5.17	**4.61**
802.11nn	2.11	**1.89**	2.11	1.94	1.94
802.11nnn	1.45	**1.43**	1.59	1.45	1.46
802.11bn	7.53	**6.99**	7.01	7.82	7.01
802.11gn	9.02	8.24	8.25	**6.92**	8.31
802.11gb	7.88	7.60	7.44	**5.65**	7.68
802.11bbg	9.10	8.79	8.68	**6.12**	8.86
802.11ggb	8.73	8.45	8.32	**5.86**	8.54
802.11bbn	8.99	8.30	8.16	**7.94**	8.40
802.11nnb	9.01	7.73	7.67	**7.59**	7.81
802.11nng	6.47	5.86	**5.63**	6.52	6.01
802.11ggn	8.62	**7.62**	7.69	7.75	7.82
802.11gbn	8.44	7.79	**7.67**	8.55	7.85

2. Larger time durations might be practically used by other coexisting technologies to perform transmissions while minimizing collision risk with 802.11 transmission. Notably, this solution is generally not feasible for lower 802.11 idle-time durations. For example, an 802.15.4 ZigBee header is 25 bytes long.

Considering ZigBee data rate of 250kbps, the header would only require 800µs for transmission, which would not be feasible within a DCF time frame.

Figure 6-14 to Figure 6-17 show idle time models compared with empirical distributions for 802.11nnn, bn, gn, and gbn combinations at medium throughput levels. Theses graphs represent previously discussed empirical distributions and their corresponding models for time durations higher than 0.8 milliseconds with linear idle-time duration axis scale. The figures show that there always exists a model that provides satisfactory representation for empirical idle-time distributions that correspond to various 802.11 combinations.

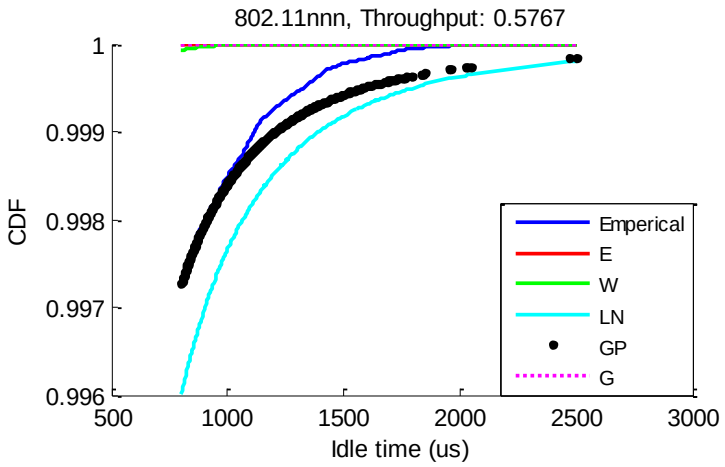

Figure 6-14. Above minimum contention window802.11nnn models vs. empirical distribution

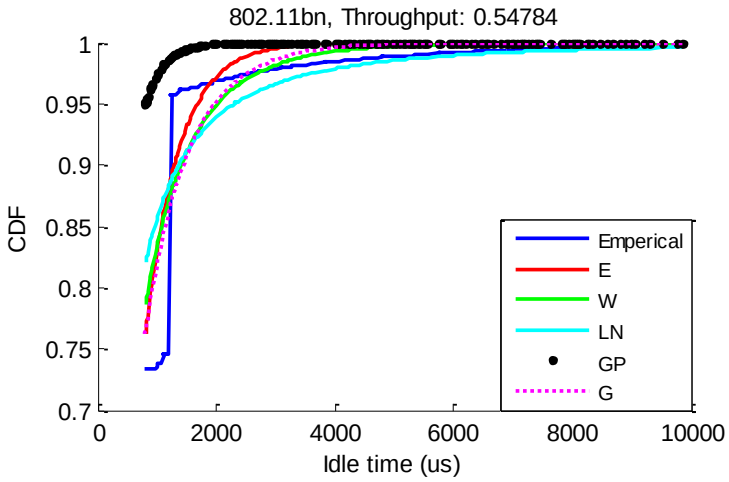

Figure 6-15. Above minimum contention window 802.11bn models vs. empirical distribution

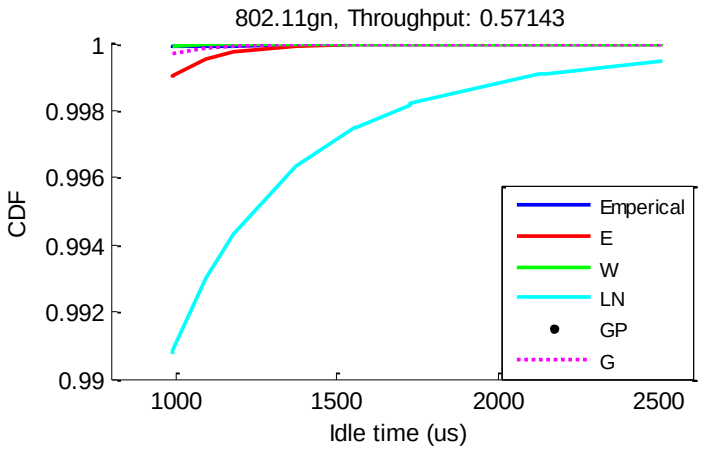

Figure 6-16. Above minimum contention window 802.11gn models vs. empirical distribution

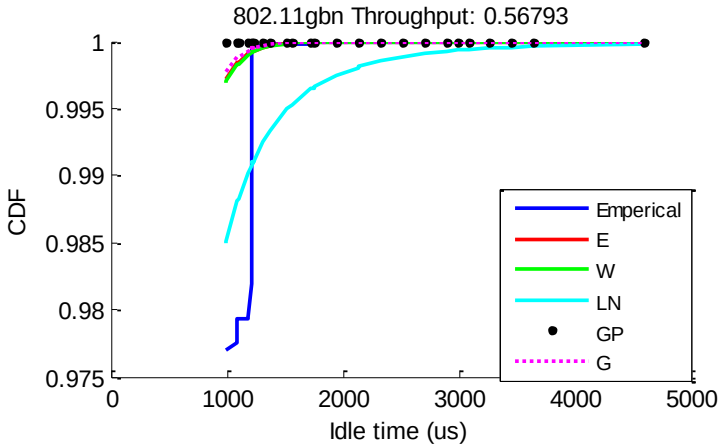

Figure 6-17. Above minimum contention window 802.11gbn models vs. empirical distribution

D_{KL} and D_B metrics were calculated and presented for idle-time durations longer than that of the minimum contention window. Such representation provides a more thorough analysis of the investigated models. In turn, this analysis supports the notion of choosing the most suitable model for each 802.11 combination.

Conclusion

A comprehensive empirical modelling of 802.11b, g and n homogeneous and heterogeneous networks idle time distributions has been presented in this chapter. Experimental data was collected for a complete set of 802.11 networks combinations at

a wide range of throughput values. Two metrics, Kullback-Leibler divergence and Bhattacharyya distance, were employed to evaluate different models and how well they describe the actual idle time distributions.

Results demonstrated that 802.11b and g homogeneous networks are best described using Weibull distribution whereas 802.11n networks can be best modeled with Log-normal models. Heterogeneous 802.11 networks combinations on the other hand were best modeled using Exponential distribution, Log-normal distribution or Generalized Pareto distribution depending on the combination. Nevertheless, it was observed that a heterogeneous distribution would generally follow a Generalized Pareto distribution whenever the medium includes transmission from one or more 802.11n pairs.

Table 11 presents mean D_{KL} for all studied 802.11 combination distributions above minimum contention window (i.e., above 0.8ms). This table also provides mathematical expressions describing best model for each of the studied 802.11 combinations at a given saturation.

Notably, homogeneous 802.11b and 802.11g for one-, two-, and three-pair combinations were best described using Weibull distribution. 802.11n homogeneous combinations are best modeled using Log-Normal distribution. 802.11n follows enhanced MAC-layer standards implementing frame aggregation, which explains the 802.11n variation from both 802.11b and g. With regard to heterogeneous 802.11 networks, all three-pair combinations containing 802.11n transmitter are best modeled using Generalized Pareto distribution. Two- and three–pair combinations containing only 802.11b and g transmitters follow an Exponential distribution. Adding a second 802.11b pair to the 802.11bg network resulted in a sharper rise in CDF. Idle-time durations are further fragmented, and their number is reduced due to a long duration of the 802.11b frame, resulting from the standard's lower data rate. Distribution parameters obtained in this work for different homogeneous and heterogeneous networks combinations can be found in Appendix I.

Conclusion

A comprehensive empirical modelling of 802.11b, g and n homogeneous and heterogeneous networks idle time distributions has been presented in this chapter. Experimental data was collected for a complete set of 802.11 networks combinations at

a wide range of throughput values. Two metrics, Kullback-Leibler divergence and Bhattacharyya distance, were employed to evaluate different models and how well they describe the actual idle time distributions.

Results demonstrated that 802.11b and g homogeneous networks are best described using Weibull distribution whereas 802.11n networks can be best modeled with Log-normal models. Heterogeneous 802.11 networks combinations on the other hand were best modeled using Exponential distribution, Log-normal distribution or Generalized Pareto distribution depending on the combination. Nevertheless, it was observed that a heterogeneous distribution would generally follow a Generalized Pareto distribution whenever the medium includes transmission from one or more 802.11n pairs.

Table 11. Above minimum contention window emperical modelling for 802.11 networks

Combination	Above minimum contention window distribution D_{KL}					Best Saturation distribution
	Exponential	Weibull	Log-normal	Generalized Pareto	Gamma	
802.11b	1.12	0.59	**0.58**	0.62	0.61	$F_w(t) = 1 - e^{-\left(\frac{t}{70.11}\right)^{0.58}}$
802.11bb	0.39	**0.14**	0.15	0.18	0.16	$F_w(t) = 1 - e^{-\left(\frac{t}{38.47}\right)^{0.63}}$
802.11bbb	0.18	**0.04**	0.06	0.10	0.06	$F_w(t) = 1 - e^{-\left(\frac{t}{45.76}\right)^{0.65}}$
802.11g	0.65	**0.46**	**0.46**	0.49	0.47	$F_w(t) = 1 - e^{-\left(\frac{t}{58.81}\right)^{0.79}}$
802.11gg	0.24	**0.12**	0.13	0.14	**0.12**	$F_w(t) = 1 - e^{-\left(\frac{t}{42.77}\right)^{0.96}}$
802.11ggg	0.03	**0.01**	**0.01**	**0.01**	**0.01**	$F_w(t) = 1 - e^{-\left(\frac{t}{43.36}\right)^{0.97}}$
802.11n	0.26	0.17	**0.16**	0.18	0.19	$F_{LN}(t) = \frac{1}{2} + \frac{1}{2}\,\mathrm{erf}\left(\frac{\ln t - 3.58}{1.25.\sqrt{2}}\right)$
802.11nn	0.08	**0.05**	**0.05**	**0.05**	0.06	$F_{LN}(t) = \frac{1}{2} + \frac{1}{2}\,\mathrm{erf}\left(\frac{\ln t - 3.3}{1.05.\sqrt{2}}\right)$
802.11nnn	0.01	0.00	**0.00**	0.00	0.00	$F_{LN}(t) = \frac{1}{2} + \frac{1}{2}\,\mathrm{erf}\left(\frac{\ln t - 3.22}{1.07.\sqrt{2}}\right)$
802.11bn	2.37	1.80	**1.66**	1.71	1.92	$F_{LN}(t) = \frac{1}{2} + \frac{1}{2}\,\mathrm{erf}\left(\frac{\ln t - 6.11}{2.1.\sqrt{2}}\right)$
802.11gn	1.45	0.77	0.69	**0.21**	0.93	$F_{GP}(t) = 1 - \left(1 - 0.57\frac{(t-0.5)}{68.19}\right)^{\frac{1}{0.57}}$
802.11gb	**0.48**	0.51	0.53	NA	0.50	$F_E(t) = 1 - e^{\frac{-t}{328.85}}$
802.11bbg	**1.29**	1.34	1.35	NA	1.33	$F_E(t) = 1 - e^{\frac{-t}{431.15}}$
802.11ggb	**0.60**	0.62	0.64	NA	0.61	$F_E(t) = 1 - e^{\frac{-t}{334.41}}$
802.11bbn	3.97	3.30	3.02	**1.82**	3.52	$F_{GP}(t) = 1 - \left(1 - 0.67\frac{(t-0.5)}{74.85}\right)^{\frac{1}{0.67}}$
802.11nnb	4.85	3.45	3.19	**1.94**	3.69	$F_{GP}(t) = 1 - \left(1 - 0.16\frac{(t-0.5)}{149.82}\right)^{\frac{1}{0.16}}$
802.11nng	1.18	0.75	0.55	**0.46**	1.00	$F_{GP}(t) = 1 - \left(1 + 1.81\frac{(t-0.5)}{26.57}\right)^{-\frac{1}{1.81}}$
802.11ggn	1.62	0.95	0.73	**0.57**	1.23	$F_{GP}(t) = 1 - \left(1 + 0.96\frac{(t-0.5)}{26.93}\right)^{-\frac{1}{0.96}}$
802.11gbn	2.18	1.49	1.32	**0.97**	1.70	$F_{GP}(t) = 1 - \left(1 - 0.36\frac{(t-0.5)}{108.03}\right)^{\frac{1}{0.36}}$

Chapter 7: Applications and Case Studies

Previous chapters have detailed temporal characterization of 802.11 networks in the ISM band. This chapter presents two applications of such characterizations: 1) 802.15.4 ZigBee adaptive packet size, and 2) Wireless standards identification through machine learning [76]. Algorithm and measurement methods used to obtain spectrum occupancy; 802.11 temporal distributions; and the empirical modelling of 802.11 idle time distributions are discussed.

The first application aims at enhancing 802.15.4 ZigBee performance in the presence of 802.11 interference by adaptively changing 802.15.4 ZigBee packet size to maximize the probability of coexistence, and thus duration, based on the mean value of 802.11g idle time distribution. Achieved results indicated reduced 802.15.4 ZigBee PER. The second application is to blindly differentiate among the various 802.11 standards and identify the number of transmitters with transmission range without demodulating 802.11 frames transmitted over the medium. This process was achieved constructing 802.11 distributions using energy detection. Features extracted from these distributions were used by machine-learning algorithms to identify wireless networks and terminals.

Notably, both experimental and simulation setups presented in Chapter 3 are employed in the work presented in this chapter to achieve the two aforementioned distributions. More details on the developed methodology to construct the applications and the obtained results are provided in the following sections.

Application 1: 802.15.4 ZigBee adaptive packet size

This section presents a case study highlighting usability of channel temporal traffic pattern occupancy awareness for enhancing performance of wireless technologies coexisting with 802.11 networks. 802.15.4 ZigBee, referred to as ZigBee from this point forward, was used as an example of ISM band technology coexisting with 802.11g network in this application. For the purpose of this proof of concept, ZigBee simulation and 802.11g simulation were used. A validation of ZigBee simulation is first discussed, and then methodology and results of this application are presented in the following subsections.

802.15.4 ZigBee simulation validation

A set of experiments was designed and executed to compare ZigBee PER results obtained from experimental test to those obtained from simulation.

Experimental setup included two 802.11g terminals (i.e., a transmitter and a receiver) placed equidistant from the ZigBee device under test (DUT), see Figure 7-1. Transmit power for 802.11g terminals was set to 16 dBm, and data was exchanged at varying DC—from low values to saturation. ZigBee RSS was maintained at -70 dBm (±1 dB) for all tests to ensure that ZigBee receiver was situated at the edge of its cell with zero percent PER [7]. Test runs were performed in a 6.6m x 4m x 3m anechoic chamber to avoid unintended interference. For each test run, 1000 ZigBee packets were sent.

To obtain ZigBee PER through simulation setup, 802.11g activity times were generated for one pair 802.11g network. ZigBee simulation was then run, wherein a packet was transmitted using the 802.15.4 CSMA/CA scheme. Both 802.11g and 802.15.4 ZigBee

simulations are described in greater detail in Chapter 3. ZigBee PER was collected for increasing 802.11g DC values.

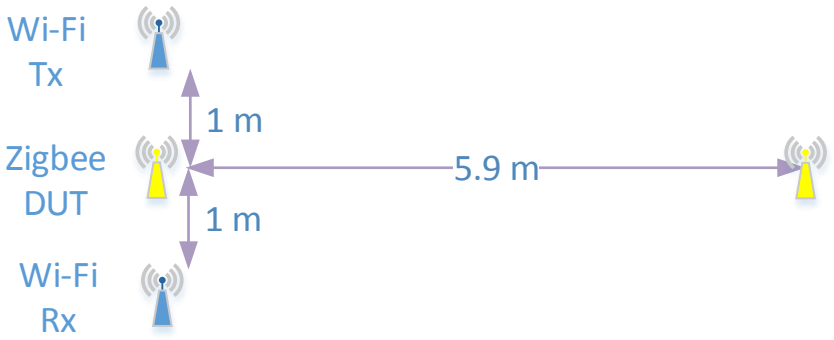

Figure 7-1. 802.15.4 ZigBee and 802.11g coexistence experimental setup

A comparison of PER results for both the experimental setup and simulation is provided in Figure 7-2. Clearly, simulation PER results are comparable with experimental PER results. PER difference was higher for larger DC values; difference in PER did not exceed 7% for all DC values.

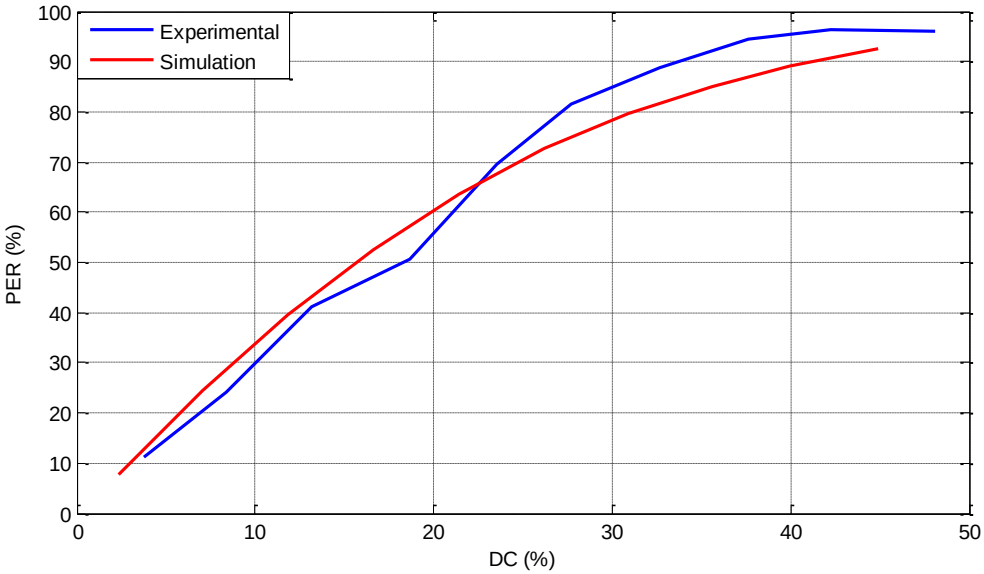

Figure 7-2. 802.15.4 ZigBee PER simulation vs. experimental results

Methodology and results

This subsection offers the methodology for implementing adaptive ZigBee packet size, as well as obtained results from this investigation. ZigBee packet size was adaptively changed based on 802.11g idle time distribution using simulation setup. Mean 802.11g idle time value was calculated for a distribution region higher than the minimum contention window (i.e., third idle time distribution region, which was described in Chapter 4). ZigBee packet size was set to the immediate integer number of Bytes with time duration smaller than calculated 802.11g idle time distribution mean. Simulation implemented a worst-case interference scenario (i.e., any overlap between ZigBee and 802.11 traffic renders a ZigBee packet corrupted).

802.15.4 ZigBee standard limits maximum ZigBee packet size to 127 Bytes, including a 25 Byte header. Adaptive packet size was constrained by the standard's boundaries in this work: an upper bound of 127 Bytes and lower bound of 26 Bytes. ZigBee adaptive packet size PER and throughput were tracked for increasing 802.11g DC. Results were compared to ZigBee fixed packet size PER and throughput. Fixed packet sizes, including headers, were 125, 100, 75, and 30 bytes. Table 12 shows calculated adaptive ZigBee packet size for various throughput/DC values.

Table 12. ZigBee adaptive packet sizes

802.11G DUTY CYCLE (%)	802.11G THROUGHPUT (MBPS)	ZIGBEE PACKET SIZE (BYTES)
2.32	1	127
7.09	3	127
11.8	5	80
16.6	7	58
21.33	9	47
26.2	11	39
30.87	13	34
35.59	15	30
39.97	17	27
44.87	19	26

Figure 7-3 and Figure 7-4 show ZigBee PER and throughput, respectively, for both adaptive (in black) and fixed packet sizes. Large fixed packet sizes exhibited a high throughput for low 802.11g DC and poor performance at high 802.11g DC. In contrast, small fixed packet sizes demonstrated poor performance for low 802.11 DC and improved performance for high DC. Results indicate a tradeoff between PER and packet payload-to-header ratio. Large packet sizes perform better at low 802.11g duty cycle due to a high ratio of packet payload-to-header, whereas small packet sizes perform better at high 802.11g DC given that they suffer fewer collisions.

The adaptive packet size method introduced in this work demonstrates a throughput comparable to the highest fixed packet size performance, regardless of 802.11g DC value, as shown in Figure 7-3. The method revealed throughput improvement of up to 66% over fixed packet size of 30 bytes at low duty cycle of 2.3%. Moreover, the method showed significant improvement over fixed packet size of 125 bytes at medium and high utilization of channel DC.

Adaptive ZigBee packet size also showed significant improvement in PER, as shown in Figure 7-4. For certain cases adaptive ZigBee packet size resulted in PER drop of up to 25% when compared to the upper end fixed packet size of 125 Bytes.

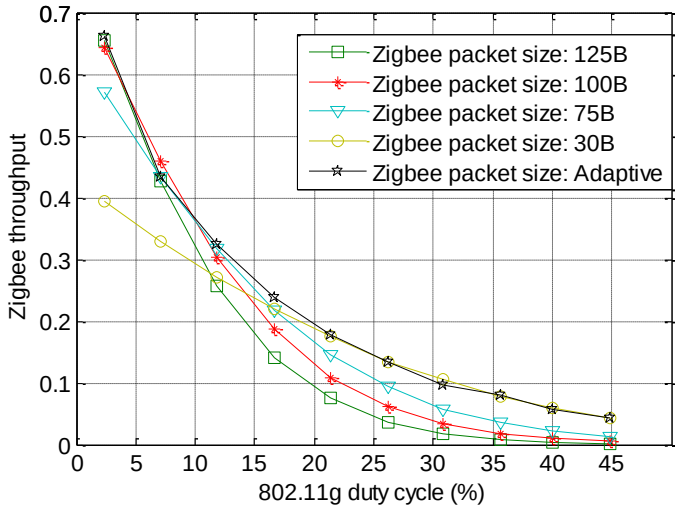

Figure 7-3. ZigBee throughput for fixed and adaptive packet sizes

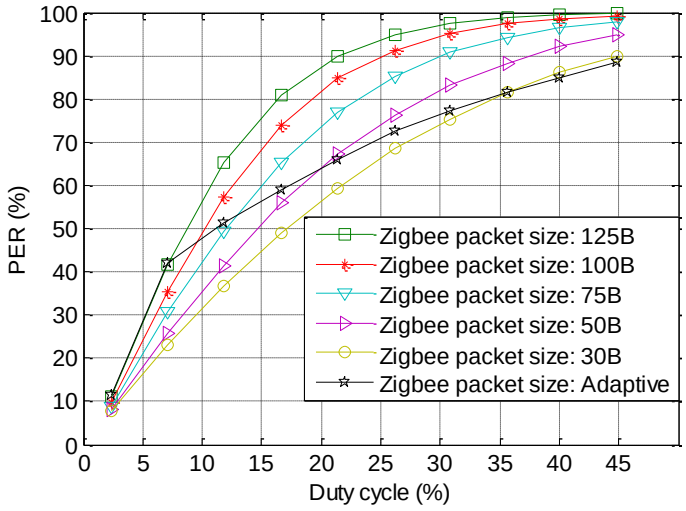

Figure 7-4. ZigBee PER for fixed and adaptive packet sizes

Application 2: Wireless technology identification through machine learning

This section presents identification of 802.11 standards and number of transmitters as an application of 802.11 temporal characterization. Identification was performed blindly using 802.11 idle time and activity distributions obtained via energy detection. Features characteristic of different standards and number of transmitters are first extracted from 802.11 idle time and activity distributions. Features are then input into a trained machine-

learning algorithm that is responsible for classifying a particular observation into corresponding standard and number of transmitters. Wireless technology identification enables situational awareness to improve coexistence and reduce interference among the devices. Details on the methodology and obtained results for this application are provided in the following subsection.

Methodology

This subsection details the methodology employed to perform wireless technology identification. Presented work is based on an energy detection technique with the following three stages:

Stage 1, Data collection and processing:

Simple energy detection scheme is implemented to measure RSS. Collected measurements are compared with a pre-set threshold to determine time periods while the channel is active (i.e., transmission is detected) or inactive (i.e., channel is idle). Temporal characteristics consisting of activity and idle time distributions are then derived by constructing histograms of active time periods and idle time periods, respectively. Time bin widths used in the histograms were: 1) 1.25μs for idle time periods; and 2) 2.5μs for activity periods. Time bin duration was short enough to accurately capture MAC layer temporal characteristics of the protocols under study (i.e., 802.11b/g/n). The lowest expected idle time period corresponds to the 802.11g/n MAC SIFS of 10μs, while the lowest expected activity period corresponds to 802.11b/g MAC acknowledgment (ACK) packet length of 30μs.

Stage 2, Feature extraction and data set construction:

Distinguishing features are extracted from activity and idle time distributions in Stage 2. A dataset consisting of features extracted from multiple scans is constructed to train a specific classifier, and then to test its accuracy for identifying the wireless technology in use. The set of features extracted from each particular energy scan is referred to as an *observation*. A set of multiple observations for different wireless technologies is referred to as a *dataset*.

Since each wireless standard/technology has a unique MAC and PHY protocol implementation, a distinguishable temporal traffic characteristic exist. Temporal traffic patterns in this work are described via activity and idle time distributions, which were constructed from energy scanning data, as discussed in great detail in Chapter 4.

Specific features able to differentiate wireless technologies are then extracted from aforementioned distributions. A combination of features were used to make an identification decision on wireless technologies utilizing the spectrum. A set of features was extracted from each distribution for a specific test run representing a single observation. Examples of such features include frequency of idle time durations at specific distribution regions; distribution mean and its standard deviation; and mean and standard deviation of a specific region within the distribution. Observations from multiple test runs are then grouped into a single dataset for further analysis. To clarify, a distribution region represents a specific time span in idle time or activity distribution. This time span contains information characteristic of a particular wireless technology (e.g., activity time region near 111μs representing 802.11b ACK). Frequency of 802.11b ACKs, along with other

characterizing features, can be employed to construct the dataset that can be used for wireless technology identification.

A total of 596 tests for 802.11 networks were used to evaluate the proposed method in this work. The experimental setup for these tests is discussed in Chapter 3. 802.11 time distributions and specific features chosen to identify different 802.11 networks are discussed in the following sections. However, these features are not discussed in this section to purposefully maintain a generic methodology. Identification of 802.11 networks is intended merely as an example of the method's functionality and presented as such. That said, the methodology presented in this work is applicable to different wireless technologies.

Stage3, Wireless technology identification:

Wireless technology identification is performed in Stage 3 using the scanned frequency channel. Figure 7-5 shows the overall structure of Stage 3. The dataset constructed in Stage 2 will train a classifier and assess its performance. This dataset is divided into two equal subsets—one for training purposes (i.e., training set) and the other to test identification accuracy rate (i.e., testing subset). Observations in testing set act as new scans for which the wireless device must perform technology identification. Note that Increasing the number of features is not associated with proportional increase in classification accuracy. On the contrary, additional features might result in poor identification accuracy because features from different classes that correspond to different technologies might overlap. As such, the classifier training process is iteratively repeated using different feature sets to select those that provide best performance.

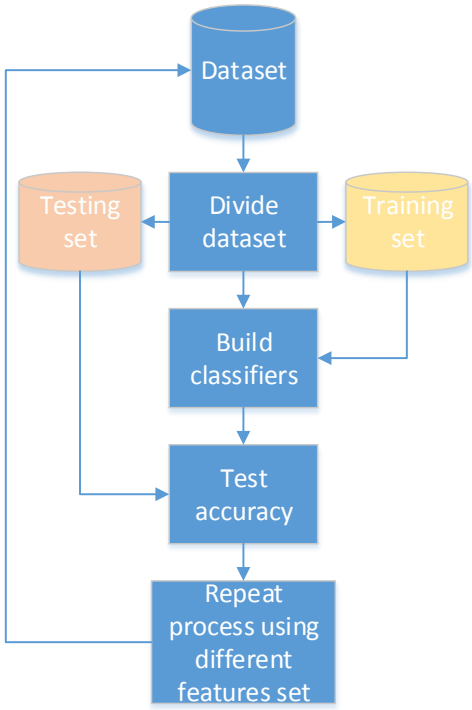

Figure 7-5. Wireless technology identification stage

Two types of classification techniques, namely naïve Bayes and K-nearest neighbor, were investigated in this research to build the classifier. Testing two machine-learning techniques aids in examining the classifier effect on the identification accuracy versus the extracted feature effect. Though machine-learning is not the focus of this work, a brief description is provided to aid in understanding utilized classification methods:

Naïve Bayes classification method:

Bayesian Networks or Belief Networks (BN) are hybrid of graph theory and probability theory. The aim of learning with BN is to determine structures and conditional probabilistic tables that distinguish between nodes via input training data [24, 25]. In a Bayesian network implementation, parent nodes (i.e., a class) represent a particular 802.11 standard or number of transmitters while other nodes (i.e., continuous) represent features used to distinguish between classes. When using a Bayesian network for

classification purposes, probability of features that are conditional on parents are estimated using a training set. These probability functions are then used later to make a classification decision using a testing set [26]. This work utilizes a Naïve Bayesian classification method, which assumes conditional independence of a feature that is conditional on its parents [27]. Thus, probability of a particular 802.11 observation $O = (f_1, f_2, \dots, f_n)$ conditional on class c is given by the following equation:

$$p(f_1, f_2, \dots, f_n|c) = \prod_{k=1}^{n} p(f_k|c) \qquad (27)$$

The probability of a class c given observation O can be obtained by:

$$p(c|O) = p(c|f_1, f_2, \dots, f_n)$$

$$= \frac{p(f_1, f_2, \dots, f_n|c)p(c)}{p(f_1, f_2, \dots, f_n)} \qquad (28)$$

$$= \frac{\prod_{k=1}^{n} p(f_k|c)p(c)}{p(f_1, f_2, \dots, f_n)}$$

Based on the value of adjacent class probabilities ratio, a classifier will make a decision on observation O. Notably, naïve Bayesian assumption of conditional independence of parents is inaccurate in most real life applications. However, this condition achieves a surprisingly superior performance. The reason being that it utilizes zero-one error function, which penalizes according to classification accuracy rather than accuracy of probability estimation. This means that given probability estimation is poor and classification is accurate, correct functionality is assumed [28].

Naïve Bayes is a simple and widely used algorithm in machine learning based on a strong assumption of independence between features and classification. Despite the unrealistic assumption of independence, Naïve Bayes is considered plausibly efficient [77]. Supervised learning is used for training the algorithm in order to predict a class based on accumulated information evidence. Simply put, the algorithm provides a classification decision that attempts to select the most probable outcome. Applications of Naïve Bayes are diverse and span from image processing [78] and text classification [79] to networking [80].

K-nearest neighbor classification method:

k-Nearest Neighbors algorithm (KNN) [81] is a non-parametric classification method wherein an algorithm polls neighbors of a data point, and then votes to assign a given class. Voting is carried out by weighting neighbor' contributions. Neighbors that are closer to the point of interest will have higher participation than those farther away from the point. An obvious drawback of this method is the high dependence on the structure of the dataset. KNN has been used to detect anomalies in wireless sensor networks in [82], to perform medical data mining in [83], and to implement biometric recognition in [84].

Results

This section details experimental wireless technology identification results obtained for 802.11 homogeneous and heterogeneous networks. This works attempts to blindly identify number of 802.11 transmitters and the transmitters' wireless technologies using statistical information obtained from 802.11 time distributions. Statistical information for a particular test run are used as input features for a machine-learning algorithm in an effort

to classify the number of wireless technologies and the number of transmitters used for the corresponding run.

Choosing a greater number of features does not necessarily guarantee improved identification performance, as aforementioned. Features corresponding to different wireless technologies might be strongly overlapping. Thus, adding such features to the training/testing datasets will confuse the classifier, as well as reduce the probability of accurate classification.

An example of overlapping features for homogeneous 802.11 technologies is depicted in Figure 7-6. Features are extracted from idle time distribution and are identified as "total idle time" and "mean of idle time region between 20μs and 180μs." Both exhibit strong overlap between 802.11 observations corresponding to different technologies/standards.

Notably, when "total idle time" was replaced by "mean of idle time region between 20μs and 305μs," as depicted in Figure 7-7, separation between observations corresponding to different technologies was enhanced considerably. This feature was extracted from idle time distribution, as well. Consequently, including features such as "total idle time" would degrade classifier performance.

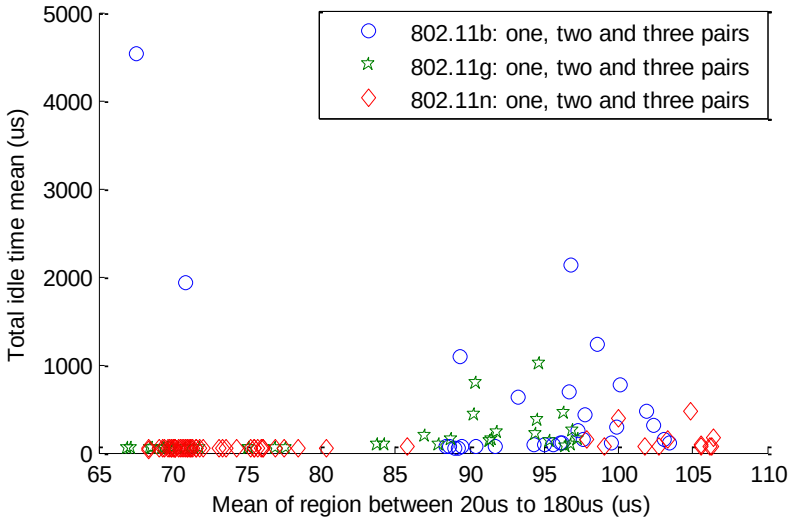

Figure 7-6. Overlapping idle time distribution features

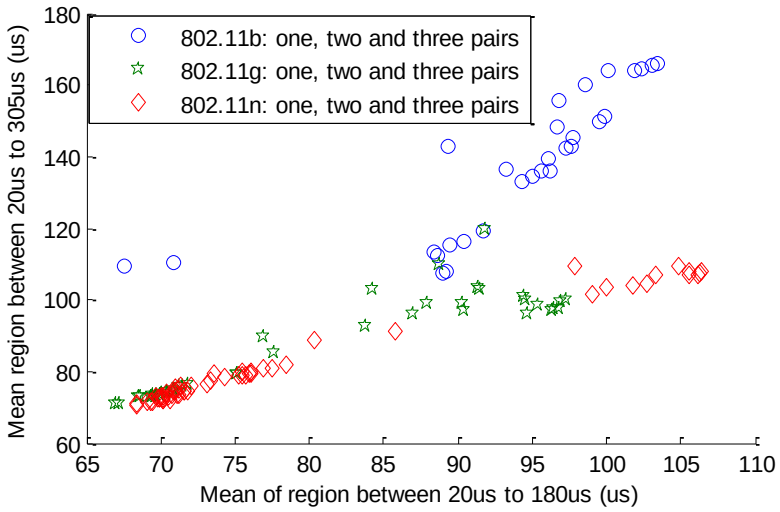

Figure 7-7. Idle time distribution features with improved technology separation

A set of five features extracted from activity distributions was used in the identification process, see Table 13. Note that "frequency of occurrence" refers to the number of occurrences that a particular fragment was repeated during unit time.

Table 13. Features used for wireless standards identification

Feature	Distribution type
Frequency of occurrences at 111µs	Activity
Frequency of occurrences between 150µs and 200µs	Activity
Frequency of occurrences between 200µs and 300µs	Activity
Frequency of occurrences between 300µs and 500µs	Activity
Frequency of occurrences between 1100µs and 1300µs.	Activity

A total of 13 features were used to perform number of transmitters identification, see Table **14.**

Table 14. Features used for number of transmitters' identification

Feature	Distribution type
Highest frequency of occurrence	Idle time
2nd highest frequency of occurrence	Idle time
Time duration of 2nd highest frequency of occurrence	Idle time
3rd highest frequency of occurrence	Idle time
Time duration of 3rd highest frequency of occurrence	Idle time
Mean of region extending from 20us to 180us	Idle time
Mean of region extending from 180us to end of distribution	Idle time
Mean of region extending from 20us to 305us	Idle time
Mean of region extending from 305us to end of distribution	Idle time
Standard deviation of region extending from 20us to 180us	Idle time
Standard deviation of region two from 180us to end of distribution	Idle time
Most contributing idle time fragment duration to the total idle time	Idle time
Number of fragments at 36us (representing number of 802.11n block acknowledgments	Activity

Homogeneous 802.11 networks identification

Technology identification for 802.11 homogeneous networks was performed using a dataset of 127 observations at variable throughput divided into training and testing sets. Frequency channel was scanned for duration of one minute per observation. One-, two-, or three-pair networks exchanged traffic at different throughput levels, ranging from low throughput to saturation. At low throughput, recorded channel utilization can be as low as 12%, whereas channel utilization can reach up to 98% for 802.11n saturation.

Figure 7-8 depicts identification accuracy obtained from both KNN and Naïve Bayes classifiers. An accuracy rate of 96.9% was achieved for homogeneous networks. Figure 7-9 shows identified observations distribution for naïve Bayes classifier. Only two out of 63 802.11g observations in the testing set failed correct identification.

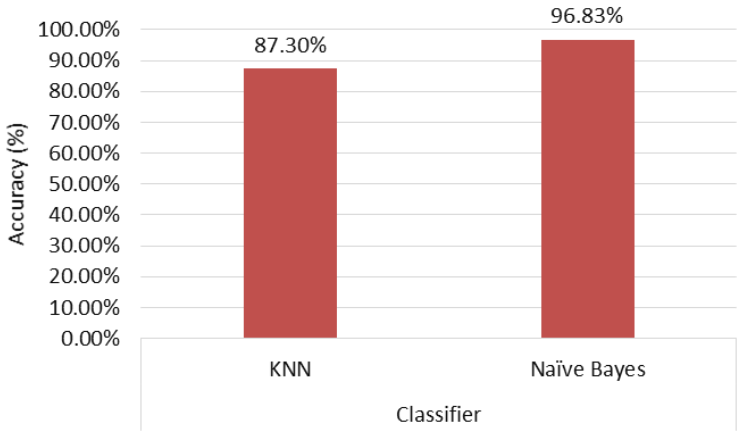

Figure 7-8. Homogeneous networks identification accuracy

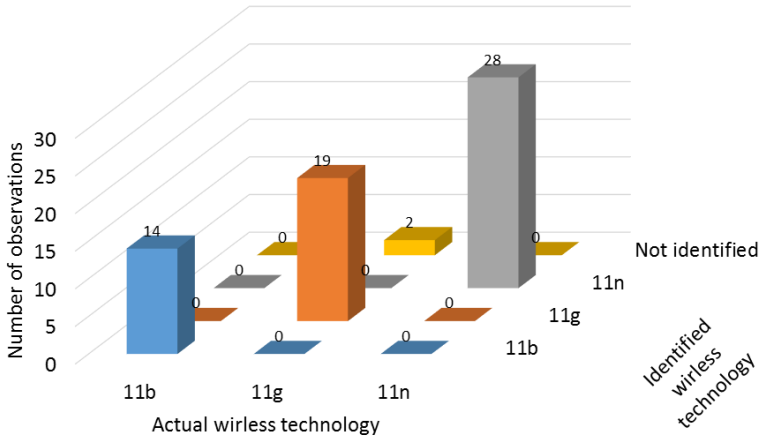

Figure 7-9. Distribution of identified observations for homogeneous networks

Number of transmitters' identification for homogeneous networks via energy detection was investigated and presented in this work, as well. An observation was classified as

one, two, or three transmitters. Maximum accuracy of 85.71% was achieved when directly implementing number of transmitters' identification to a certain observation. See Figure 7-10.

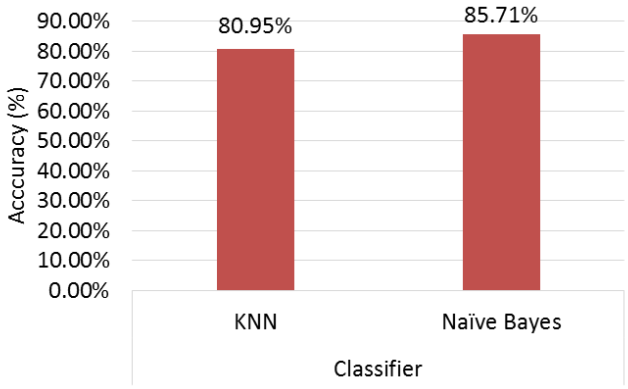

Figure 7-10. Number of transmitters' identification accuracy

A two-stage classifier can be implemented wherein a wireless technology/standard is identified at first, and then transmitter number is identified. As a means to enhance accuracy, number of transmitter identification was investigated in two stages. The reason for this approach is the satisfactory accuracy rate obtained from homogeneous standards identification presented earlier. Per-standard accuracy rates for two stages of transmitter identification is depicted in Figure 7-11.

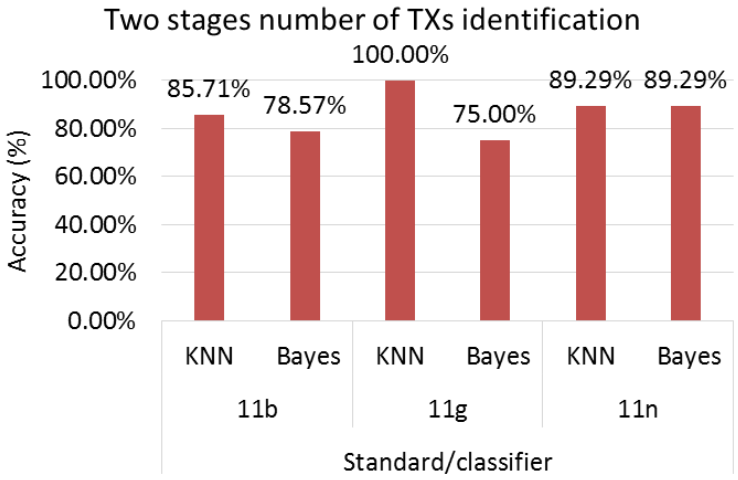

Figure 7-11. Per-standard, two stages, number of transmitters' identification accuracy

Heterogeneous 802.11 networks identification

This section provides identification results for a combined dataset comprised of both homogeneous and heterogeneous 802.11 networks. Heterogeneous 802.11 networks may consist of two- or three-pair networks operating on different 802.11 standards. A total of 469 observations were collected and utilized to construct the dataset. Observations were collected at varying throughput values for the following combinations:

- One-pair: 802.11b, g and n.
- Two-pair: 802.11bb, gg, nn, bg, bn and gn.
- Three-pair: 802.11bbb, ggg, nnn, bbg, bbn, ggb, ggn, nnb, nng and bgn.

Figure 7-12 depicts achieved identification accuracy. An accuracy of up to 85.9% was obtained when using a Naïve Bayes classifier. Figure 7-13 shows distribution of identified observations over various 802.11 standard combinations.

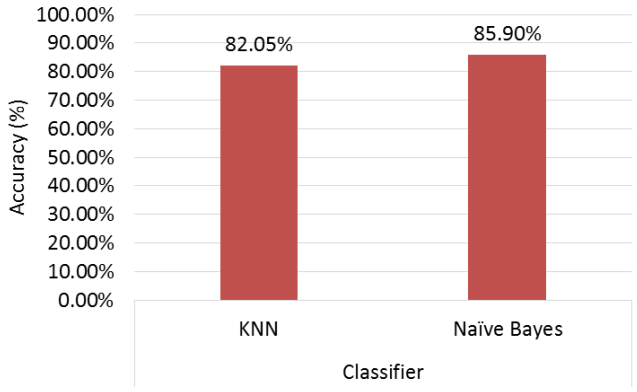

Figure 7-12. Heterogeneous networks identification accuracy

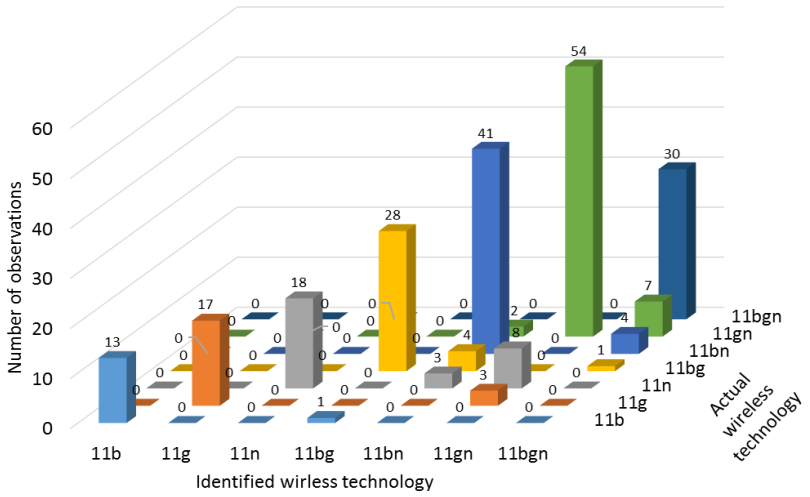

Figure 7-13. Distribution of identified observations for heterogeneous networks

Figure 7-13 demonstrates that overlap occurred between combinations characterized with the same wireless technology. For example, a major overlap was observed between 802.11n one-pair and two- and three-pair heterogeneous networks with 802.11gn combination. The overlap results from temporal parameter similarities between the two technologies at low 802.11n throughput values. Whenever 802.11n transmitter aggregates two sub-frames, it results in aggregated frame duration comparable to 802.11g frame size.

Three-pair 802.11bgn combination observations were identified correctly at an accuracy rate of 100%. Observations for other combinations composed of two technologies were confused with the 802.11bgn combination, although error rate for these cases did not exceed 10%.

Notably, Naïve Bayes classifier outperformed KNN classifier for all reported homogeneous and heterogeneous technology identification experiments. KNN classifier provided better results than Naïve Bayes only for homogeneous two-stage number of transmitter identification.

Conclusion

This chapter presented two applications of 802.11 temporal characterization aimed at providing situational awareness to wireless technologies coexisting with 802.11 networks and enhancing their performance. Spectrum utilization awareness provides coexisting wireless devices with an opportunity to enhance performance.

An application based on channel-timing parameters was investigated and presented wherein an adaptive rather than a fixed 802.15.4 ZigBee packet size was implemented. The method demonstrated superior performance over traditional fixed packet size.

A novel method for wireless technology and number of transmitter identification using simple energy detection techniques was researched, as well. The presented method does not require demodulation, making its application feasible when using the majority of currently used transceivers. Experimental results have been provided to investigate applicability of the proposed identification method and to assess its performance. Various 802.11 homogeneous and heterogeneous wireless networks were utilized in experimental assessment. Identification accuracy of up to 96.9% was achieved under homogeneous network conditions and up to 85.9% under heterogeneous condition.

Chapter 8: Conclusion and Future Work

An extensive temporal characterization of 802.11b, g and n spectrum occupancy and traffic patterns was presented in this dissertation. Applications that benefit from such characterization were introduced and implemented.

Literature review was provided, including an overview of wireless technologies employed in this work. An energy detection methodology free from frame demodulation was provided and implemented. Presented results delivered critical information about channel utilization in terms of DC, throughput, activity distributions, and idle time distributions.

Comprehensive empirical modelling of 802.11b, g and n networks was also presented in this work. Experimental data was collected for a complete set of 802.11 network combinations at a wide range of throughput values. Results demonstrated that 802.11b and g homogeneous networks are best-described using Weibull distribution; 802.11n homogeneous networks are best modeled with Log-Normal models. Heterogeneous 802.11 network combinations were best-modeled using exponential distribution, Log-normal distribution, or Generalized Pareto distribution, depending on the combination of standards employed. A heterogeneous distribution was found to generally follow a Generalized Pareto distribution when the medium included transmission from one or more 802.11n pairs.

Two applications based on channel-timing parameters were also presented and discussed in an effort to highlight usability of 802.11 temporal characterization for enhancing coexistence in the ISM band. The first application introduced adaptive 802.15.4 ZigBee

packet size based on detected 802.11 temporal distributions. ZigBee packet size was changed adaptively to reduce interference with an 802.11g network and to take advantage of longer idle time durations. The method demonstrated superior performance over traditional fixed packet size.

The second application presented a novel method for wireless technology identification using simple energy detection techniques. The presented application enables transceivers to identify wireless technology and the number of transmitters using the spectrum. Results of identifying 802.11 homogeneous and heterogeneous wireless networks were presented to prove the concept. Identification accuracy of up to 96.9% was achieved for homogeneous networks; 85.9% accuracy was achieved for heterogeneous networks.

Future work

Work presented in earlier chapters provided a comprehensive study of 802.11 temporal behavior in the 2.4GHz ISM band. The experimental setup was designed to focus on the core operational scenarios that would represent a wide range of spectrum temporal behavior variations for the investigated networks. Nevertheless, outlier scenarios may exist which could introduce changes to the investigated networks behavior. To accommodate for such scenarios, topology of the networks being studied in the experimental setup can be modified. Notably, when changes to the topology are introduced, we may start observing phenomena resulting for both PHY and MAC layers rather than only isolated MAC layer effects. Two test topologies, depicted in Figure 8-2 and Figure 8-3 are proposed as future work. Test setup depicted in Figure 8-1 aims at investigating effects of hidden node on the spectrum behavior. It is of interest to observe

spectrum occupancy near the hidden node transmitter and receiver and the other transmitters in the network. 802.11 networks operate at frequency above 2.4GHz with limited transmit power leading to increased levels of attenuation. As such, spectrum temporal behavior may prove to be localized and demonstrate different results at either communication end. Figure 8-3 depicts a test setup intended for investigating over exposed node effects. Similarly, spectrum measurements shall be conducted at both 802.11 transmitter and receiver to characterize the resulting spectrum temporal behavior. Realizing these test setups would obviously require changes to spacing between nodes and modification of transmit power for different transmitters to replicate the hidden node and exposed node problems. Details of the hidden node and over exposed node problems can be found in [85]. Investigating such test scenario is directly achievable using methods and tools presented in this dissertation.

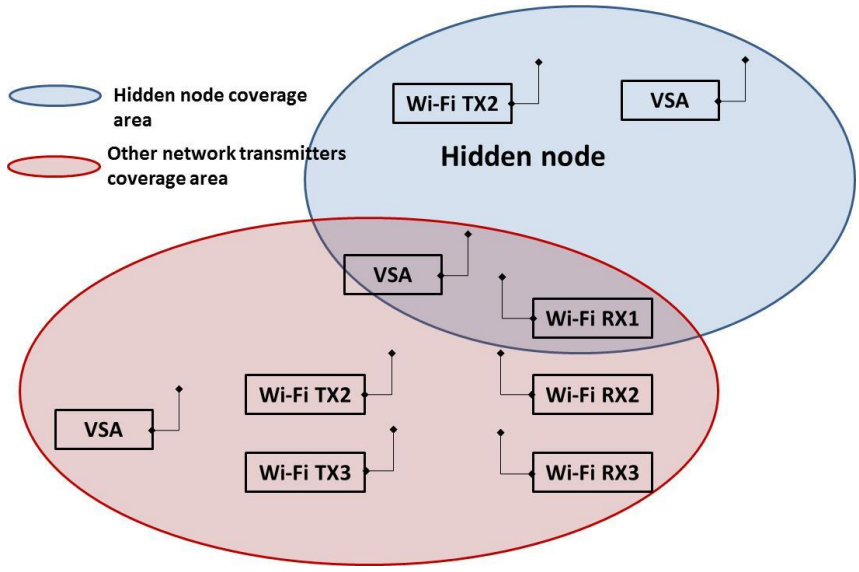

Figure 8-2. Proposed hidden node test setup

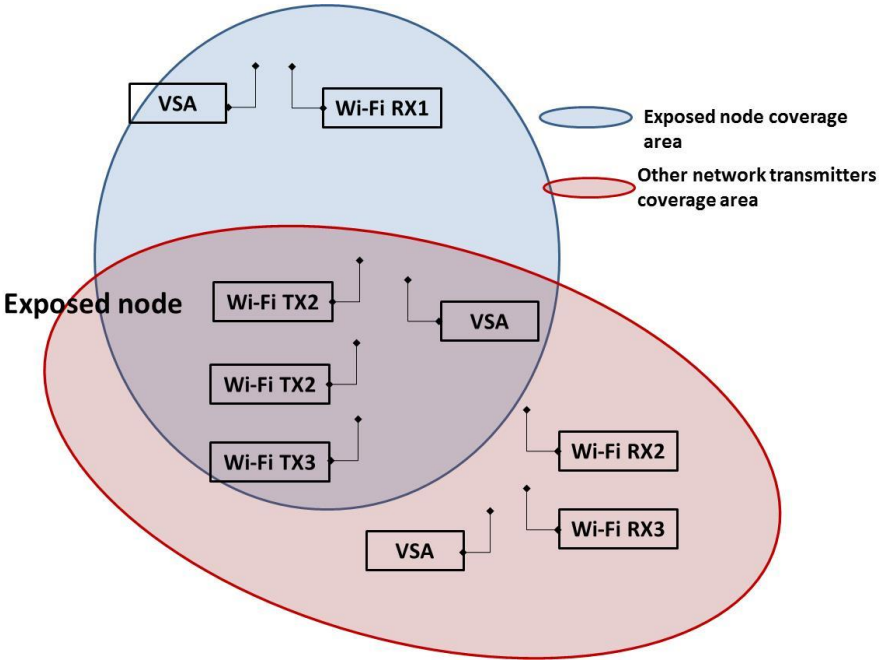

Figure 8-3. Proposed exposed node test setup

Future work also includes performing a temporal and frequency characterization of coexisting wireless technologies in the ISM band. Wireless technology identification study can then performed for such wireless technologies similar to the one performed for 802.11 networks. This helps in providing a holistic view and understanding of the ISM band spectrum occupancy. Also, it serves as a step to enable implementation of extensive cognitive functionality of coexisting devices in unlicensed bands based on temporal and frequency characterization. Such activities help in providing a better wireless devices performance and an efficient use of available spectrum.

Extending these efforts to the 5.9GHz band is proposed as a future work as well. U.S Federal Communication Commission has allocated a 75MHz in the 5.9GHz band for Directed Short-Range Communications (DSRC). Wireless Access in Vehicular Environment (WAVE) is the base communication technology for V2X systems in the United States. PHY and MAC layers implementation for Wave is defined in IEEE

802.11p [86] and IEEE 1609 [87] standards. Wi-Fi alliance is expected to share this band as a secondary user [88]. Efficient use of the band while avoiding interference with V2X network shall be investigated. Work presented in this dissertation provides a method for characterizing available time and frequency in the 5.9GHz band to enable an improved coexistence between

Also, these efforts can be extended to other unlicensed bands to investigate their spectrum occupancy in an effort to increase efficiency of spectrum utilization and improve performance of wireless technologies utilizing these spectrum bands.

References

[1] David Watkins (Strategy Analytics), “Embedded WLAN (Wi-Fi) CE Devices: US Market Forecast,” 2013. [Online]. Available: http://www.strategyanalytics.com/default.aspx?mod=reportabstractviewer&a0=8452.

[2] H. Takagi and B. H. Walke, *Spectrum requirement planning in wireless communications: Model and methodology for IMT-Advanced*, vol. 2. John Wiley & Sons, 2008.

[3] “IEEE Recommended Practice for Information technology-- Local and metropolitan area networks-- Specific requirements-- Part 15.2: Coexistence of Wireless Personal Area Networks with Other Wireless Devices Operating in Unlicensed Frequency Bands,” *IEEE Std 802.15.2-2003*. pp. 1–150, 2003.

[4] Y. Zhu, X. Tian, and J. Zheng, “Performance analysis of the binary exponential backoff algorithm for IEEE 802.11 based mobile ad hoc networks,” *2011 IEEE Int. Conf. Commun.*, 2011.

[5] A. Sikora and V. F. Groza, “COEXISTENCE OF STANDARDIZED WIRELESS SYSTEMS IN THE 2 . 4 GHZ-ISM-BAND *,” vol. 4, no. 1, pp. 5–11, 2005.

[6] L. Angrisani, M. Bertocco, D. Fortin, and A. Sona, “Experimental study of coexistence issues between IEEE 802.11b and IEEE 802.15.4 wireless networks,” *IEEE Trans. Instrum. Meas.*, vol. 57, no. 8, pp. 1514–1523, 2008.

[7] N. J. LaSorte, S. a Rajab, and H. H. Refai, “Developing a reproducible non-line-of-sight experimental setup for testing wireless medical device coexistence utilizing ZigBee.,” *IEEE Trans. Biomed. Eng.*, vol. 59, no. 11, pp. 3221–9, Nov. 2012.

[8] N. LaSorte, S. Rajab, and H. Refai, “Experimental Assessment of Wireless Coexistence for 802.15. 4 in the Presence of 802.11 g/n,” *2012 IEEE Int. Symp. Electromagn. Compat.*, pp. 473–479, 2012.

[9] W. Guo, W. M. Healy, and M. Zhou, “Impacts of 2.4-GHz ISM band interference on IEEE 802.15.4 wireless sensor network reliability in buildings,” *IEEE Trans. Instrum. Meas.*, vol. 61, no. 9, pp. 2533–2544, 2012.

[10] “Radio Frequency Wireless Technology in Medical Devices - Guidance for Industry and Food and Drug Administration Staff,” 2013. [Online]. Available: http://www.fda.gov/MedicalDevices/DeviceRegulationandGuidance/GuidanceDocuments/ucm077210.htm. [Accessed: 01-Jan-2014].

[11] S. Atapattu, C. Tellambura, and H. Jiang, “Energy Detection for Spectrum Sensing in Cognitive Radio,” *Springer*, 2014.

[12] A. Mariani, A. Giorgetti, and M. Chiani, “SNR Wall for Energy Detection with Noise Power Estimation,” *2011 IEEE Int. Conf. Commun.*, pp. 1–6, Jun. 2011.

[13] J. Avila and K. Thenmozhi, “Boosted Energy Detector Based Spectrum Sensing Methodology For Cognitive Radio,” *Middle-East J. Sci. Res.*, vol. 20, no. 9, pp. 1031–1035, 2014.

[14] K. Chabbra, G. Mahendru, and P. Banerjee, “Effect of dynamic threshold & noise uncertainty in energy detection spectrum sensing technique for cognitive radio systems,” *2014 Int. Conf. Signal Process. Integr. Networks*, vol. 1, no. 2, pp. 377–361, Feb. 2014.

[15] H. M. Baradkar and S. G. Akojwar, “Implementation of Energy Detection Method for Spectrum Sensing in Cognitive Radio Based Embedded Wireless Sensor Network Node,” *2014 Int. Conf. Electron. Syst. Signal Process. Comput. Technol.*, pp. 490–495, Jan. 2014.

[16] M. Matinmikko, M. Mustonen, M. Höyhtyä, T. Rauma, H. Sarvanko, and A. Mämmelä, “Distributed and directional spectrum occupancy measurements in the 2.4 GHz ISM band,” in *2010 7th International Symposium on Wireless Communication Systems (ISWCS)*, 2010, pp. 976–980.

[17] M. Matinmikko, M. Mustonen, M. Höyhtyä, T. Rauma, H. Sarvanko, and A. Mämmelä, “Cooperative spectrum occupancy measurements in the 2.4 GHz ISM band,” in *2010 3rd International Symposium on Applied Sciences in Biomedical and Communication Technologies (ISABEL)*, 2010, vol. 00, no. 134624.

[18] D. Denkovski, M. Pavloski, V. Atanasovski, and L. Gavrilovska, “Parameter setting for 2.4GHz ISM spectrum measurement,” in *2010 3rd International Symposium on Applied Sciences in Biomedical and Communication Technologies (ISABEL)*, 2010, pp. 3–7.

[19] S. Geirhofer, L. Tong, and B. M. Sadler, “Dynamic Spectrum Access in the Time Domain: Modeling and Exploiting White Space,” *IEEE Commun. Mag.*, vol. 45, no. 5, pp. 66–72, 2007.

[20] L. Stabellini, “Quantifying and modeling spectrum opportunities in a real wireless environment,” in *2010 IEEE Wireless Communications and Networking Conference (WCNC)*, 2010.

[21] M. Lopez-Benitez and F. Casadevall, “Empirical time-dimension model of spectrum use based on a discrete-time markov chain with deterministic and stochastic duty cycle models,” *IEEE Trans. Veh. Technol.*, vol. 60, no. 6, pp. 2519–2533, 2011.

[22] M. López-Benıtez and F. Casadevall, “Time-dimension models of spectrum usage for the analysis, design and simulation of cognitive radio networks,” *IEEE Trans. Veh. Technol*, vol. 62, no. 5, pp. 2091–2104, 2013.

[23] X. Wang, A. Wong, and P. Ho, “Extended knowledge-based reasoning approach to spectrum sensing for cognitive radio,” *IEEE Trans. Mob. Comput.*, vol. 9, no. 4, pp. 465–478, Apr. 2010.

[24] L. Tang, Y. Chen, E. L. Hines, and M.-S. Alouini, “Effect of primary user traffic on sensing-throughput tradeoff for cognitive radios,” *IEEE Trans. Wirel. Commun.*, vol. 10, no. 4, pp. 1063–1068, 2011.

[25] K. Chang and B. Senadji, “Spectrum sensing optimisation for dynamic primary user signal,” *IEEE Trans. Commun.*, vol. 60, no. 12, pp. 3632–3640, 2012.

[26] S. Zarrin and T. Lim, “Throughput-sensing tradeoff of cognitive radio networks based on quickest sensing,” *2011 IEEE Int. Conf. Commun.*, pp. 1–5, Jun. 2011.

[27] M. Guerrini, L. Rugini, and P. Banelli, “Sensing-throughput tradeoff for cognitive radios,” *2013 IEEE 14th Work. Signal Process. Adv. Wirel. Commun.*, pp. 115–119, Jun. 2013.

[28] F. Zhang, W. Wang, and Z. Zhang, “A primary traffic aware opportunistic spectrum sensing for cognitive radio networks,” *2011 IEEE 22nd Int. Symp. Pers. Indoor Mob. Radio Commun. (PIMRC)*, pp. 700–704, 2011.

[29] Y. Lin and V. W. S. Wong, “WSN01-1: Frame Aggregation and Optimal Frame Size Adaptation for IEEE 802.11n WLANs,” *Global Telecommunications Conference, 2006. GLOBECOM ’06. IEEE*. pp. 1–6, 2006.

[30] Y.-D. Lin, J.-H. Yeh, T.-H. Yang, C.-Y. Ku, S.-L. Tsao, and Y.-C. Lai, “Efficient dynamic frame aggregation in IEEE 802.11s mesh networks,” *Int. J. Commun. Syst.*, vol. 22, no. 10, pp. 1319–1338, 2009.

[31] N. Hajlaoui, I. Jabri, and M. Ben Jemaa, “Analytical study of frame aggregation in error-prone channels,” *2013 9th Int. Wirel. Commun. Mob. Comput. Conf.*, pp. 237–242, Jul. 2013.

[32] M. Kim and C. Choi, “Joint rate and fragment size adaptation in IEEE 802.11 n wireless LANs,” *... Netw. Conf. (CCNC), 2011 IEEE*, pp. 942–947, 2011.

[33] G. Kim, C. Shin, and H. Park, “Adaptive frame size estimation using extended Kalman filter for high-stressed WLANs,” *2012 IEEE 23rd Int. Symp. Pers. Indoor Mob. Radio Commun. -*, pp. 272–277, Sep. 2012.

[34] P. Teymoori, A. Dadlani, K. Sohraby, and K. Kim, “An Optimal Packet Aggregation Scheme in Delay-Constrained IEEE 802.11n WLANs,” *Wireless Communications, Networking and Mobile Computing (WiCOM), 2012 8th International Conference on*. pp. 1–4, 2012.

[35] J. Deng and M. Davis, “An adaptive packet aggregation algorithm for wireless networks,” *Wireless Communications & Signal Processing (WCSP), 2013 International Conference on*. pp. 1–6, 2013.

[36] D. Kim and S. An, “Throughput enhancement by Dynamic Frame Aggregation in multi-rate WLANs,” *Communications and Vehicular Technology in the Benelux (SCVT), 2012 IEEE 19th Symposium on*. pp. 1–5, 2012.

[37] J. Yin, X. Wang, and D. P. Agrawal, “Optimal packet size in error-prone channel for IEEE 802.11 distributed coordination function,” *Wireless Communications and Networking Conference, 2004. WCNC. 2004 IEEE*, vol. 3. pp. 1654–1659 Vol.3, 2004.

[38] E. Rocha, D. Corujo, and R. Aguiar, “Implementing and evaluating improved MAC efficiency through payload extension in 802.11n networks,” *Communications Workshops (ICC), 2013 IEEE International Conference on*. pp. 982–987, 2013.

[39] E. N. Ciftcioglu and O. Gurbuz, “Opportunistic Scheduling with Frame Aggregation for Next Generation Wireless LANs,” *Communications, 2006. ICC ’06. IEEE International Conference on*, vol. 11. pp. 5228–5233, 2006.

[40] N. Shetty, S. Pollin, and P. Paweczak, “Identifying Spectrum Usage by Unknown Systems using Experiments in Machine Learning,” *Wireless Communications and Networking Conference, 2009. WCNC 2009. IEEE*. pp. 1–6, 2009.

[41] H. Nguyen, N. Nguyen, G. Zheng, Z. Han, and R. Zheng, “Binary Blind Identification of Wireless Transmission Technologies for Wide-Band Spectrum Monitoring,” *Global Telecommunications Conference (GLOBECOM 2011), 2011 IEEE*. pp. 1–6, 2011.

[42] R. Miller, W. Xu, P. Kamat, and W. Trappe, “Service Discovery and Device Identification in Cognitive Radio Networks,” in *2007 2nd IEEE Workshop on Networking Technologies for Software Define Radio Networks*, 2007, pp. 40–47.

[43] K. Kim, C. M. Spooner, I. Akbar, and J. H. Reed, “Specific Emitter Identification for Cognitive Radio with Application to IEEE 802.11,” in *IEEE GLOBECOM 2008 - 2008 IEEE Global Telecommunications Conference*, 2008, pp. 1–5.

[44] V. Brik, S. Banerjee, M. Gruteser, and S. Oh, “Wireless device identification with radiometric signatures,” in *Proceedings of the 14th ACM international conference on Mobile computing and networking - MobiCom ’08*, 2008, p. 116.

[45] Z. Shi, M. Liu, and L. Huang, “Transient-based identification of 802.11b wireless device,” in *2011 International Conference on Wireless Communications and Signal Processing (WCSP)*, 2011, pp. 1–5.

[46] C. Neumann, O. Heen, and S. Onno, “An Empirical Study of Passive 802.11 Device Fingerprinting,” in *2012 32nd International Conference on Distributed Computing Systems Workshops*, 2012, pp. 593–602.

[47] S. Hu, Y. Yao, and Z. Yang, “MAC protocol identification using support vector machines for cognitive radio networks,” *IEEE Wirel. Commun.*, vol. 21, no. 1, pp. 52–60, Feb. 2014.

[48] R. Challoo, a. Oladeinde, N. Yilmazer, S. Ozcelik, and L. Challoo, “An overview and assessment of wireless technologies and coexistence of ZigBee, bluetooth and wi-fi devices,” *Procedia Comput. Sci.*, vol. 12, pp. 386–391, 2012.

[49] P. Chatzimisios, A. C. Boucouvalas, and V. Vitsas, “Effectiveness of RTS/CTS handshake in IEEE 802.11a Wireless LANs,” *Electronics Letters*, vol. 40, no. 14. pp. 915–916, 2004.

[50] IEEE, “Supplement to IEEE Standard for Information Technology- Telecommunications and Information Exchange Between Systems- Local and Metropolitan Area Networks- Specific Requirements- Part 11: Wireless LAN Medium Access Control (MAC) and Physical Layer (PHY) Sp,” *IEEE Std 802.11b-1999*. pp. i–90, 2000.

[51] I. Ramachandran and S. Roy, “Clear channel assessment in energyconstrained wideband wireless networks,” *Wireless Communications, IEEE*, vol. 14, no. 3. pp. 70–78, 2007.

[52] I. Ramachandran and S. Roy, “WLC46-2: On the Impact of Clear Channel Assessment on MAC Performance,” *Global Telecommunications Conference, 2006. GLOBECOM ’06. IEEE*. pp. 1–5, 2006.

[53] B. Pearson, “Complementary code keying made simple,” *Intersil, Milpitas, CA, USA, Appl. Notes AN9850*, vol. 1, 2000.

[54] B. E. Henty, “A Brief Tutorial on the PHY and MAC layers of the IEEE 802.11 b Standard,” *July*, vol. 12, pp. 12–16, 2001.

[55] IEEE, “IEEE Standard for Information Technology- Telecommunications and Information Exchange Between Systems- Local and Metropolitan Area Networks- Specific Requirements Part Ii: Wireless LAN Medium Access Control (MAC) and Physical Layer (PHY) Specifications,” *IEEE Std 802.11g-2003 (Amendment to IEEE Std 802.11, 1999 Edn. (Reaff 2003) as amended by IEEE Stds 802.11a-1999, 802.11b-1999, 802.11b-1999/Cor 1-2001, and 802.11d-2001)*. pp. i–67, 2003.

[56] M. Debbah, “Short introduction to OFDM,” *White Pap. Mob. Commun. Group, Inst. Eurecom*, 2004.

[57] M. Ergen, “IEEE 802.11 Tutorial,” *Univ. Calif. Berkeley*, vol. 70, 2002.

[58] IEEE, “IEEE Standard for Information technology-- Local and metropolitan area networks-- Specific requirements-- Part 11: Wireless LAN Medium Access Control (MAC)and Physical Layer (PHY) Specifications Amendment 5: Enhancements for Higher Throughput,” *IEEE Std 802.11n-2009 (Amendment to IEEE Std 802.11-2007 as amended by IEEE Std 802.11k-2008, IEEE Std 802.11r-2008, IEEE Std 802.11y-2008, and IEEE Std 802.11w-2009)*. pp. 1–565, 2009.

[59] A. Saif and M. Othman, “Frame Aggregation in Wireless Networks: Techniques and Issues.,” *IETE Tech. Rev.*, vol. 28, no. 4, p. 336, 2011.

[60] Z. Alliance, “IEEE 802.15. 4, ZigBee standard,” *http//www. zigbee. org*, 2009.

[61] IEEE, *IEEE Standard for Telecommunications and information Local and metropolitan area networks — Specific requirements Part 15 . 4 : Wireless Medium Access Control (MAC) and Physical Layer (PHY) Specifications for Low-Rate Wireless Personal Area Networks (*, vol. 2006, no. September. 2006.

[62] “RouterBoard.com : RB433UAH.” [Online]. Available: http://routerboard.com/RB433UAH. [Accessed: 16-Oct-2015].

[63] “Manual:TOC - MikroTik Wiki.” [Online]. Available: http://wiki.mikrotik.com/wiki/Manual:TOC. [Accessed: 16-Oct-2015].

[64] “RF Signal Analyzers - National Instruments.” [Online]. Available: http://sine.ni.com/nips/cds/view/p/lang/en/nid/203041. [Accessed: 16-Oct-2015].

[65] N. LaSorte, D. Bloom, S. Rajab, S. Asadallahi, H. H. Refai, R. Zhang, and W. He, “Comparison of duty cycle measurement techniques of 802.11 b/g in the frequency and time domain,” *2013 IEEE Int. Instrum. Meas. Technol. Conf.*, 2013.

[66] M. Lopez-Benitez and F. Casadevall, “Methodological aspects of spectrum occupancy evaluation in the context of cognitive radio,” *Wireless Conference, 2009. EW 2009. European*. pp. 199–204, 2009.

[67] A. Holt and C.-Y. Huang, *802.11 Wireless Networks: Security and Analysis*, 1st ed. Springer Publishing Company, Incorporated, 2010.

[68] S. A. Rajab, W. Balid, and H. H. Refai, “Comprehensive study of spectrum occupancy for 802.11b/g/n homogeneous networks,” in *2015 IEEE International Instrumentation and Measurement Technology Conference (I2MTC) Proceedings*, 2015, pp. 1741–1746.

[69] W. Balid, S. A. Rajab, and H. H. Refai, “Comprehensive study of spectrum utilization for 802.11 b/g/n networks,” in *Wireless Communications and Mobile Computing Conference (IWCMC), 2015 International*, 2015, pp. 1526–1531.

[70] J. O. Rawlings, S. G. Pantula, and D. A. Dickey, *Applied regression analysis: a research tool. 1998*. Springer, 1998.

[71] “r2, a measure of goodness-of-fit of linear regression,” 2014. [Online]. Available: http://www.graphpad.com/guides/prism/6/curve-fitting/index.htm?r2_ameasureofgoodness_of_fitoflinearregression.htm.

[72] D. Mercedes, M. Plata, Á. Gabriel, and A. Reátiga, “Evaluation of energy detection for spectrum sensing based on the dynamic selection of detection-threshold,” vol. 35, pp. 135–143, 2012.

[73] C. Walck, “Hand-book on STATISTICAL DISTRIBUTIONS for experimentalists,” *Hand-b. Stat. Distrib. Exp.*, no. September, pp. 26–35, 2007.

[74] W. H. Press, S. A. Teukolsky, W. T. Vetterling, and B. P. Flannery, *Numerical Recipes 3rd Edition: The Art of Scientific Computing*, 3rd ed. New York, NY, USA: Cambridge University Press, 2007.

[75] A. Bhattacharyya, “On a measure of divergence between two multinomial populations,” *Sankhyā Indian J. Stat.*, pp. 401–406, 1946.

[76] S. A. Rajab, W. Balid, M. O. Al Kalaa, and H. H. Refai, “Energy Detection and Machine Learning for the Identification of Wireless MAC Technologies,” in *Wireless Communications and Mobile Computing Conference (IWCMC), 2015 11th International. IEEE*, 2015.

[77] H. Zhang, “The optimality of naive Bayes,” in *FLAIRS*, 2004.

[78] S. Aksoy, K. Koperski, C. Tusk, G. Marchisio, and J. C. Tilton, “Learning bayesian classifiers for scene classification with a visual grammar,” *IEEE Trans. Geosci. Remote Sens.*, vol. 43, no. 3, pp. 581–589, Mar. 2005.

[79] S. Kim, K. Han, H. Rim, and S. H. Myaeng, “Some Effective Techniques for Naive Bayes Text Classification,” *IEEE Trans. Knowl. Data Eng.*, vol. 18, no. 11, pp. 1457–1466, Nov. 2006.

[80] C. Livadas, R. Walsh, D. Lapsley, and W. Strayer, “Usilng Machine Learning Technliques to Identify Botnet Traffic,” in *Proceedings. 2006 31st IEEE Conference on Local Computer Networks*, 2006, pp. 967–974.

[81] T. Cover and P. Hart, “Nearest neighbor pattern classification,” *IEEE Trans. Inf. Theory*, vol. 13, no. 1, pp. 21–27, Jan. 1967.

[82] M. Xie, J. Hu, S. Han, and H.-H. Chen, “Scalable hypergrid k-NN-Based online anomaly detection in wireless sensor networks,” *IEEE Trans. Parallel Distrib. Syst.*, vol. 24, no. 8, pp. 1661–1670, Aug. 2013.

[83] M. Tseng, “Medical data mining using BGA and RGA for weighting of features in fuzzy k-NN classification,” in *2009 International Conference on Machine Learning and Cybernetics*, 2009, no. July, pp. 3070–3075.

[84] E. Acar and M. S. Ozerdem, “An iris recognition system by laws texture energy measure based k-NN classifier,” in *2013 21st Signal Processing and Communications Applications Conference (SIU)*, 2013, pp. 1–4.

[85] A. Jayasuriya, S. Perreau, A. Dadej, and S. Gordon, “Hidden vs exposed terminal problem in ad hoc networks.” ATNAC 2004, 2004.

[86] “IEEE Std. 802.11-2007, Part 11 : Wireless LAN Medium Access Control (MAC) and Physical Layer (PHY) specifications,” 2007.

[87] “IEEE 1609.4-2006 WAVE Multi-Channel Operation,” 2006.

[88] M. O’Rielly and J. Rosenworcel, “Steering into the Future with More Wi-Fi by Sharing the Upper 5 GHz Band,” 2015. [Online]. Available: https://www.fcc.gov/news-events/blog/2015/09/16/steering-future-more-wi-fi-sharing-upper-5-ghz-band.

APPENDIX A

This appendix provides distributions parameters that were obtained from the empirical modelling activities presented in this work.

Table 15. Homogeneous networks idle time distributions empirical modelling distributions parameters

Combination	Throughput	Scale	Shape	Location	Distribution
802.11b	0.140845	1151.251	0.31634	NA	Weibull
	0.28169	440.6714	0.331248	NA	
	0.422535	288.5521	0.352516	NA	
	0.56338	216.5685	0.38959	NA	
	0.704225	150.3286	0.420093	NA	
	0.84507	110.6426	0.457851	NA	
	0.985915	80.31762	0.533705	NA	
802.11bb	0.25641	454.4337	0.327704	NA	Weibull
	0.512821	154.6577	0.36692	NA	
	0.769231	91.01028	0.429571	NA	
	0.948718	56.419	0.532209	NA	
	0.512821	137.558	0.371585	NA	
	0.641026	112.3662	0.397244	NA	
	0.897436	64.70541	0.486399	NA	
	0.948718	54.43224	0.512986	NA	
	0.769231	83.78105	0.435607	NA	
	0.935897	42.97834	0.587049	NA	
	0.948718	45.56229	0.578959	NA	
802.11bbb	0.395257	235.6976	0.358938	NA	Weibull
	0.922266	64.30312	0.552894	NA	
	0.948617	58.17729	0.595449	NA	
	0.948617	59.0059	0.579327	NA	
	0.943347	47.31613	0.64903	NA	
	0.961792	58.52603	0.57807	NA	
	0.988142	45.27752	0.659201	NA	
802.11g	0.177936	296.2906	0.401876	NA	Weibull
	0.355872	188.0788	0.474716	NA	
	0.533808	136.1997	0.545248	NA	
	0.711744	94.95738	0.613136	NA	
	0.907473	67.13438	0.720941	NA	

802.11gg	0.20202	243.4112	0.420061	NA	Weibull
	0.3367	150.9766	0.459805	NA	
	0.484848	92.07866	0.522523	NA	
	0.673401	80.93936	0.582589	NA	
	0.750842	57.12293	0.666552	NA	
	0.37037	175.1613	0.4992	NA	
	0.673401	87.96291	0.595932	NA	
	0.838384	61.70147	0.69289	NA	
	0.905724	49.57255	0.775471	NA	
	0.538721	119.0187	0.581204	NA	
	0.96633	43.87613	0.94169	NA	
	0.707071	90.92134	0.645902	NA	
802.11ggg	0.505051	118.8617	0.524905	NA	Weibull
	0.673401	87.09919	0.60096	NA	
	0.973064	46.49123	0.928603	NA	
	0.96633	46.475	0.933612	NA	
	0.841751	63.76732	0.718561	NA	
	0.96633	43.60345	0.989488	NA	
	0.96633	44.32544	0.975629	NA	
	0.962963	43.71256	0.985164	NA	
	0.969697	44.02202	0.968904	NA	
	0.942761	44.77692	0.95326	NA	
	0.912458	51.25997	0.807983	NA	
	0.962963	44.60241	0.947918	NA	
	0.976431	44.68183	0.951513	NA	
	0.986532	43.60212	0.982651	NA	
	0.979798	43.47336	0.97884	NA	
	0.976431	43.22909	0.984923	NA	
	1	44.22538	0.979422	NA	
	0.983165	43.74223	0.978745	NA	
	0.976431	43.30836	0.969737	NA	
802.11n	0.177305	2.069346	NA	4.203107	Log-normal
	0.35461	1.592815	NA	3.822592	
	0.531915	1.211674	NA	3.534159	
	0.707447	1.202277	NA	3.527166	
	0.884752	1.204307	NA	3.533672	
802.11nn	0.204461	1.945643	NA	4.148856	Log-normal
	0.371747	1.60833	NA	3.732821	
	0.557621	1.201955	NA	3.382773	
	0.743494	1.056183	NA	3.35401	
	0.923792	0.970632	NA	3.410213	

	0.966543	1.043055	NA	3.324704	
	0.390335	1.492385	NA	3.828994	
	0.743494	1.007904	NA	3.401058	
	0.921933	1.063105	NA	3.344005	
	0.979554	1.053032	NA	3.311238	
	0.576208	1.109256	NA	3.554679	
	0.762082	1.117833	NA	3.554234	
	0.901487	1.118302	NA	3.537706	
802.11nnn	0.576699	1.269116	NA	3.318556	Log-normal
	0.743689	1.232356	NA	3.188379	
	0.860194	1.171053	NA	3.225668	
	0.881553	1.189282	NA	3.195587	
	0.850485	1.111687	NA	3.207965	
	0.741748	1.189706	NA	3.226072	
	0.879612	1.162332	NA	3.201583	
	0.885437	1.092253	NA	3.197527	
	0.891262	1.124227	NA	3.193137	
	0.897087	1.098211	NA	3.200927	
	0.838835	1.0693	NA	3.205014	
	0.794175	1.082335	NA	3.187564	
	0.825243	1.101089	NA	3.19606	
	0.928155	1.11306	NA	3.218478	
	0.88932	1.086084	NA	3.195579	
	0.908738	1.068917	NA	3.211776	
	0.757282	1.122891	NA	3.210936	
	0.893204	1.112785	NA	3.206724	
	0.924272	1.118681	NA	3.208861	
	0.88932	1.098844	NA	3.223486	
	0.926214	1.210991	NA	3.211035	
	0.902913	1.140704	NA	3.222747	
	0.92233	1.097092	NA	3.186204	
	0.961165	1.104124	NA	3.18189	
	0.912621	1.060313	NA	3.20389	
	0.873786	1.083727	NA	3.192075	
	0.906796	1.058571	NA	3.187935	
	0.935922	1.063335	NA	3.200623	
	0.897087	1.095473	NA	3.188811	
	0.92233	1.070957	NA	3.176276	
	0.933981	1.103175	NA	3.185043	
	0.953398	1.13054	NA	3.203061	
	0.945631	1.12596	NA	3.198065	

	0.920388	1.126939	NA	3.193299	
	0.947573	1.113638	NA	3.184497	

Table 16. Heterogeneous networks idle time distributions empirical modelling distributions parameters

Combination	Throughput	Scale	Shape	Location	Mean	Distribution
802.11bn	0.272682	1.10298	0	4.656476	0	Log-normal
	0.520575	1.069559	0	4.618012	0	
	0.76351	1.295357	0	4.757562	0	
	0.979177	1.908868	0	5.704975	0	
	1	2.113918	0	6.109859	0	
	0.366882	1.333006	0	5.227343	0	
	0.547843	1.44634	0	5.363297	0	
	0.783342	1.653392	0	5.498698	0	
	0.884978	1.845906	0	5.751182	0	
	0.840357	1.939403	0	5.778878	0	
	0.371839	1.326488	0	5.231814	0	
	0.540407	1.447206	0	5.356055	0	
	0.701537	1.508741	0	5.405192	0	
	0.946951	1.913603	0	5.810937	0	
802.11gn	0.285714	52.27314	-0.34669	0.5	0	Generalized Pareto
	0.47619	52.9427	-0.33988	0.5	0	
	0.666667	132.3694	-0.27529	0.5	0	
	0.853333	167.4889	-0.03088	0.5	0	
	0.952381	79.08634	-0.49533	0.5	0	
	0.380952	58.46963	-0.49444	0.5	0	
	0.571429	47.67757	-0.25662	0.5	0	
	0.739048	37.33339	0.33333	0.5	0	
	0.845714	27.90672	0.814537	0.5	0	
	0.99619	70.99381	-0.57591	0.5	0	
	0.502857	72.43361	-0.46505	0.5	0	
	0.620952	73.51602	-0.17785	0.5	0	
	0.75619	46.95976	0.132992	0.5	0	
	0.857143	40.27006	0.485429	0.5	0	
	0.980952	73.88522	-0.50547	0.5	0	
	0.51619	58.16333	-0.37951	0.5	0	
	0.6	45.64311	-0.13294	0.5	0	
	0.739048	135.7636	-0.1678	0.5	0	
	0.851429	28.60806	0.775861	0.5	0	
802.11gb	0.242915	0	0	0	240.6198	Exponential

	0.445344	0	0	0	408.0854	
	0.850202	0	0	0	445.5406	
	1	0	0	0	197.1214	
	0.404858	0	0	0	331.6408	
	0.607287	0	0	0	341.6722	
	0.615385	0	0	0	172.9214	
	0.611336	0	0	0	336.0893	
	0.453441	0	0	0	329.7796	
	0.59919	0	0	0	169.3101	
	0.623482	0	0	0	329.5189	